ALL-OPTICAL MICROWAVE SIGNAL PROCESSING BASED ON OPTICAL PHASE MODULATION

By

Fei Zeng

A thesis submitted in partial fulfillment of the
requirements for the degree of

Doctor of Philosophy

Ottawa-Carleton Institute of Electrical and Computer Engineering
School of Information Technology and Engineering
Faculty of Engineering
University of Ottawa

December 2006

Your file Votre référence
ISBN: 978-0-494-49404-2
Our file Notre référence
ISBN: 978-0-494-49404-2

uOttawa

L'Université canadienne
Canada's university

FACULTÉ DES ÉTUDES SUPÉRIEURES ET POSTOCTORALES

uOttawa

L'Université canadienne
Canada's university

FACULTY OF GRADUATE AND POSDOCTORAL STUDIES

Fei Zeng

AUTEUR DE LA THÈSE / AUTHOR OF THESIS

Ph.D. (Electrical Engineering)

GRADE / DEGREE

School of Information Technology and Engineering

FACULTÉ, ÉCOLE, DÉPARTEMENT / FACULTY, SCHOOL, DEPARTMENT

All-Optical Microwave Signal Processing Based on Optical Phase Modulation

TITRE DE LA THÈSE / TITLE OF THESIS

Jianping Yao

DIRECTEUR (DIRECTRICE) DE LA THÈSE / THESIS SUPERVISOR

CO-DIRECTEUR (CO-DIRECTRICE) DE LA THÈSE / THESIS CO-SUPERVISOR

EXAMINATEURS (EXAMINATRICES) DE LA THÈSE / THESIS EXAMINERS

Jacques Albert

Pierre Berini

José Azana

Tet Yeap

Gary W. Slater

Le Doyen de la Faculté des études supérieures et postdoctorales / Dean of the Faculty of Graduate and Postdoctoral Studies

ABSTRACT

This thesis presents a theoretical and experimental study of optical phase modulation and its applications in all-optical microwave signal processing, which include all-optical microwave filtering, all-optical microwave mixing, optical code-division multiple-access (CDMA) coding, and ultrawideband (UWB) signal generation.

All-optical microwave signal processing can be considered as the use of opto-electronic devices and systems to process microwave signals in the optical domain, which provides several significant advantages such as low loss, low dispersion, light weight, high time bandwidth products, and immunity to electromagnetic interference. In conventional approaches, the intensity of an optical carrier is modulated by a microwave signal based on direct modulation or external modulation. The intensity-modulated optical signal is then fed to a photonic circuit or system to achieve specific signal processing functionalities. The microwave signal being processed is usually obtained based on direct detection, i.e., an opto-electronic conversion by use of a photodiode.

In this thesis, the research efforts are focused on the optical phase modulation and its applications in all-optical microwave signal processing.

To avoid using coherent detection which is complicated and costly, simple and effective phase modulation to intensity modulation (PM-IM) conversion schemes are pursued. Based on a theoretical study of optical phase modulation, two approaches to achieving PM-IM conversions are proposed. In the first approach, the use of chromatic dispersion induced by a dispersive device to alter the phase relationships among the sidebands and the optical carrier of a phase-modulated optical signal to realize PM-IM conversion is investigated. In the second approach, instead of using a dispersive device, the PM-IM conversion is realized based on optical frequency discrimination implemented using an optical filter. We show that the proposed PM-IM conversion schemes can be implemented by use of commercially available devices without increasing significantly the system complexity compared to IM-based systems. More importantly, the PM-IM conversions bring a number of very interesting features which would

be used to implement different signal processing functionalities. First, the PM-IM conversion plus direct detection has a frequency response with a notch at the dc, this feature can be used to achieve all-optical microwave bandpass filtering. Second, in the PM-IM conversion based on frequency discrimination, the polarity of the detected electrical signal can be easily reversed by simply tuning the optical wavelength, which provides the possibility to achieve bipolar operation, a feature highly desirable and extremely important in all-optical microwave signal processing.

In this thesis, the use of the PM-IM conversion features for all-optical signal processing is investigated. Specifically,

(1) We propose and demonstrate three different filter architectures for all-optical microwave bandpass filtering.

(2) We propose and demonstrate, for the first time, an all-optical microwave signal processor that can realize all-optical mixing and filtering simultaneously.

(3) We propose and demonstrate a scheme to implement unipolar-bipolar phase-time encoding/decoding for optical CDMA.

(4) UWB pulses are usually generated in the electrical domain for short-range high-data rate wireless communications. To extend its coverage, UWB signal distributed over optical fiber is a topic of interest recently. In the thesis, we propose and demonstrate two approaches to generating and distributing UWB pulses in the optical domain.

ACKNOWLEDGMENTS

First of all, I owe a deep sense of gratitude to my supervisor, Professor Jianping Yao. He has been a source of constant encouragement and enthusiasm. I thank him for providing continuous support and valuable directions throughout this work.

I would also like to thank the following people, who are current or former colleagues working with me in the Microwave Photonics Research Laboratory at the School of Information Technology and Engineering, University of Ottawa: Guohua Qi, Jun Wang, Sebastien Blais, Zhichao Deng, Jian Yao, Dr. Jian Liu, Dr. Xiangfei Chen, Dr. Junqiang Sun, Howard Rideout, Blerim Qela, Dr. Qing Wang, and Dr. Chi Hao. Their strong supports and generous help greatly improved my research work. I will always cherish memories of the good times we have had both inside and outside the laboratory.

Special thanks also go to Optical Communications and Electro-photonics Group of the Communications Research Centre Canada for sharing their facilities and fruitful collaborations.

Finally, I am greatly indebted to my beloved family: my father Zhaoguo Zeng, my mother Xiaogui Zeng, my wife Huilan Yang, and my daughter Amy. They have always been the biggest support, physically and mentally, to my study.

TABLE OF CONTENTS

CHAPTER 1
INTRODUCTION

1.1 Background review

Nowadays many applications in the fields such as radar and communication systems are calling for ever-increasing speed, bandwidth and dynamic range [1]-[4]. Features like small size, light weight, large tunability and low power consumption are also required. Digital electronics has been the most widely used approach for those purposes [5]-[6]. However, its speed is normally less than several gigahertzes, which is limited by the fact that the required sampling speed increases in direct proportion to the bandwidth of the signal to be processed. Being important, the electronic bottleneck is by no means the only source of limitation on current signal processing techniques, since electromagnetic interference (EMI) and frequency dependent losses can also be sources of important impairments. All-optical signal processing, with several significant advantages, such as low loss, low dispersion, light weight, high time bandwidth products, and immunity to EMI, has been recognized as one of the promising candidates to process high frequency and wideband signals [2]-[4].

In addition, digital optical communication systems now carry the bulk of terrestrial long-distance communications traffic and fiber is increasingly being brought into the local access networks. With deploying long-distance systems having minimum channel rates of 10 Gb/s and the evolution of the Ethernet standard to encompass a transmission rate of 10 Gb/s, it is expected that all-optical signal processing techniques will be utilized in most of future optical digital communication systems. Moreover, in response to the demand for high-throughput broadband wireless access networks, radio-over-fiber technologies based on the combined and complementary aspects of RF/microwave/millimeter-wave and optical links for integrated network operation have been attracted intensive research and development interests. This combination of radio and fiber technologies will extend the fiber-optic backbone closer to the end-user and more importantly, into the wireless domain. In fact, the use of photonic techniques in radio systems has now become a commercial reality in fiber-radio access networks and there

are emerging applications in phase arrayed antennas and electronic warfare as well. Consequently, the capability of processing high frequency and wideband signals directly in the optical domain, without the need of inefficient and costly intermediate conversions to and from the optical and electrical domains, is highly desired for the direct interfacing of all-optical signal processors with high-speed optical digital communication systems and radio-over-fiber networks [7].

Motivated by the above reasons, over the past thirty years, many research groups have been working on all-optical microwave signal processing for a number of frequency- and time-domain applications, such as filtering, correlation, differentiation and Fourier transformation. The first work on fiber delay-line microwave signal processing can be traced back to the seminal paper of Wilner and Van de Heuvel, who noted that the low loss and high modulation bandwidth of optical fibers are ideal for broadband signal processing [8]. Following it, several experimental investigations on all-optical microwave signal processing using multimode fibers were performed during 1970s [9]-[10]. Between 1980 and 1990, an intensive theoretical and experimental research work using single-mode fiber (SMF) delay lines was carried by researchers at Stanford University [11]-[12]. With the advent of some key optical components, including optical amplifiers, variable couplers, high-speed modulators and electrooptic switches, more flexible structures employing these components have been put forth [13]-[31]. Moreover, the availability of fiber Bragg gratings (FBGs) [32]-[56] and arrayed waveguide gratings (AWGs) [57]-[60] has opened a new perspective toward the implementation of fully reconfigurable and tunable all-optical microwave signal processors.

Among all the configurations mentioned above, an electrooptic intensity modulator (EOIM) is mainly used to modulate a microwave signal on an optical carrier, which is partially due to the fact that intensity modulation is a mature technology widely used in optical digital communication systems based on on-off-keying (OOK) formats. After passing through a specific photonic circuit or system, the intensity-modulated optical signal is then fed to a photodiode (PD) which produces an electrical current that is proportional to the input light intensity (this is usually called direct detection, since the PD directly detects the intensity of the incident light); subsequently, the processed microwave signal is obtained at the output of the PD. However, since only the intensity of the optical signal can be manipulated which is positive,

limited functions can be achieved. For instances, it is known that delay-line filters with all-positive coefficients can only function as a lowpass filter; and in an incoherent optical CDMA only unipolar codes can be utilized, which results in large multiple-access interference and hence a small amount of users can access the network simultaneously. Most recently, a lot of research interests and efforts have been focused on the development of different techniques to achieve incoherent all-optical signal processing with bipolar operation capability [61]-[68].

On the other hand, electrooptic phase modulation has recently become a hot topic with the renaissance of the differential-phase-shift-keying (DPSK) technique [69]-[71], which stimulates a lot of interest in exploring the optical signal processing techniques based on optical phase modulation. From the point-of-view of optical spectrum, phase modulation is different from intensity modulation, in which, the two first-order optical sidebands are π out of phase while the two sidebands are in phase in intensity modulation (under small signal condition, only the two first-order sidebands are considered). When the phase-modulated optical carrier is applied to a PD, no microwave signal would be generated because the beating between the optical carrier and the upper first-order sideband will completely cancel the beating between the optical carrier and the lower first-order sideband. Although a coherence detection scheme can be used to detect phase modulated signal, it needs a local oscillator light with high phase stability, which makes the system complicated and costly. To incorporate with the simple direct detection scheme, proper schemes to perform phase modulation to intensity modulation (PM-IM) conversion are thus essential. Meanwhile, all-optical signal processing based on electrooptic phase modulation are required to have the capability that achieves desired processing functions and the PM-IM conversions simultaneously, without adding extra photonic components or increasing the system complexity.

1.2 Major contributions

Motivated by these objectives mentioned in Sec. 1.1, we perform a comprehensive study on optical phase modulation and its applications for all-optical signal processing. To the best of our knowledge, we are the first research group in the world who introduce the optical phase modulation to all-optical microwave signal processing. The major contributions of this work are listed as follows.

(1) Two different methods to realize PM-IM conversion are proposed and demonstrated. In the first approach, the use of chromatic dispersion induced by a dispersive device, such as a length of dispersive fiber or a linearly-chirped FBG (LCFBG), to alter the phase relationships among the sidebands and the optical carrier of a phase-modulated optical signal to realize PM-IM conversion is investigated. In the second approach, the PM-IM conversion is realized based on optical frequency discrimination implemented using an optical filter, which can be a fiber-based Sagnac-loop filter or a uniform FBG (UFBG). The proposed PM-IM conversions present some interesting features. First, the frequency response of the PM-IM conversions has a notch at dc, which eliminates the baseband resonance and can be directly applied for highpass microwave filtering. Second, the PM-IM conversion based on frequency discrimination can generate microwave signals that are out of phase by using dispersive devices with opposite dispersions or optical bandpass filters with opposite frequency response slopes. This feature is highly desirable since it provides the possibility to implement bipolar operations, and eventually achieve more complex signal processing functionalities with flexible structures.

(2) Based on the PM-IM conversions, three different architectures for all-optical microwave bandpass filtering are proposed and demonstrated. In the first structure, bandpass filtering is directly obtained by applying chromatic dispersion based PM-IM conversion. In the second approach, all-optical microwave bandpass filtering with multiple taps is achieved by emerging the PM-IM conversion into a laser-array-based photonic delay-line structure. Some important aspects of the filter performance, including the mainlobe to sidelobe suppression ratio, the reconfigurability, tunability, and the dynamic range, are also discussed. In the third approach, a novel method to realize negative filter coefficients is proposed and demonstrated.

(3) For the first time, an optical phase modulation based all-optical signal processor that can perform both microwave mixing and bandpass filtering simultaneously in a radio-over-fiber link is proposed and presented. First, a two-tone approach to performing an up-conversion of a microwave signal from 3 GHz to 11.8 GHz in an SMF link is demonstrated. Then, as a continuation of the two-tone approach, subcarrier frequency up-conversion and filtering with a digital baseband signal on the subcarrier is investigated and experimentally demonstrated.

(4) By using the frequency discriminator based PM-IM conversion, a novel approach to implementing unipolar-bipolar phase-time encoding/decoding in optical CDMA networks is proposed. Two FBG arrays can be employed to perform encoding/decoding and the proposed scheme is equivalent to a sequence inversion keyed (SIK) direct-sequence CDMA, which can provide an improved performance compared to that of a conventional incoherent scheme using optical orthogonal codes.

(5) UWB signal distribution over optical fiber, or UWB-over-fiber, has been considered a promising solution to extend the coverage of UWB wireless communications. Based on optical phase modulation, two approaches to generating UWB pulse signals in the optical domain are proposed and experimentally demonstrated. Implementation of UWB pulse polarity and pulse shape modulation by use of these approaches is also discussed, which provides the potential for fully exploiting the advantages aroused by UWB-over-fiber networks.

1.3 Organization of this thesis

The thesis consists of six chapters. In Chapter 1, a brief review of the background of all-optical microwave signal processing is first presented, and then the motivations and major contributions of this research are summarized. In Chapter 2, a theoretical study of the electrooptic phase modulation and its comparison to intensity modulation is presented. Two methods to convert phase-modulated signal to intensity-modulated signal are discussed in this Chapter. Based on the proposed PM-IM conversions, three approaches to achieving equivalent microwave bandpass filtering and microwave filtering with negative coefficients are presented in Chapter 3. In Chapter 4, an approach to performing simultaneously all-optical microwave mixing (subcarrier frequency conversion) and bandpass filtering in a radio-over-fiber link is investigated. In Chapter 5, FBG-based frequency discrimination is studied. Its applications for unipolar-encoding/bipolar-decoding in optical CDMA and UWB pulse signal generation are discussed. Finally, a conclusion is drawn in Chapter 6.

The term microwave will be used throughout this thesis to designate RF, microwave, or millimeter-wave.

References

[1] P. M. Grant and R. S. Withers, "Recent advances in analog signal processing," IEEE Trans. Aerospace and Electron. System, vol. 26, no. 5, pp. 818-849, Sept. 1990.

[2] K. P. Jackson, S. A. Newton, B. Moslehi, M. Tur, C. C. Culter, J. W. Goodman, and H. J. Shaw, "Optical fiber delay-line signal processing," IEEE Trans. Microwave Theory Tech., vol. 33, no. 3, pp. 193-210, Mar. 1985.

[3] J. L. Horner, *Optical Signal Processing*, Academic Press, 1987.

[4] J. Capmany, B. Ortega, D. Pastor, and S. Sales, "Discrete-time optical processing of microwave signals," J. Lightwave Technol., vol. 23, no. 2, pp. 702-723, Feb. 2005.

[5] A. Oppenheim, R. Schaffer, and J. R. Buck, *Discrete-time signal processing*, Upper Saddle River, NJ: Prentice-Hall, 1988.

[6] J. G. Proakis and D. G. Manolakis, *Digital signal processing: principles, algorithms and applications*, Upper Saddle River, NJ: Prentice-Hall, 1996.

[7] A. J. Seeds, "Microwave photonics," IEEE Trans. Microwave Theory Tech., vol. 50, no. 3, pp. 877-887, Mar. 2002.

[8] K. Wilner and A. P. Van den Heuvel, "Fiber-optic delay lines for microwave signal processing," Proc. IEEE, vol. 64, no. 5, pp. 805-807, May 1976.

[9] C. Chang, J. A. Cassaboom, and H. F. Taylor, "Fiber optic delay line devices for RF signal processing," Electron. Lett., vol. 13, pp. 678-680, Jul. 1977.

[10] H. F. Taylor, "Fiber and integrated optical devices for signal processing," Proc. SPIE, vol. 176, pp. 17-27, Mar. 1979.

[11] B. Moslehi, J. W. Goodman, M. Tur, and H. J. Shaw, "Fiber-optic lattice signal processing," Proc. IEEE., vol. 72, no. 7, pp. 909-930, Jul. 1984.

[12] K. Jackson, S. Newton, B. Moslehi, M. Tur, C. Culter, J. Goodman, and H. J. Shaw, "Optical fiber delay-line signal processing," IEEE Trans. Microwave Theory Tech., vol. 33, no. 3, pp. 193-204, Mar. 1985.

[13] B. Moslehi, "Fiber-optic filters employing optical amplifiers to provide design flexibility," Electron. Lett., vol. 28, no. 3, pp. 226-228, Jan. 1992.

[14] M. C. Vázquez, B. Vizoso, M. López-Amo, and M. A. Muriel, "Single and double amplified recirculating delay lines as fiber-optic filters," Electron. Lett., vol. 28, no. 11, pp. 1017-1019, May 1992.

[15] J. Capmany and J. Cascón, "Optical programmable transversal filters using fiber amplifiers," Electron. Lett., vol. 28, no. 13, pp. 1245-1246, Jun. 1992.

[16] J. Capmany and J. Cascón, "Direct form I fiber-optic discrete-time signal processors using optical amplifiers and embedded Mach-Zehnder structures," IEEE Photon. Technol. Lett., vol. 32, no. 3, pp. 842–844, Mar. 1993.

[17] J. Capmany and J. Cascón, "Discrete-time fiber-optic signal processors using optical amplifiers," J. Lightwave Technol., vol. 12, no. 1, pp. 106–117, Jan. 1994.

[18] M. C. Vazquez, R. Civera, M. López-Amo, and M. A. Muriel, "Analysis of double-parallel amplified recirculating optical delay lines," Appl. Opt., vol. 33, no. 6, pp. 1015–1021, Feb. 1994.

[19] B. Vizoso, C. Vazquez, R. Civera, M. Lopez-Amo, and M. A. Muriel, "Amplified fiber-optic recirculating delay lines," J. Lightwave Technol., vol.12, no. 2, pp. 294–305, Feb. 1994.

[20] V. Polo, F. Ramos, J. Marti, D.Wake, and D. Moodie, "Synthesis of photonic microwave filters based on external optical modulators and wideband chirped fiber gratings," J. Lightwave Technol., vol. 18, no. 2, pp. 213–220, Feb. 2000.

[21] J. Capmany, "Amplified double recirculating delay line using a 3x3 coupler," J. Lightwave Technol., vol.12, no. 7, pp. 1136–1143, Jul. 1994.

[22] A. Ho Quoc and S. Tedjini, "Experimental investigation on the optical unbalanced Mach-Zehnder interferometers as microwave filters," IEEE Microwave Guided Wave Lett., vol. 4, no.6, pp. 183–185, Jun. 1994.

[23] D. Pastor, S. Sales, J. Capmany, J. Martí, and J. Cascón, "Amplified double-coupler fiber-optic delay line filter," IEEE Photon. Technol. Lett., vol. 7, no. 1, pp. 75–77, Jan. 1995.

[24] E. Heyde and R. A. Minasian, "A solution to the synthesis problem of recirculating delay line filters," IEEE Photon. Technol. Lett., vol. 6, no. 7, pp. 833–835, Jul. 1995.

[25] S. Sales, J. Capmany, J. Martí, and D. Pastor, "Novel and significant results on the nonrecirculating delay line with a fiber loop," IEEE Photon. Technol. Lett., vol.7, no. 12, pp. 1439–1440, Dec. 1995.

[26] S. Sales, J. Capmany, J. Martí, and D. Pastor, "Solutions to the synthesis problem of optical delay line filters," Opt. Lett., vol. 20, no.23, pp. 2438–2440, Dec. 1995.

[27] N. You and R. A. Minasian, "A novel tunable microwave optical notch filter," IEEE Trans. Microwave Theory Tech., vol. 49, no. 10, pp. 2002–2005, Oct. 2001.

[28] D. Norton, S. Johns, C. Keefer, and R. Soref, "Tunable microwave filtering using high dispersion fiber time delays," IEEE Photon. Technol. Lett., vol. 6, no.7, pp. 831–832, Jul. 1994.

[29] M. Y. Frankel and R. D. Esman, "Fiber-optic tunable microwave transversal filter," IEEE Photon. Technol. Lett., vol. 7, no. 2, pp. 191–193, Feb. 1995.

[30] J. Capmany, D. Pastor, and B. Ortega, "Fiber-optic microwave and millimeter-wave filter with high density sampling and very high sidelobe suppression using subnanometer optical spectrum slicing," Electron. Lett., vol. 35, no. 6, pp. 494–496, Mar. 1999.

[31] J. Capmany, J. Cascón, J. L. Marín, S. Sales, D. Pastor, and J. Martí, "Synthesis of fiber-optic delay line filters," J. Lightwave Technol., vol. 13, no. 10, pp. 2003–2012, Oct. 1995.

[32] G. A. Ball, W. H. Glenn, and W. W. Morey, "Programmable fiber optic delay line," IEEE Photon. Technol. Lett., vol. 6, no. 6, pp. 741–743, Jun. 1994.

[33] D. B. Hunter and R. A. Minasian, "Reflectivity tapped fiber-optic transversal filter using in-fiber Bragg gratings," Electron Lett., vol. 31, no. 12, pp. 1010–1012, Jun. 1995.

[34] D. B. Hunter and R. A. Minasian, and P. A. Krug, "Tunable transversal filter based on chirped gratings," Electron. Lett., vol. 31, no. 25, pp. 2205–2207, Dec. 1995.

[35] D. B. Hunter and R. A. Minasian, "Microwave optical filters using in-fiber Bragg grating arrays," IEEE Microwave Guided Wave Lett., vol. 6, no. 2, pp. 103–105, Feb. 1996.

[36] D. B. Hunter and R. A. Minasian, "Photonic signal processing of microwave signals using active-fiber Bragg-grating-pair structure," IEEE Trans. Microwave Theory Tech., vol. 8, no. 8, pp. 1463–1466, Aug. 1997.

[37] W. Zhang, J. A. R. Williams, L. A. Everall, and I. Bennion, "Fiber-optic radio frequency notch filter with linear and continuous tuning by using a chirped fiber grating," Electron. Lett., vol. 34, no. 18, pp. 1770–1772, Sept. 1998.

[38] D. Pastor and J. Capmany, "Fiber optic tunable transversal filter using laser array and linearly chirped fiber grating," Electron. Lett., vol. 34, no. 17, pp. 1684–1685, Aug. 1998.

[39] W. Zhang and J. A. R. Williams, "Fiber optic bandpass transversal filter employing fiber grating arrays," Electron. Lett., vol. 35, no.12, pp. 1010–1011, Jun. 1999.

[40] N. You and R. A. Minasian, "A novel high-Q optical microwave processor using hybrid delay line filters," IEEE Trans. Microwave Theory Tech., vol. 47, no. 7, pp. 1304–1308, Jul. 1999.

[41] D. B. Hunter and R. A. Minasian, "Tunable microwave fiber-optic bandpass filters," IEEE Photon. Technol. Lett, vol. 11, no. 7, pp. 874–876, Jul. 1999.

[42] J. Capmany, D. Pastor, and B. Ortega, "New and flexible fiber-optic delay line filters using chirped Bragg gratings and laser arrays," IEEE Trans. Microwave Theory Tech., vol. 47, no. 7, pp. 1321–1327, Jul. 1999.

[43] N. You and R. A. Minasian, "Synthesis of WDM grating-based optical microwave filter with arbitrary impulse response," in Int. Top. Meeting on Microwave Photon. MWP '99, vol. 1, pp. 223–226, Nov. 1999.

[44] D. Pastor, J. Capmany, and B. Ortega, "Experimental demonstration of parallel fiber-optic-based RF filtering using WDM techniques," IEEE Photon. Technol. Lett., vol. 12, no. 1, pp. 77–79, Jan. 2000.

[45] G. Yu, W. Zhang, and J. A. R.Williams, "High-performance microwave transversal filter using fiber Bragg grating arrays," IEEE Photon. Technol. Lett., vol. 12, no. 9, pp. 1183–1185, Sept. 2000.

[46] W. Zhang, G. Yu, and J. A. R. Williams, "Tap multiplexed fiber grating-based optical transversal filter," Electron. Lett., vol. 36, no. 20, pp. 1708–1710, Sept. 2000.

[47] W. Zhang, J. A. R. Williams, and I. Bennion, "Optical fiber recirculating delay line incorporating a fiber grating array," IEEE Microwave Wireless Compon. Lett., vol. 11, no. 5, pp. 217–219, May 2001.

[48] W. Zhang, J. A. R. Williams, and I. Bennion, "Polarization synthesized optical transversal filter employing high birefringence fiber gratings," IEEE Photon. Technol. Lett., vol. 13, no. 5, pp. 523–525, May 2001.

[49] D. Pastor, J. Capmany, and B. Ortega, "Broad-band tunable microwave transversal notch filter based on tunable uniform fiber Bragg gratings as slicing filters," IEEE Photon. Technol. Lett., vol. 13, no. 7, pp. 726–728, Jul. 2001.

[50] R. A. Minasian, K. E. Alameh, and E. H. W. Chan, "Photonics-based interference mitigation filters," IEEE Trans. Microwave Theory Tech., vol. 49, no. 10, pp. 1894–1899, Oct. 2001.

[51] D. Pastor, J. Capmany, S. Sales, P. Munoz, and B. Ortega, "Reconfigurable fiber-optic-based RF filters using current injection in multimode lasers," IEEE Photon. Technol. Lett., vol. 13, no. 11, pp. 1224–1226, Nov. 2001.

[52] J. Mora, B. Ortega, J. Capmany, J. L. Cruz, M. V. Andres, D. Pastor, and S. Sales, "Automatic tunable and reconfigurable fiber optic microwave filters based on a broadband optical source sliced by uniform fiber Bragg gratings," Opt. Express, vol. 10, no. 22, pp. 1291–1298, Nov. 2002.

[53] E. H. W. Chan, K. E. Alameh, and R. A. Minasian, "Photonic bandpass filter with high skirt selectivity and stopband attenuation," J. Lightwave Technol., vol. 20, no. 11, pp. 1962–1967, Nov. 2002.

[54] J. Mora, B. Ortega, M. V. Andres, J. Capmany, D. Pastor, J. L. Cruz, and S. Sales, "Tunable chirped fiber Bragg grating device controlled by variable magnetic fields," Electron. Lett., vol. 38, no.3, pp. 118–119, Jan. 2002.

[55] F. Zeng, J. P. Yao, and S. Mihailov, "Genetic algorithm for fiber Bragg grating based all-optical microwave filter synthesis," Opt. Eng., vol. 42, no. 8, pp. 2250-2256, Aug. 2003.

[56] F. Zeng and J. P. Yao, "All-optical microwave filters using uniform fiber Bragg gratings with identical reflectivities," J. Lightwave Technol., vol. 23, no. 3, pp. 1410-1418, Mar. 2005.

[57] S. Yegnanarayanan, P. D. Trinh, and B. Jalali, "Recirculating photonic filter: a wavelength-selective time delay for phased-array antennas and wavelength code-division multiple access," Opt. Lett., vol. 21, no. 10, pp. 740–742, May 1996.

[58] F. Coppinger, S. Yegnanarayanan, P. D. Trinh, B. Jalali, and I. L. Newberg, "Nonrecursive photonic filter using wavelength-selective true time delay," IEEE Photon. Technol. Lett., vol. 8, no. 9, pp. 1214-1216, Sept. 1996.

[59] F. Coppinger, S. Yegnanarayanan, P. D. Trinh, and B. Jalali, "Continuously tunable photonic radio-frequency notch filter," IEEE Photon. Technol. Lett, vol. 9, no. 3, pp. 339–341, Mar. 1997.

[60] D. Pastor, B. Ortega, J. Capmany, S. Sales, A. Martinez, and P. Munoz, "Flexible and tunable microwave filters based on arrayed waveguide gratings," in Proc. IEEE Int. Topical Meeting on Microwave Photon., pp. 189–192, Nov. 2002.

[61] S. Sales, J. Capmany, J. Martí, and D. Pastor, "Experimental demonstration of fiber-optic delay line filters with negative coefficients," Electron. Lett, vol. 31, no. 13, pp. 1095-1096, Jun. 1995.

[62] F. Coppinger, S. Yegnanarayanan, P. D. Trinh, and B. Jalali, "All-optical RF filter using amplitude inversion in a semiconductor optical amplifier," IEEE Trans. Microwave Theory Tech., vol. 45, no. 8, pp. 1473-1477, Aug. 1997.

[63] X. Wang and K. T. Chan, "Tunable all-optical incoherent bipolar delay-line filter using injection-locked Fabry-Perot laser and fiber Bragg gratings," Electron. Lett., vol. 36, no. 24, pp. 2001-2002, Dec. 2000.

[64] S. Li, K. S. Chiang, W. A. Gambling, Y. Liu, L. Zhang, and I. Bennion, "A novel tunable all-optical incoherent negative-tap fiber-optic transversal filter based on a DFB laser diode and fiber Bragg gratings," IEEE Photon. Technol. Lett., vol. 12, no. 9, pp. 1207-1209, Sept. 2000.

[65] J. Mora, B. Ortega, M. V. Andrés, J. Capmany, J. L. Cruz, D. Pastor, and S. Sales, "Tunable all-optical negative multi-tap microwave filters based on uniform fiber Bragg gratings," Opt. Lett., vol. 28, no. 15, pp. 1308-1310, 2003.

[66] J. Capmany, D. Pastor, A. Martinez, B. Ortega, and S. Sales, "Microwave photonic filters with negative coefficients based on phase inversion in an electro-optic modulator," Opt. Lett., vol. 28, no. 16, pp. 1415-1417, 2003.

[67] D. Pastor, J. Capmany, B. Ortega, A. Martinez, L. Pierno, and M. Varasi, "Reconfigurable RF-photonic filter with negative coefficients and flat top resonances using phase inversion in a newly designed 2 × 1 integrated Mach-Zehnder modulator," IEEE Photon. Technol. Lett., vol. 16, no. 9, pp.216-2128, Sept. 2004.

[68] D. B. Hunter, "Incoherent bipolar tap microwave photonic filter based on a balanced bridge electro-optic modulator," Electron. Lett., vol. 40, no. 14, pp. 856-857, July 2004.

[69] E. Ciaramella, G. Contestabile, and A. D'Errico, "A novel scheme to detect optical DPSK signals," IEEE Photon. Technol. Lett, vol. 16, no. 9, pp. 2138–2140, 2004.

[70] A. H. Gnauck and P. J. Winzer, "Optical phase-shift-keyed transmission," J. Lightwave Technol., vol. 23, no. 1, pp. 115-130, Jan. 2005.

[71] I. Lyubomirsky and C. C. Chien, "DPSK demodulator based on optical discriminator filter," IEEE Photon. Technol. Lett, vol. 17, no. 2, pp. 492–494, 2005.

CHAPTER 2

THEORETICAL BASES

Electrooptic phase modulation and its conversion to intensity modulation are the bases of the research for all-optical microwave signal processing. In this Chapter, a review of the mathematical expressions of an EOPM and its implementation is presented. Then, two methods to convert a phase-modulated optical signal to an intensity-modulated signal by use of a dispersive device and an optical bandpass filter are presented.

2.1 Electrooptic phase modulation

In this section, frequency domain analysis of a phase-modulated optical signal is presented. Operation principle and general structure of a Lithium Niobate ($LiNbO_3$) crystal based EOPM are introduced. A comparison of a phase-modulated signal and an intensity-modulated signal in terms of their spectra and detection methods is carried out.

2.1.1 Mathematical expression

The optical field of a phase-modulated optical carrier $e_{PM}(t)$ can be expressed as

$$e_{PM}(t) = e_o \cdot \cos[\omega_o t + \Delta\varphi(t)], \tag{2.1}$$

where e_o and ω_o are the amplitude and angular frequency of the optical carrier, and $\Delta\varphi(t)$ is the modulating signal induced phase change. Without loss of generality, $\Delta\varphi(t)$ can be expressed as

$$\Delta\varphi(t) = \beta_{PM} \cdot f(t), \tag{2.2}$$

where β_{PM} is the phase modulation index, defined as the phase change of the carrier when unit voltage is applied (rad/volt); and $f(t)$ represents the modulating electrical signal.

A. A general approximation

If the amplitude of $f(t)$ is small enough, we have the following approximations

$$\begin{cases} \cos\Delta\varphi(t) = \cos[\beta_{PM} \cdot f(t)] \approx 1 \\ \sin\Delta\varphi(t) = \sin[\beta_{PM} \cdot f(t)] \approx \beta_{PM} \cdot f(t). \end{cases} \tag{2.3}$$

Then, Eq. (2.1) can be written as

$$\begin{aligned} e_{PM}(t) &= e_o\{\cos\omega_o t \cdot \cos[\beta_{PM} \cdot f(t)] - \sin\omega_o t \cdot \sin[\beta_{PM} \cdot f(t)]\} \\ &\approx e_o[\cos\omega_o t - \beta_{PM} \cdot f(t) \cdot \sin\omega_o t]. \end{aligned} \tag{2.4}$$

Applying Fourier transform to both sides of Eq. (2.4) we obtain

$$E_{PM}(\omega) \approx \pi e_o[\delta(\omega-\omega_o) + \delta(\omega+\omega_o)] + \frac{j}{2} e_o \beta_{PM}[F(\omega-\omega_o) - F(\omega+\omega_o)], \tag{2.5}$$

where $E_{PM}(\omega)$ and $F(\omega)$ represent the Fourier transforms of $e_{PM}(t)$ and $f(t)$ respectively. Observing Eq. (2.5), we can conclude that the spectral band of $F(\omega-\omega_o)$ has a $\pi/2$ phase shift with respect to $\delta(\omega-\omega_o)$ while $F(\omega+\omega_o)$ has a - $\pi/2$ phase shift with respect to $\delta(\omega+\omega_o)$, which indicates that $F(\omega-\omega_o)$ and $F(\omega+\omega_o)$ are out of phase.

B. Small-signal and one-tone modulating

To further understand Eq. (2.5) and to have an accurate description of the relationship among all the frequency components of a phase modulated signal, we assume $f(t)$ is a single-frequency sinusoidal signal with zero initial phase,

$$f(t) = V_e \cdot \cos\omega_m t, \tag{2.6}$$

where V_e and ω_m are the amplitude and angular frequency of the modulating signal respectively.

Then Eq. (2.1) can be expanded in terms of Bessel functions of the first kind without loss of generality,

$$e_{PM}(t) = e_o \cdot \sum_{n=-\infty}^{+\infty} J_n(\beta_{PM} V_e) \cdot \cos[(\omega_o + n\omega_m)t + \frac{1}{2} n\pi], \tag{2.7}$$

where $J(.)$ denotes the nth-order Bessel function of the first kind. To simplify, the argument $(\beta_{PM} V_e)$ will be omitted in the remainder of the text. From Eq. (2.7), we can see that the phase modulation generates a series of sidebands with amplitude coefficients determined by the Bessel functions. The approximation condition in Eq. (2.3) can be quantified by calculating the coefficients in Eq. (2.7), which leads to the conclusion that for small signal modulation, only the first-order upper and lower sidebands need to be considered and the higher-order sidebands can be ignored. The intensities of the carrier and the sidebands, plotted as a function of $\beta_{PM} V_e$ in Fig. 2.1, are proportional to the square of the coefficients of the corresponding terms in Eq. (2.7).

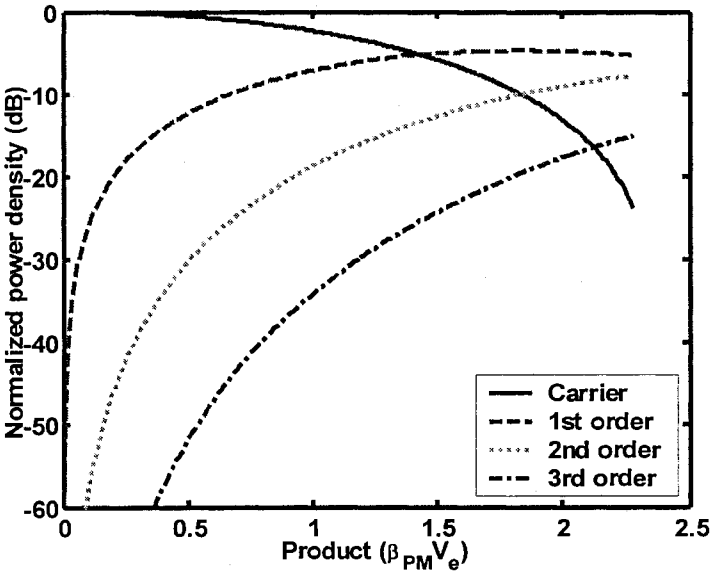

Fig. 2.1 Normalized intensities of the carrier and the sidebands as a function of $\beta_{PM} V_e$.

Eq. (2.7) can be further simplified as

$$e_{PM}(t) = e_o \cdot \{J_o \cos \omega_o t + J_1 \cos[(\omega_o + \omega_m)t + \frac{\pi}{2}] + J_{-1} \cos[(\omega_o - \omega_m)t - \frac{\pi}{2}]. \tag{2.8}$$

For Bessel functions, we have

$$J_n = -J_{-n}, \text{ when } n \text{ is odd.} \tag{2.9}$$

Applying the Fourier transform to Eq. (2.8), we have

$$E_{PM}(\omega) \approx \pi\, e_o J_o[\delta(\omega-\omega_o)+\delta(\omega+\omega_o)] - j\pi\, e_o J_1[\delta(\omega+\omega_o+\omega_m)-\delta(\omega-\omega_o-\omega_m)] - j\pi\, e_o J_1[\delta(\omega+\omega_o-\omega_m)-\delta(\omega-\omega_o+\omega_m)]. \quad (2.10)$$

Fig. 2.2 illustrates the spectra of the modulating electrical signal and the corresponding optical phase-modulated signal (by Eq. (2.10)). From the plots, it is interesting to note that the lower sideband and upper sideband are exactly out of phase.

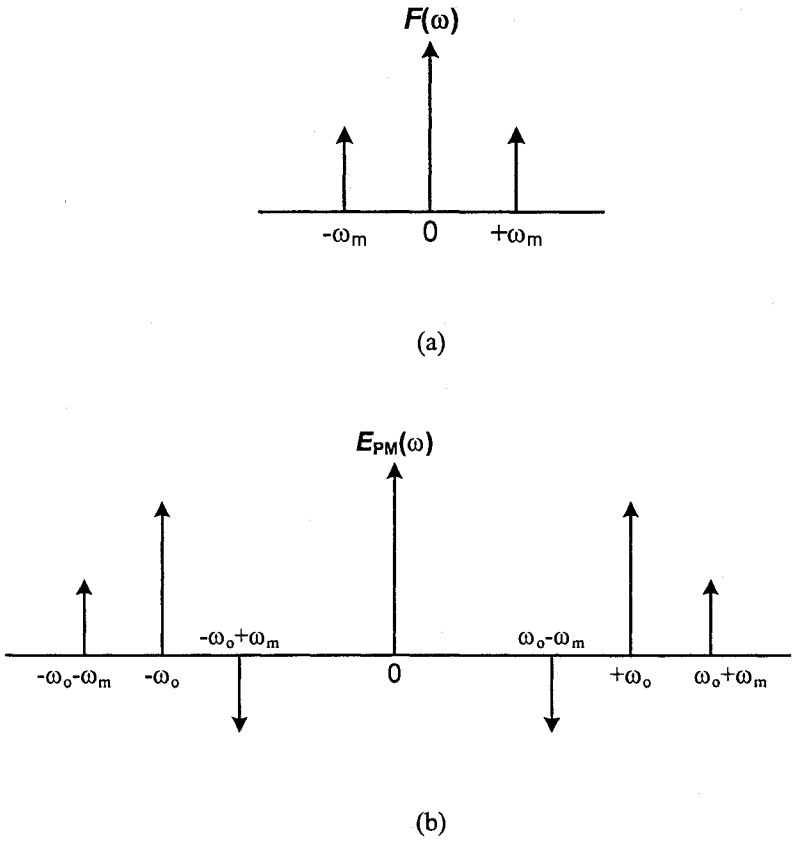

Fig. 2.2 Schematic diagram showing the spectra of (a) the single-frequency sinusoidal modulating signal, and (b) the optical phase-modulated signal.

C. Large-signal and two-tone modulating

If $\beta_{PM}V_e$ is relatively large and the power levels of the higher-order sidebands are comparable to or even higher than those of the carrier and the first-order sidebands, the modulation is no

longer linear, which is the basis to achieving microwave frequency synthesis by upconverting a low frequency tone (ω_m) to its higher-order harmonics ($2\omega_m$, $3\omega_m$, ...).

In addition, if the input RF signal contains two frequency components ω_{m1} and ω_{m2}, the phase modulated optical field will be expressed as

$$E(t) = \sum_{n=-\infty}^{\infty}\sum_{k=-\infty}^{\infty} J_n(m_p V_1)\cdot J_k(m_p V_2)\cdot\cos[(\omega_c + n\omega_{m1} + k\omega_{m2})t + \frac{1}{2}n\pi + \frac{1}{2}k\pi], \qquad (2.11)$$

where V_1 and V_2 represent the amplitudes of the modulating signal at frequencies ω_{m1} and ω_{m2}, respectively; n and k are integers representing the orders of the harmonics. From Eq. (2.11), the sidebands having frequency variations from the carrier of $\pm\omega_{m1}$, $\pm\omega_{m2}$, $\pm 2\omega_{m1}$, $\pm 2\omega_{m2}$,..., and $\omega_{m1} \pm \omega_{m2}$, $2\omega_{m1} \pm \omega_{m2}$, $\omega_{m1} \pm 2\omega_{m2}$,... are observed, which indicates that inter-modulation products at $|\omega_{m1} \pm \omega_{m2}|$, $|2\omega_{m1} \pm \omega_{m2}|$, and $|\omega_{m1} \pm 2\omega_{m2}|$,..., may also be obtained if proper PM-IM conversion and detection schemes are applied to this phase-modulated optical signal. This is actually the basic operation principle of all-optical microwave mixing.

2.1.2 Physical implementation

Optical phase modulation can be realized based on electrooptic effect, i.e., an external electrical field applied to an electrooptic material would lead to a change to the refractive index in that material. When a light beam propagates through this material, its phase will be changed by the applied electrical field. A Lithium Niobate ($LiNbO_3$) crystal is one of the materials with such electrooptic effect. Throughout this research work, the phase modulation is implemented using a $LiNbO_3$ straight-line EOPM. The structure of an EOPM is shown in Fig. 2.3.

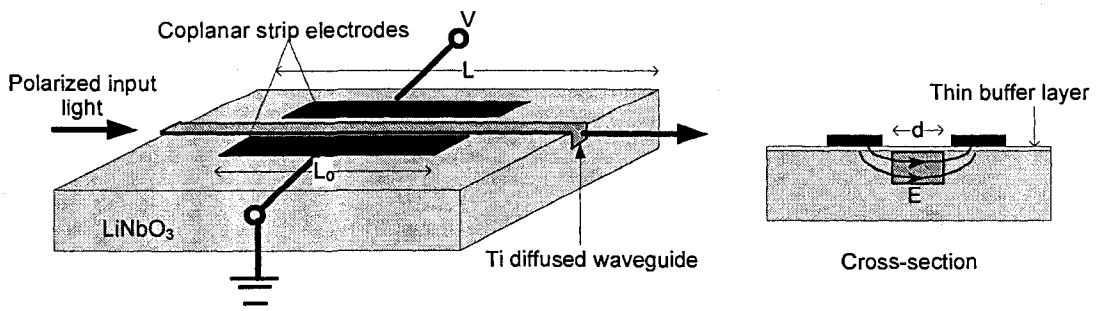

Fig. 2.3 Block diagram of a $LiNbO_3$ EOPM.

As can be seen that when the modulating signal is applied to the EOPM via two electrodes, a refractive index change is thus resulted,

$$\delta_n(E) = -\frac{1}{2} r n^3 E, \tag{2.12}$$

where r is the electrooptic effect coefficient, n is the effective refractive index of the crystal, and E is the applied electrical field which is given by

$$E = -V_e / d, \tag{2.13}$$

where V_e is the amplitude of the modulating voltage and d is the distance between the two faces of the crystal across which the electrical field is applied, as shown in Fig. 2.3.

The phase shift φ introduced to the lightwave propagating through the EOPM is given by

$$\varphi = \underbrace{\frac{2\pi n L}{\lambda_o}}_{\varphi_0} + \underbrace{\frac{2\pi \delta_n(E) L_0}{\lambda_o}}_{\Delta\varphi}, \tag{2.14}$$

where L is the total length of the EOPM, L_0 is the length of the $LiNbO_3$ crystal to which the electrical field E is applied, λ_o is the wavelength of the incident light, φ_0 is the phase shift of the light after propagating through the EOPM of length L, and $\Delta\varphi$ is the phase shift induced by the refractive index change within the length L_0. The phase shift φ_0 is constant, which is independent of the modulating signal and can be ignored. By substituting Eqs. (2.12), (2.13), and (2.6) into Eq. (2.14), the modulating signal induced phase change is

$$\Delta\varphi = \frac{\pi r n^3 L_o \cdot f(t)}{d\lambda_o}. \tag{2.15}$$

An important parameter of an EOPM is the half-wave voltage V_π, given by

$$V_\pi = \frac{d}{L_0} \cdot \frac{\lambda_o}{r n^3}. \tag{2.16}$$

It is the voltage by which $\Delta\varphi$ equals to π. Under single-frequency sinusoidal signal modulation, Eq. (2.15) can be rewritten as

$$\Delta\varphi = \pi \cdot \frac{V_e}{V_\pi} \cdot \cos(\omega_m t). \tag{2.17}$$

Comparing Eq. (2.17) and Eq. (2.2), we obtain the relationship between β_{PM} (the phase modulation index given in the theoretical analysis) and V_π (the parameter given with a specific EOPM),

$$\beta_{PM} = \frac{\pi}{V_\pi} = \frac{\pi r n^3 L_o}{d\lambda_o}. \tag{2.18}$$

Being different from a phase modulator, an intensity modulator is implemented by putting an EOPM in one arm of an MZI, as shown in Fig. 2.4.

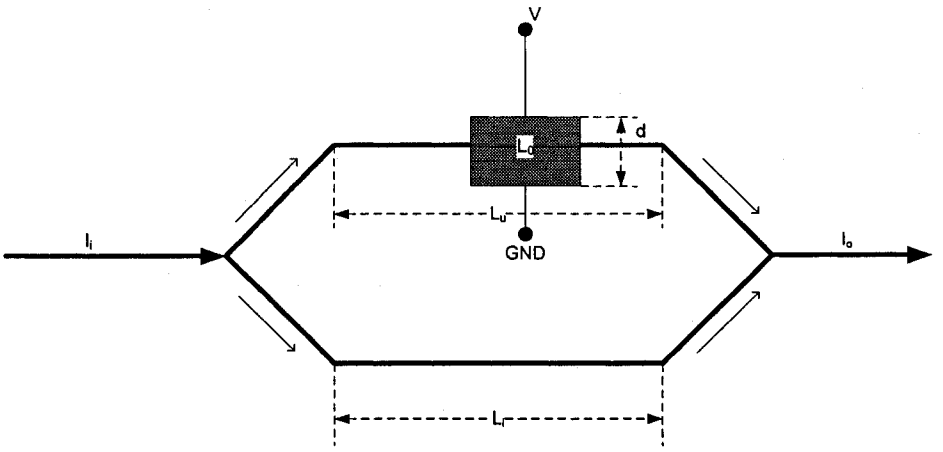

Fig. 2.4 Block diagram of a Mach-Zehnder interferometer (MZI) based intensity modulator.

Assuming that the EOPM is located at the upper branch of the MZI, based on Eq. (2.14), the light propagating through the upper arm will experience a phase shift φ_u given by

$$\varphi_u = \underbrace{\frac{2\pi n L_u}{\lambda_o}}_{\varphi_{uo}} + \underbrace{\pi \cdot \frac{V(t)}{V_\pi}}_{\Delta\varphi_u}, \tag{2.19}$$

where L_u is the total length of the upper arm, φ_{uo} is the phase shift of the light after propagating along the upper arm, and $\Delta\varphi_u$ is the phase change induced by modulating signal.

The phase shift φ_l induced by the lower arm is

$$\varphi_l = \frac{2\pi n L_l}{\lambda_o}, \tag{2.20}$$

where L_l is the total length of the lower arm.

If the input light is distributed equally into the two arms of the MZI, the electrical field $e_{MZI}(t)$ at the output of the modulator is

$$\begin{aligned} e_{MZI}(t) &= \frac{1}{2} e_o \cos(\omega_o t + \varphi_u) + \frac{1}{2} e_o \cos(\omega_o t + \varphi_l) \\ &= e_o \cos(\omega_o t + \frac{\varphi_u + \varphi_l}{2}) \cos(\frac{\varphi_u - \varphi_l}{2}) \\ &= e_o \cos(\omega_o t + \frac{\varphi_u + \varphi_l}{2}) \cos[\frac{\pi n}{\lambda_o}(L_u - L_l) + \frac{\pi}{2} \cdot \frac{f(t)}{V_\pi}]. \end{aligned} \tag{2.21}$$

The transmittance of the MZI modulator $T(V)$ defined as the ratio between the output optical intensity and input optical intensity is given by

$$T(V) = \cos^2[\frac{\pi\, n(L_u - L_l)}{\lambda_o} + \frac{\pi}{2} \cdot \frac{f(t)}{V_\pi}]. \tag{2.22}$$

By properly choosing the length difference (L_u-L_l) between the upper arm and the lower arm of the MZI, which can be fine-adjusted by tuning the dc voltage applied on the EOPM at the upper branch, the first term at the right side of Eq. (2.22) can be set as $\pi/2$. Consequently Eq. (2.22) is written as

$$T(V) = \frac{1}{2}\{1 - \sin[\pi \cdot \frac{f(t)}{V_\pi}]\}. \tag{2.23}$$

Again, under small signal condition, Eq. (2.23) can be approximated as

$$T(V) = \frac{1}{2}[1 - \frac{\pi}{V_\pi} \cdot f(t)], \tag{2.24}$$

where π / V_π is the intensity modulation index, defined as β_{IM}. Then we can conclude that the MZI modulator acts as a linear intensity modulator when it is operating at the linear region of a sinusoidal function under small signal condition.

2.1.3 Comparison with intensity modulation

In Sec. 2.1.1, the spectrum of a phase-modulated optical signal has been derived, in which the lower first-order sideband and the upper first-order sideband are out of phase. If this signal is directly applied to a PD, only a dc current would be generated. This can be easily understood because a PD is actually an envelope detector. For phase modulation, the envelope is a constant. Mathematically, the output current from a PD can be written as

$$i_{PD} = \Re \cdot \left\langle |e(t)|^2 \right\rangle, \tag{2.25}$$

where $\Re$ is the responsivity of the PD, and $\langle\ \rangle$ represents the ensemble average operation. Substituting Eq. (2.8) into Eq. (2.25), we can see that the beating between the optical carrier and the upper sideband will exactly cancel the beating between the optical carrier and the lower sideband; and eventually only a dc current is obtained.

In contrary, for the MZI-based intensity modulation, the modulating signal can be obtained directly at the output of the PD, which can also be explained by using the frequency domain analysis as follows.

The electrical field at the output of a MZI, as illustrated by Eq. (2.21), can be expanded in the form of Bessel functions as

$$\begin{aligned} e_{MZI}(t) = {} & e_o \cdot \cos(\omega_o t) \cdot \cos(\frac{\varphi_o}{2}) \cdot \{J_0 + 2\sum_{n=1}^{\infty} J_{2n} \cos[2n(\frac{\pi}{2} - \omega_m t)]\} \\ & - e_o \cdot \cos(\omega_o t) \cdot \sin(\frac{\varphi_o}{2}) \cdot \{2\sum_{n=1}^{\infty} J_{2n-1} \sin[(2n-1)(\frac{\pi}{2} - \omega_m t)]\}, \end{aligned} \tag{2.26}$$

where $\varphi_o \equiv \pi n(L_u - L_l)/\lambda_o$.

Assuming that the modulator is operating at its linear region, i.e., $\varphi_o = \pi/2$. Under small signal condition, only the first-order sidebands need to be considered. Then Eq. (2.26) can be re-written as

$$e_{MZI}(t) = \frac{\sqrt{2}}{2} e_o \{J_0 \cos(\omega_o t) - J_1 \cos(\omega_o + \omega_m)t - J_1 \cos(\omega_o - \omega_m)t\}. \tag{2.27}$$

Its spectrum is

$$\begin{aligned} E_{MZI}(\omega) = \frac{\sqrt{2}}{2} \pi \cdot e_o \{ & J_0 \cdot [\delta(\omega - \omega_o) + \delta(\omega + \omega_o)] \\ & - J_1 \cdot [\delta(\omega - \omega_o - \omega_e) - \delta(\omega + \omega_o + \omega_e)] \\ & - J_1 \cdot [\delta(\omega - \omega_o + \omega_e) - \delta(\omega + \omega_o - \omega_e)]\}. \end{aligned} \tag{2.28}$$

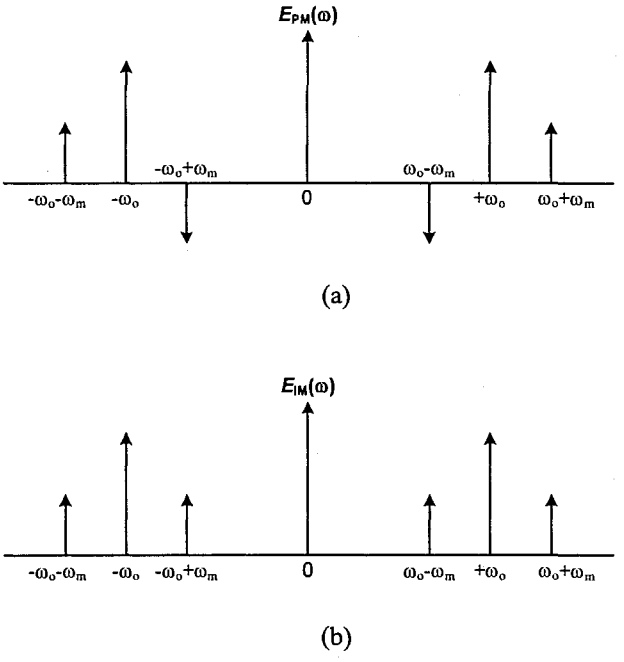

Fig. 2.5 Spectra of (a) a phase-modulated optical signal, and (b) an intensity-modulated signal.

Fig. 2.5(b) illustrates the spectrum of the intensity-modulated signal described in Eq. (2.28). For comparison, the spectrum of the phase-modulated signal is illustrated in Fig. 2.5(a). From Fig. 2.5(b) we can see that the lower sideband and upper sideband of an intensity-modulated signal

are exactly in phase, therefore the beating between the upper sideband and the carrier is also in phase with the beating between the lower sideband and the carrier. Consequently, photo current reflecting the modulating signal could be obtained.

2.2 PM-IM conversion

To recover the information carried by the optical phase, a coherent detection (heterodyne or homodyne) scheme can be used, in which the phase-modulated optical signal is mixed with a local oscillator light. However, the construction of a local oscillator light source with high frequency and phase stability is difficult at present. In addition, the temperature and mechanical vibrations in the transmission line will result in phase and polarization fluctuations of the transmitted light, which would appear as noise after photodetection. In this Section, two methods to convert the phase-modulated signal to intensity-modulated signal are presented. In the first method, chromatic dispersion induced by a dispersive device is applied to change the phase relationships of the two sidebands from out of phase to in phase. The second method, which is very similar to the detection of an optical phase-shift-keyed (PSK) signal, is to use an optical filter that acts as a frequency discriminator. This operation can be explained that the magnitude relationships among the sidebands and the carrier are changed, leading to the detection of the phase-modulated signal. After the PM-IM conversions, a PD is then used to detect the intensity-modulated signal reflecting the modulating information.

2.2.1 PM-IM conversion based on a dispersive device

Fig. 2.6 shows the principle of the chromatic dispersion based PM-IM conversion, in which a phase-modulated signal (described by Eq. (2.8)) propagates through a dispersive device and then is fed to a PD.

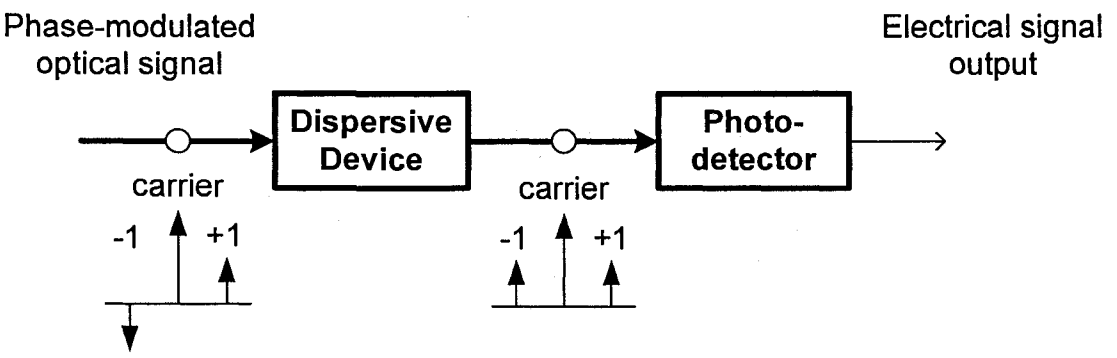

Fig. 2.6 Diagram of chromatic dispersion based PM-IM conversion plus direct detection.

Assume the dispersive device has a unity magnitude response (which is true if the dispersive device is a length of dispersive fiber with a very low loss) but a quadratic phase response. Then the optical signal at the output of the dispersive device can be expressed as

$$\begin{aligned} e_{DD}(t) = e_o \cdot \{ & J_o \cos(\omega_o t + \theta_o) \\ & + J_1 \cos[(\omega_o + \omega_m)t + \frac{\pi}{2} + \theta_{+1}] \\ & - J_1 \cos[(\omega_o - \omega_m)t - \frac{\pi}{2} + \theta_{-1}], \end{aligned} \tag{2.29}$$

where θ_0, θ_{-1} and θ_{+1} are the phase shifts experienced by the carrier, the lower sideband and the upper sideband, respectively.

Generally, the phase shift induced by the dispersive device can be expressed as

$$\theta = \beta z, \tag{2.30}$$

where β is the propagation constant and z is the distance traveled. Expanding β in a Taylor series and substituting it into Eq. (2.30) yields

$$\theta = z\beta(\omega_o) + z\beta'(\omega_o)(\omega - \omega_o) + \frac{1}{2} \cdot z\beta''(\omega_o)(\omega - \omega_o)^2 + \cdots, \tag{2.31}$$

where the β' and β'' are the first- and second-order derivatives of β with respect to the optical angular frequency ω.

We know that group delay $\tau(\omega)$ is defined as $d\theta/d\omega$, i.e.,

$$\tau(\omega) \equiv \frac{d\theta}{d\omega} = z\beta'(\omega_o) + z\beta''(\omega_o)(\omega - \omega_o) + \frac{1}{2} \cdot z\beta'''(\omega_o)(\omega - \omega_o)^2 + \cdots. \tag{2.32}$$

For a dispersive device with a quadratic phase response, its group delay response is linear and the third- or higher-order derivatives of β in Eq. (2.32) can be ignored. Then Eq. (2.32) is simplified as

$$\tau(\omega) = \underbrace{z\beta'(\omega_o)}_{\tau_o} + z\beta''(\omega_o)(\omega - \omega_o), \tag{2.33}$$

where the first term (τ_o) is the group delay experienced by the optical carrier at frequency ω_o, and the second term describes the group delay variation as a linear function with respect to angular frequency ω.

Dispersion is defined as the first-order derivative of the group delay with respect to the angular frequency ω, it is a constant in this case,

$$D_\omega = z\beta''(\omega_o). \tag{2.34}$$

Evaluating θ at the optical carrier of ω_o and the sidebands of $\omega_o \pm \omega_m$, we have

$$\begin{cases} \theta_o = z\beta(\omega_o) \\ \theta_{-1} = z\beta(\omega_o) - \tau_o\omega_m + \frac{1}{2}D\omega_m^2 \\ \theta_{+1} = z\beta(\omega_o) + \tau_o\omega_m + \frac{1}{2}D\omega_m^2. \end{cases} \tag{2.35}$$

When the lightwave passed through a dispersive device, a photo current is generated at the PD by using Eq. (2.25). Taking only the RF signal centered at the modulating frequency ω_m and ignoring the dc current and the higher-order harmonics, we have

$$i_{PD} \propto \sin(\frac{\theta_{+1}+\theta_{-1}}{2}-\theta_o)\cdot\cos(\omega_m t+\frac{\theta_{+1}-\theta_{-1}}{2})$$
$$=\underbrace{\sin(\frac{1}{2}D_\omega\omega_m^2)}_{H_{PM-IM}(\omega_m)}\cdot\cos[\omega_m(t-\tau_o)]. \tag{2.36}$$

From Eq. (2.36) we can see that the proposed chromatic dispersion based PM-IM conversion with direct detection has a frequency response given by

$$H_{PM-IM}(\omega_m)=\sin(\frac{1}{2}D_\omega\omega_m^2). \tag{2.37}$$

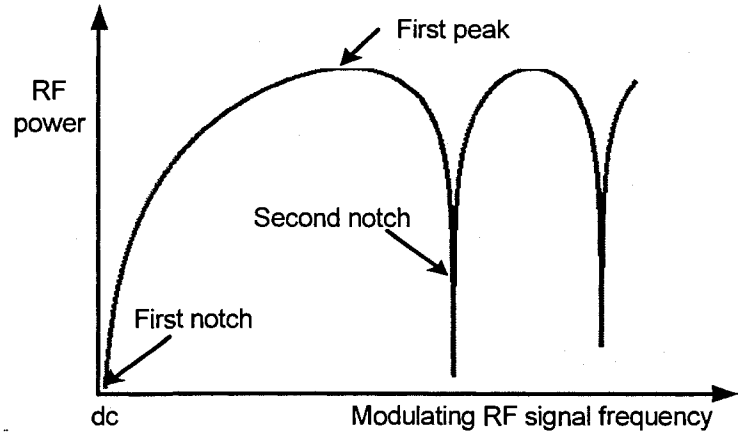

Fig. 2.7 Frequency response of the chromatic-dispersion-based PM-IM conversion.

The frequency response is shown in Fig. 2.7, from which a quasi-periodic function with a notch at the dc frequency is observed. The first peak and the second notch can be determined by letting $D_\omega\omega_m^2/2=\pi/2$ and π, respectively. The frequency response between the first two notches forms a pass band, which can be directly used to shape spectrum of the modulating signal, as we will show in Sec. 3.2 of Chapter 3. Furthermore, if this dispersion-induced frequency response is combined with a frequency response of a conventional all-optical transversal lowpass filter, the intrinsic baseband resonance of the lowpass filter is eliminated, leading to an all-optical bandpass filter. More details about the bandpass filter implemented based on chromatic-dispersion-based PM-IM conversion will be presented in Sec. 3.3 of Chapter 3. In addition, since $\sin(D_\omega\omega_m^2/2)$ is an odd function, if the PM-IM conversion is implemented with positive or negative chromatic dispersion D_ω, the resulted RF signals will be

out of phase. This feature can be applied to implement all-optical microwave filters with both positive and negative coefficients, which will be discussed in Sec. 3.4 of Chapter 3.

2.2.2 PM-IM conversion based on an optical filter

Based on the theoretical analysis of a phase-modulated signal, we know that PM-IM conversion can also be realized by changing the magnitude relationship among the carrier and the sidebands. For instance, using an optical filter to eliminating either a sideband or the carrier would lead to the PM-IM conversion. In this following, a more general discussion on optical-filter-based PM-IM conversion is presented, in which an optical bandpass filter having two linear slopes is used as a frequency discriminator.

Fig. 2.8 shows the frequency response of an ideal optical filter. It has two linear slopes, by locating the carrier of the phase modulated signal at either slopes of the filter, PM-IM conversion can be realized.

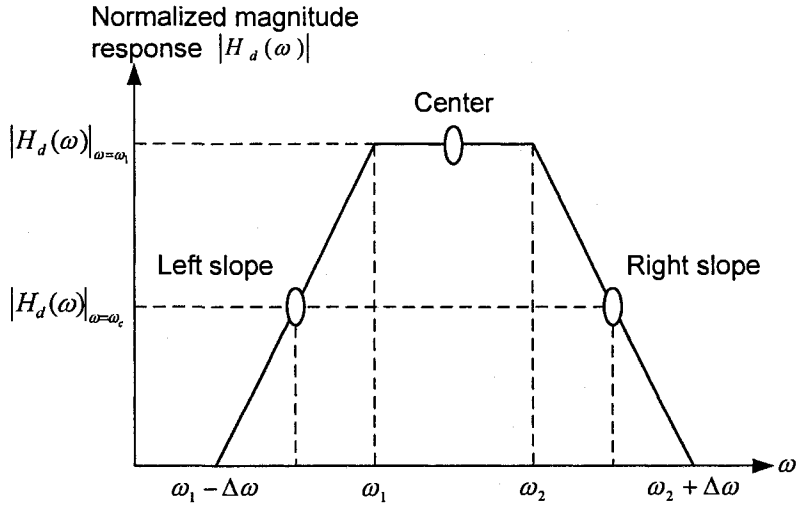

Fig. 2.8 The ideal frequency response of an optical filter with two linear slopes and flat top.

Mathematically, the frequency response of the optical filter shown in Fig. 2.8 can be written as

$$|H_d(j\omega)| = \begin{cases} K\omega - K(\omega_1 - \Delta\omega);\ \omega_1 - \Delta\omega \le \omega \le \omega_1 & (\textit{left slope}) \\ K \cdot \Delta\omega;\ \omega_1 \le \omega \le \omega_2 & (\textit{center}) \\ K(\omega_2 + \Delta\omega) - K\omega;\ \omega_2 \le \omega \le \omega_2 + \Delta\omega & (\textit{right slope}) \\ 0;\ \textit{otherwise}, \end{cases} \tag{2.38}$$

where K is the slope steepness factor of the filter ($K > 0$), and ω is the optical frequency. From Eq. (2.38) we can see that the frequency response of the optical filter consists of three linear sections, i.e., the left slope, the center, and the right slope. To simplify the derivation, we assume that within each section the phase response is linear (In Sec. 5.1 of Chapter 5, a properly apodized FBG is used to perform the PM-IM conversion. Both the simulation and experiment results show that under small signal condition the effect of this assumption on the proposed frequency discriminator is negligible). In addition, if the phase-modulated optical signal has a narrow bandwidth and the optical carrier is properly selected to make its spectrum be totally located within each spectral section of the frequency response of the optical filter, as shown in Fig. 2.8, the impulse response of the optical filter $h_d(t)$ can be approximated

$$h_d(t) \approx \begin{cases} -K(\omega_1 - \Delta\omega)\cdot\delta(t) - jK\cdot\delta'(t); & \textit{left slope} \\ K\cdot\Delta\omega\cdot\delta(t); & \textit{center} \\ K(\omega_2 + \Delta\omega)\cdot\delta(t) + jK\cdot\delta'(t); & \textit{right slope}, \end{cases} \tag{2.39}$$

where the group delay derived from the linear phase response is neglected, $\delta(t)$ is the unit impulse, and $\delta'(t)$ is the first-order derivative of the unit impulse. Note that

$$\begin{aligned} &\delta(t) \xleftrightarrow{FT} 1 \\ &\frac{d}{dt}x(t) \xleftrightarrow{FT} j\omega\cdot X(\omega). \end{aligned} \tag{2.40}$$

After the phase-modulated optical signal passing through the optical filter with the carrier located at one of the three sections, we obtain the optical field

$$\begin{aligned} e_d(t) &= e_{PM}(t) * h_d(t) \\ &\approx \begin{cases} e_{PM}(t)\cdot[K(\omega_o - \omega_1 + \Delta\omega) + K\cdot\beta_{PM}\cdot f'(t)]; & \textit{left slope} \\ e_{PM}(t)\cdot K\cdot\Delta\omega; & \textit{center} \\ e_{PM}(t)\cdot[K(\omega_2 + \Delta\omega - \omega_o) - K\cdot\beta_{PM}\cdot f'(t)]; & \textit{right slope}, \end{cases} \end{aligned} \tag{2.41}$$

where $*$ denotes convolution operation, and $f'(t)$ is the first-order derivative of the modulating signal $f(t)$.

Again using Eq. (2.25), the photo current at the output of the PD is given by

$$i_{PD}(t) \sim \begin{cases} K^2\{(\omega_o - \omega_1 + \Delta\omega)^2 + [\beta_{PM} \cdot f'(t)]^2 + 2(\omega_o - \omega_1 + \Delta\omega) \cdot \beta_{PM} \cdot f'(t)\}; & \textit{left slope} \\ K^2\Delta\omega^2; & \textit{center} \\ K^2\{(\omega_2 + \Delta\omega - \omega_o)^2 + [\beta_{PM} \cdot f'(t)]^2 - 2(\omega_2 + \Delta\omega - \omega_o) \cdot \beta_{PM} \cdot f'(t)\}; & \textit{right slope.} \end{cases} \tag{2.42}$$

The first term on the right side for each case, which equals $|H_d(\omega)|_{\omega=\omega_o}$, represents a dc and can be eliminated by using a dc blocker. When the optical carrier ω_o is located at the left or the right slope with an assumption of small signal modulation, the second term is much smaller than the third term and can be neglected. Finally, we obtain the recovered RF signal,

$$r(t) \sim \begin{cases} 2K^2(\omega_o - \omega_1 + \Delta\omega) \cdot \beta_{PM} \cdot f'(t); & \textit{left slope} \\ 0; & \textit{center} \\ -2K^2(\omega_2 + \Delta\omega - \omega_o) \cdot \beta_{PM} \cdot f'(t); & \textit{right slope.} \end{cases} \tag{2.43}$$

Observing Eq. (2.43), we can conclude that 1) no signal can be recovered if the optical carrier is located at the center of the optical filter passband, 2) the recovered signal is the first-order derivative of the modulating signal when the optical carrier is located at either slope of the optical filter, and 3) the amplitude of the detected signals have different signs when the carriers are located at the opposite slopes which is a very important feature and would find many interesting applications in all-optical signal processing. In Chapter 5, to implement encoding/decoding for optical CDMA systems, and to generate UWB pulses in UWB-over-fiber systems, will be discussed.

CHAPTER 3

ALL-OPTICAL MICROWAVE FILTERS

3.1 Introduction

An all-optical microwave filter is a system used to implement microwave filtering in the optical domain. The use of an all-optical microwave filter would bring many advantages such as low loss, broad bandwidth, large tunable range, high Q factor, and immunity to electromagnetic interference. In addition, since the signal to be processed is in the optical domain, it can be directly incorporated into a radio-over-fiber (RoF) system without the need for an additional electrical to optical (E/O) conversion.

A general structure of an all-optical microwave filter is shown in Fig. 3.1.1. It consists of a light source (either narrowband or broadband, single wavelength or multiple wavelengths), an optical modulator (either intensity modulator or phase modulator), an optical delay line module, and a PD. To avoid optical interference which is very sensitive to environmental changes, the time delayed signals after the delay line module should be added incoherently.

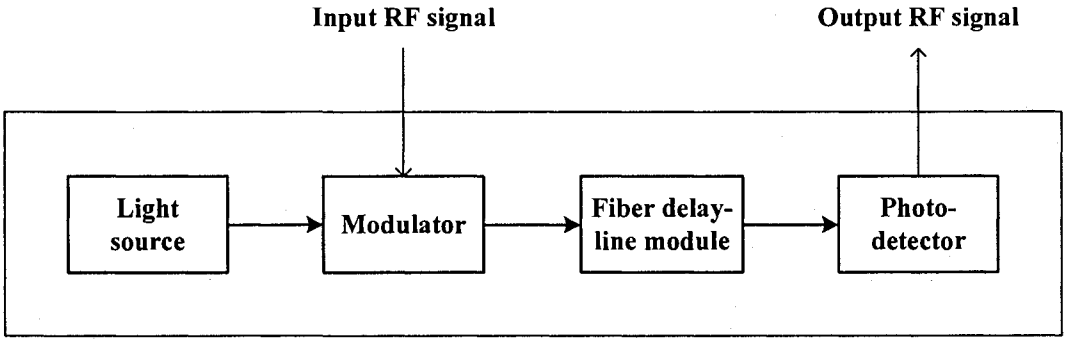

Fig. 3.1.1 General diagram of an all-optical microwave filter.

A. Using electrooptic intensity modulator (EOIM)

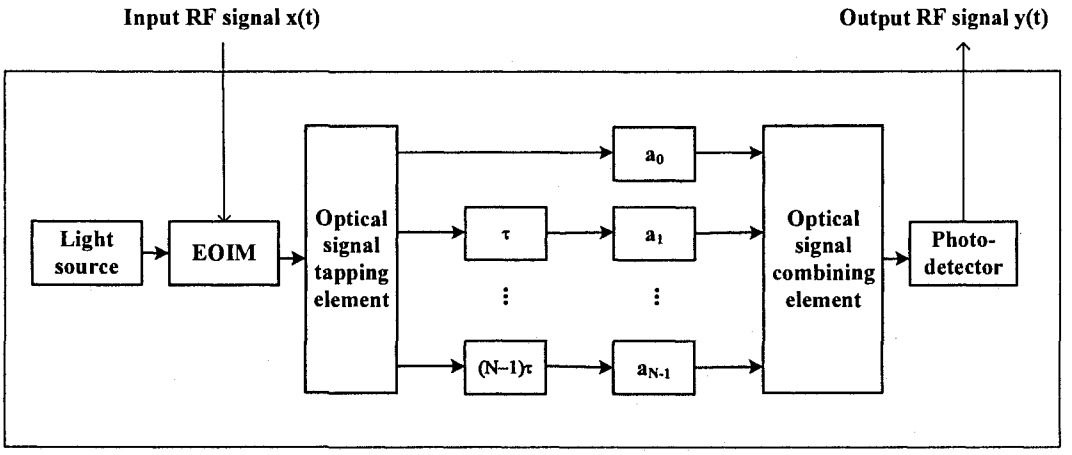

Fig. 3.1.2 Block diagram of an EOIM-based all-optical microwave transversal filter.

Traditionally, an EOIM is used to converting a microwave signal to be processed, $x(t)$, to an optical-intensity-modulated signal, as shown in Fig. 3.1.2. Then the optical signal is sent to the tapped delay-line module, where it is split into several channels with different time delays and attenuations and then summed incoherently at a PD. The filtered electrical signal $y(t)$ is obtained at the output of the PD. Provided that the nonlinear effects in the system are small and negligible, the entire system can be considered as a linear, time-invariant system, in which the output $y(t)$ can be written as

$$y(t) \propto \sum_{k=0}^{N} a_k \cdot x(t - k\tau), \tag{3.1.1}$$

where τ represents the time delay difference between two adjacent taps, and a_k is the attenuation index of the k-th optical path.

Applying the Fourier transforms to both sides of Eq. (3.1.1), the system transfer function is then obtained,

$$H_{FIR}(\omega) \propto \sum_{k=0}^{N-1} a_k \cdot e^{-j\omega k\tau}, \tag{3.1.2}$$

where the time delay unit τ determines the free spectral range (FSR) of the all-optical microwave filter, and the attenuation index a_k determines the k-th filter coefficient, which is proportional to the optical intensity of the k-th optical path and can not be negative. So the frequency response described by Eq. (3.1.2) is a typical transfer function of a finite impulse response (FIR) delay-line filter with all-positive coefficients. Based on signal processing theory, a delay-line filter with all-positive coefficients would operate always as a lowpass filter. However, for many applications, such as RoF systems, bandpass filters are required.

B. Using electrooptic phase modulator (EOPM)

To solve the problem discussed above, in this research, the efforts are focused on optical phase modulation. Fig. 3.1.3 shows a general architecture of an all-optical microwave filter using an EOPM, in which the EOPM is used to modulate the phase of the optical carrier with the RF input, and at each tap a PM-IM conversion module is added, compared to the structure shown in Fig. 3.1.2.

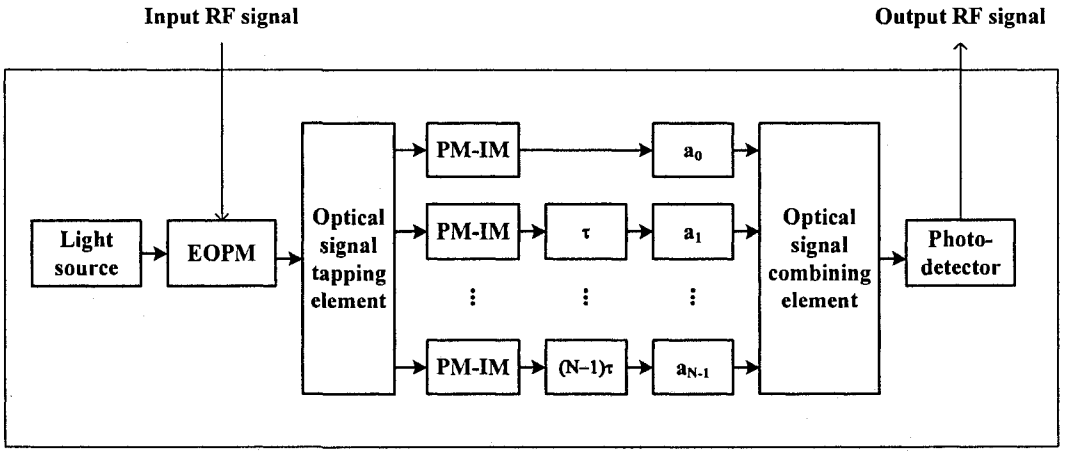

Fig. 3.1.3 Schematic diagram of an EOPM-based all-optical microwave filter with N taps.

If the frequency transfer function of the k-th PM-IM conversion is $H_{PM-IM}^{(k)}(\omega)$, and the time delayed signals with different weights are combined incoherently, the transfer function of the whole system is given by

$$H_{EOPM}(\omega) \propto \sum_{k=0}^{N-1} H_{PM-IM}^{(k)}(\omega) \cdot a_k \cdot e^{-j\omega k\tau}. \tag{3.1.3}$$

If $H_{PM-IM}^{(k)}(\omega)$ is identical for all the channels and is denoted as $H_{PM-IM}(\omega)$, Eq. (3.1.3) can thus be written as

$$H_{EOPM}(\omega) \propto H_{PM-IM}(\omega) \cdot \underbrace{\sum_{k=0}^{N-1} a_k \cdot e^{-j\omega k\tau}}_{H_{FIR}(\omega)} . \tag{3.1.4}$$

As can be seen from Eq. (3.1.4), the filter frequency response is a multiplication of the frequency response of the PM-IM conversion ($H_{PM-IM}(\omega)$) with the frequency response of the transfer function of an EOIM-based all-optical microwave filter ($H_{FIR}(\omega)$). As discussed in Sec. 2.2, $H_{PM-IM}(\omega)$, the frequency response of a chromatic-dispersion-based PM-IM conversion, has a notch at dc, as shown in Fig. 2.6. Based on this property, the baseband resonance of the microwave filter with all-positive coefficients would be eliminated by the dc notch, with an overall frequency response $H_{EOPM}(\omega)$ equivalent to a bandpass filter.

On the other hand, if $H_{PM-IM}^{(k)}(\omega)$ is different for each tap, especially if $H_{PM-IM}^{(1)}(\omega) = -H_{PM-IM}^{(2)}(\omega)$, Eq. (3.1.4) can be written as

$$H_{Filter}(\omega) \propto \left|H_{PM-IM}(\omega)\right| \cdot \sum_{k=0}^{N-1} (-1)^m \cdot a_k \cdot e^{-j\omega k\tau} . \tag{3.1.5}$$

In Eq. (3.1.5), m = 1 corresponds to a negative efficient, and m = 2 corresponds to a positive efficient. Based on the analysis in Sec. 2.2, a positive or negative sign of $H_{PM-IM}(\omega)$ can be achieved by applying the phase-modulated optical signal to a dispersive device with a positive or negative chromatic dispersion or an optical filter at its positive or negative frequency response slope. Using this property, negative taps can be generated. Consequently, implementation of bandpass filter with flat-top passband and larger mainlobe-to-sidelobe ratio (MSR) is possible.

In this Chapter, three different architectures for all-optical microwave bandpass filtering will be presented. In Sec. 3.2, an equivalent bandpass filter with only "one tap" (N=1) is implemented to generate an UWB pulse signal with a spectrum meeting the regulation of the Federal

Communication Commission (FCC). In Sec. 3.3, an all-optical microwave bandpass filter with multiple taps is experimentally implemented by emerging the PM-IM conversions into a laser-array-based delay-line structure. In Sec. 3.4, a method to realize negative filter coefficients is presented.

3.2 A single-tap all-optical microwave bandpass filter using an EOPM

In this Section, an equivalent bandpass filter with only "one tap" is experimentally implemented. The motivation of design and implementation of this single-tap filter is to use its bandpass frequency response to shape the spectrum of Gaussian pulses, to generate ultrawideband (UWB) doublets in the optical domain. The filter consists of a single-wavelength laser source, an EOPM that performs the optical phase modulation, a length of single-mode fiber (SMF) that acts as a dispersive device to perform the PM-IM conversion, and a PD that performs the direct detection. By applying electrical Gaussian pulses to the proposed all-optical microwave bandpass filter, Gaussian doublet pulses are obtained at the PD output, which can provide several gigahertz bandwidths for applications in high-bit-rate UWB wireless communications. In addition, owing to the use of the SMF as a transmission medium to connect a central station to a wireless access point, UWB pulse signals are not only generated but also distributed to a remote site.

An Approach to Ultra-Wideband Pulse Generation and Distribution over Optical Fiber[1]

Fei Zeng, *Student Member, IEEE* and Jianping Yao, *Senior Member, IEEE*
Microwave Photonics Research Laboratory
School of Information Technology and Engineering
University of Ottawa, Ottawa, Ontario, Canada
Email: jpyao@site.uottawa.ca

Abstract

We propose a novel approach to generating and distributing UWB pulse signals over optical fiber. The proposed system consists of a single-wavelength laser source, an electrooptic phase modulator (EOPM), a length of single-mode fiber (SMF) and a photodetector. The combination of the EOPM, the SMF link and the photodetector forms an all-optical microwave bandpass filter, which is used to generate a UWB signal with a spectrum meeting the regulation of the Federal Communication Commission. Gaussian doublet pulses are obtained at the receiver front-end, which can provide several gigahertz bandwidths for applications in high-bit-rate UWB wireless communications. Experimental results measured in both temporal and frequency domains are presented.

Index terms: Ultra-wideband, electro-optic phase modulation, chromatic dispersion, direct sequence impulse radio, bandpass filter, radio-over-fiber.

1. Introduction

Ultra-wideband (UWB) wireless systems have recently attracted considerable interests for short range high-throughput wireless communication and sensor networks thanks to their intrinsic properties, such as the immunity to multipath fading, extremely short time duration, carrier free, low duty cycle, wide occupied bandwidth, and low power spectral density [1-2]. Specifically, the indoor and hand-held UWB systems must operate in the frequency range from 3.1 to 10.6

[1] Published in IEEE Photonics Technology Letters, vol. 18, no. 7, pp. 823-825, April 2006.

GHz with an effective isotropic radiated power level of less than -41dBm/MHz, as required by the United States Federal Communication Commission (FCC) [3].

However, by wireless transmission, UWB signals are only limited in short distance of a few to tens of meters. Such short-range wireless networks can operate mainly in indoor environments in standalone mode, with a nearly nonexistent integration into the fixed wired networks or wireless wide-area infrastructures. To offer availability of undisrupted service across different networks and eventually achieve high-rate data access at any time and from any place, UWB-over-fiber technology combined with fiber-to-the-home (FTTH) topology may provide an effective solution [4].

On the other hand, one of the most attractive technologies to generate UWB signals is based on direct-sequence impulse radio technology. It is a carrier-free modulation scheme that does not use the complicated frequency mixer and intermediate frequency, hence the cost can be greatly reduced compared to that of multi-band orthogonal frequency multiplexing scheme. The selection of the impulse signal types is one of the fundamental considerations in designing UWB circuits and systems because the impulse types determine the performance of the UWB systems. As described in [5], Gaussian mono-cycle pulses and doublets can provide a better bit-error-rate (BER) and multipath performance among different impulse signals. Basically these desired waveforms can be created by a sort of bandpass filtering of a Gaussian pulse, i.e., the filtering acts in a manner similar to taking the derivation of the Gaussian waveform. For instance, a Gaussian mono-cycle is the first-order derivative of a Gaussian pulse and has a single zero crossing; while a Gaussian doublet with an additional zero crossing is the second-order derivative of a Gaussian pulse [2]. However, with the current stage of technology, it is rather expensive and difficult to make such a pulse with a fractional bandwidth even greater than 100% at the central frequency of around 7 GHz [6-8].

In fact, since UWB-over-fiber is essential to integrate the local UWB environment into the fixed networks or other wireless-wide-area infrastructures, it is highly desirable that the distributed UWB signals can be created directly in the fiber link and are ready to radiate at the receiver front-end, which can simplify the system by centralizing the operation. In this letter, we propose a novel approach to achieving both UWB pulse generation and distribution in a simple and

efficient way. By using an electrooptic phase modulator (EOPM), an optical carrier is phase modulated by a Gaussian pulse train representing the data sequence to be transmitted. A length of single-mode fiber (SMF) is then employed as transmission medium to send the information to a remote site. Thanks to the SMF-induced chromatic dispersion, which is usually considered a negative effect in traditional intensity-modulation and direct-detection (IM-DD) systems, in our approach the combination of the EOPM and the SMF link forms an all-optical microwave bandpass filter [9] that can be designed to shape the input Gaussian pulses into UWB pulses that meet the UWB spectral requirement. In this letter, a point-to-point UWB-over-fiber connection is experimentally implemented. The experimental result shows that Gaussian doublet pulses are obtained at the end of the fiber link with a spectrum meeting the FCC regulation.

2. Principle and Experiment

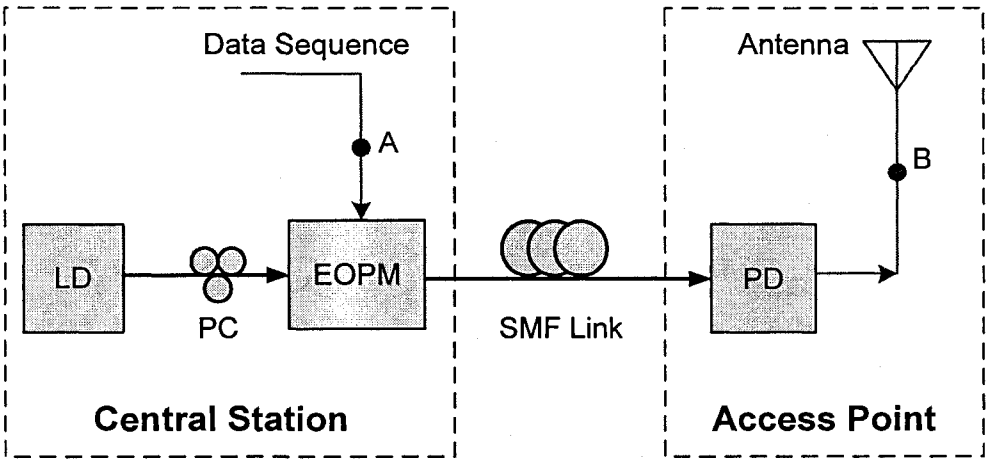

Fig. 1 Block diagram of the proposed UWB-over-fiber system.

The block diagram of the proposed UWB-over-fiber system connecting a central station (CS) and an access point (AP) is shown in Fig. 1. At the CS, light from a laser diode (LD) is fiber coupled to an EOPM which is driven by the data sequence to be transmitted. The phase-modulated optical signal is then applied to a length of SMF that serves as a transmission medium as well as a dispersive device. In our approach the information is carried by the optical phase, if the phase-modulated optical signal is directly fed to a power-detection device, e.g., a photodetector (PD), no information but a dc can be detected. Thanks to the chromatic dispersion induced by the SMF, at the AP the phase information is converted to the optical intensity, and

the modulating electrical signal is then obtained at the output of the PD [9, 10], which is ready to radiate via an antenna.

Under small-signal condition, the frequency response of the proposed system with respect to the modulating signal (between point A and B) can be written as [10]

$$H(\omega) = \cos(\frac{\pi\chi\lambda_0^2 f_m^2}{c} + \frac{\pi}{2}) \cdot H_{EOPM}(\omega) \cdot H_{PD}(\omega) \quad , \tag{1}$$

where the first term on the right side represents the dispersion-based phase-modulation to intensity-modulation (PM-IM) conversion, c is the optical wave propagation velocity in free space, χ is the accumulated dispersion of the SMF link, λ_0 denotes the wavelength of the optical carrier, and f_m is the frequency of the modulating signal; $H_{EOPM}(\omega)$ and $H_{PD}(\omega)$ represent the radio frequency responses of the EOPM and PD, respectively. Based on Eq. (1), some unique properties can be concluded [10]. First, a quasi-periodic change of the response with a notch at the dc frequency is expected. Second, radio frequency responses of the EOPM and PD are usually bandwidth limited, which have a significant degradation at high frequency. Therefore, only the first null-to-null frequency range need to be considered and higher frequency response can be ignored, and eventually bandpass filtering is achieved. Furthermore, since the proposed frequency response is the function of the optical carrier wavelength λ_0 and the dispersion of the transmission medium, e.g., the peak and the second null are obtained by letting $\pi\chi\lambda_0^2 f_m^2 / c = \pi/2$ and π respectively, it indicates that by varying λ_0 or χ, the bandwidth and shape of the proposed bandpass filter can be tuned and hence the spectrum of the generated UWB signals can be optimized.

The proposed UWB bandpass filter in an optical link is experimentally implemented based on the configuration shown in Fig. 1. An LD with a wavelength of 1550 nm is used as the light source. A 25-km standard SMF-28 fiber is employed to transmit UWB signal from the CS to the AP. The SMF-28 fiber has a chromatic dispersion of $17\ ps/nm \cdot km$ at 1550 nm. 25-km of this fiber has a accumulated dispersion of $\chi = 425\ ps/nm$. The frequency response between point A and point B, as shown in Fig. 2, is measured via a vector network analyzer (Agilent E8364A) by sweeping the modulating frequency from 45 MHz to 20 GHz while keeping the

same output power of 3 dBm. From Fig. 2, we can see that a notch at the dc is observed. The passband peak, the lower and higher -10 dB cutoff frequencies are of 10.5, 4.1 and 15.9 GHz respectively, which provide a fractional bandwidth of about 112%. It should be noted that this frequency response does not need to meet the spectral mask authorized by the FCC, but the spectrum of the shaped pulses should meet that regulation.

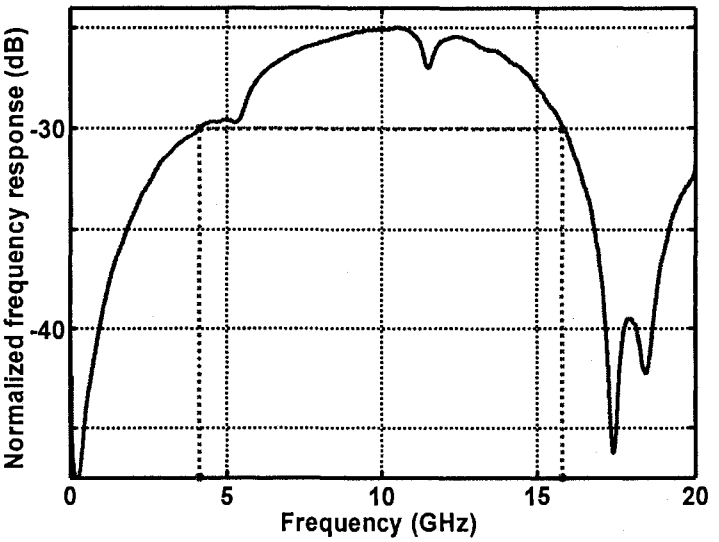

Fig. 2 Measured frequency response of the proposed UWB-over-fiber system.

To further verify the pulse shaping function of our proposed system, at the CS, a 13.5-Gb/s pseudo random bit sequence (PRBS) 2^7-1 signal is applied to the EOPM, which is generated by use of a bite error tester (Agilent N4901B). The temporal waveform representing a single bit is measured by use of a high-speed sampling oscilloscope (Agilent 86116A), as shown in Fig. 3(a). We can see that it has a Gaussian-like shape and a full width at half of the maximum (FWHM) of about 63 ps. The spectrum of the pulse train is also measured by use of an electrical spectrum analyzer (Agilent E4448A), as shown in Fig. 3(b).

After passing through the 25-km SMF-28 fiber link, the phase-modulated optical signal is then fed to the PD located at the AP. The output of the PD is then measured in both temporal and frequency domain as we did at the CS. Fig. 4(a) shows that a Gaussian doublet pulse is obtained at the receiver front-end, which has an FWHM of about 40 ps. From Fig. 4(b), we can see that the measured spectrum has a central frequency of about 7 GHz, and the lower and higher frequencies at -10 dB points are around 3.0 and 10.9 GHz, respectively, which indicates that the

generated UWB signal achieves a fractional bandwidth of about 113%. In particular, the FCC assigned bandwidth and spectral mask for indoor communications is also illustrated in Fig. 4(b). We can see that the resulting pulses in our approach not only meet the FCC's mask, but also optimally exploit the allowable bandwidth and power. A spectral line at 13.5 GHz is observed in the spectrum, which is due to the use of a short code-length of the PRBS pattern, i.e., 2^7-1. By employing longer code-length PRBS patterns or by using pulse position modulation or pulse polarity modulation, this spectral line can be significantly reduced.

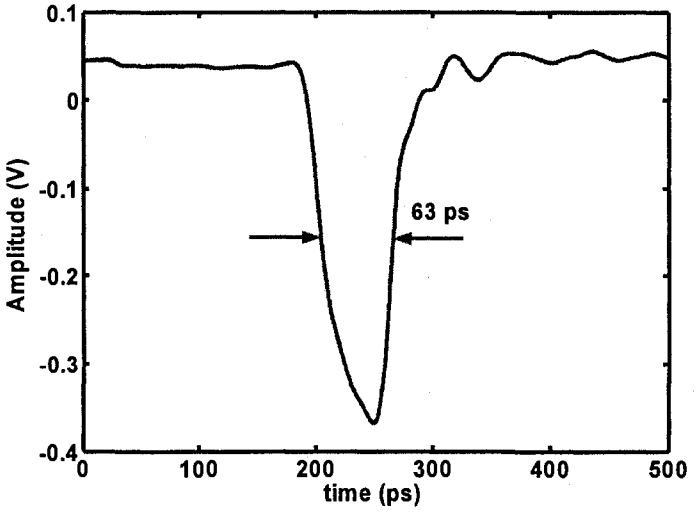

(a)

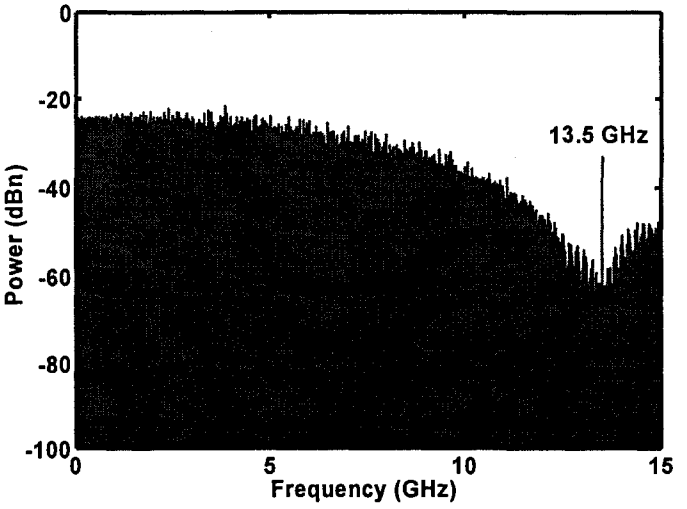

(b)

Fig. 3 When a 13.5 Gb/s PBRS 2^7-1 signal is applied to the EOPM, (a) the waveform of a single bit, and (b) the power spectrum of the modulating signal are measured at point A.

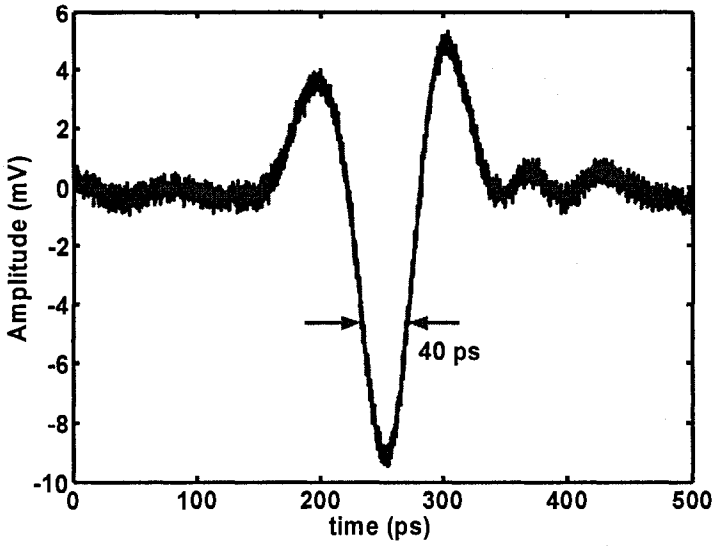

(a)

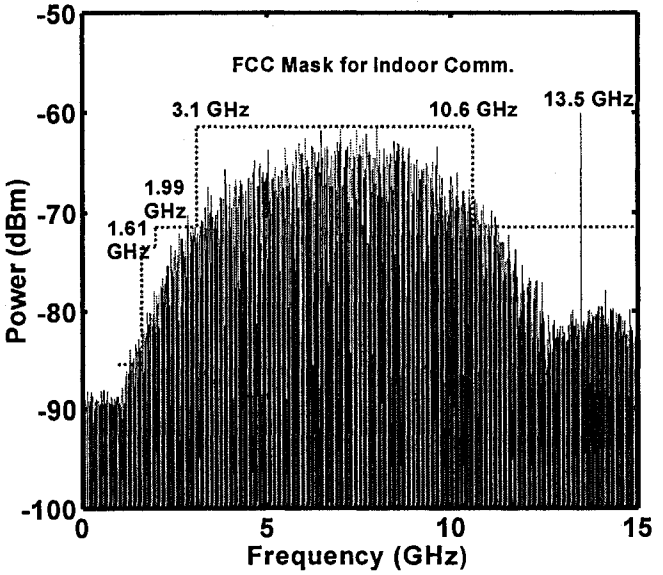

(b)

Fig. 4 (a) Waveform of the Gaussian doublet pulse, and (b) power spectrum of the shaped 13.5 Gb/s PBRS 2^7-1 signal obtained at the end of the fiber link (point B in Fig. 1). Dashed line: FCC spectral mask for indoor applications.

3. Conclusion

A novel and simple UWB-over-fiber system to generate and distribute UWB signals has been proposed and experimentally implemented. In the proposed approach, a passband all-optical microwave filter realized by use of an EOPM, a length of SMF and a photodetector was implemented to generate a UWB signal with a spectrum meeting the regulation of the FCC. The SMF in the system has two functions, as a dispersive device for all-optical bandpass filtering and transmission medium to connect a CS to an AP. Therefore, UWB signals were not only generated but also distributed to at a remote site. Owing to the use of the EOPM, the chromatic-dispersion-induced power penalty existing in traditional IM-DD systems does not exist in the proposed system. On the contrary, it is a positive effect that contributes to the generation of UWB pulse signals. If the proposed system is only used for short distance distribution, e.g., hundreds of meters or a few kilometers, a linearly chirped fiber Bragg grating may be used to generate the required chromatic dispersive. In addition, the use of the EOPM has some other advantages over an intensity modulator, which include a lower insertion loss, no bias control, and simpler system design. The experimental results showed that the doublet pulses generated by the proposed system had a central frequency of about 7 GHz with the lower and higher frequencies at -10 dB points of 3.0 and 10.9 GHz, which meets well the FCC regulation.

References:

[1] D. Porcine, P. Research, and W. Hirt, "Ultra-wideband radio technology: Potential and challenges ahead," IEEE Commun. Mag., vol. 41, no. 7, pp. 66-74, Jul. 2003.

[2] M. Ghavami, L. B. Michael, and R. Kohno, Ultra Wideband Signals and Systems in Communication Engineering. West Sussex, England: Wiley, 2004.

[3] G. R. Aiello and G. D. Rogerson, "Ultra-wideband wireless systems," IEEE Microw. Mag., vol. 4, no. 2, pp. 36-47, Jun. 2003.

[4] S. Kim, H. Jang, S. Choi, Y. Kim, and J. Jeong, "Performance evaluation for UWB signal transmission with different modulation schemes in multi-cell environment distributed using ROF technology," in Proc. Int. Workshop Ultra Wideband Systems, pp. 187-191, May 2004.

[5] X. Chen and S. Kiaei, "Monocycle shapes for ultra wide-band system," in IEEE Int. Symp. Circuits and Systems, vol. 1, pp. 26-29, 2002.

[6] H. Ishida and K. Araki, "Design and analysis of UWB bandpass filter with ring filter," in IEEE MTT-S Int. Dig., vol. 3, pp. 1307-1310, Jun. 2004.

[7] L. Zhu, S. Sun, and W. Menzel, "Ultra-wideband (UWB) bandpass filters using multiple-mode resonator," IEEE Microw. Wireless Compon. Lett., vol. 15, no. 11, pp. 796-798, Nov. 2005.

[8] W. P. Lin and J. Y. Chen, "Implementation of a new ultrawide-band impulse system," IEEE. Photon. Technol. Lett., vol. 17, no. 11, pp. 2418-2420, Nov. 2005.

[9] F. Zeng and J. P. Yao, "All-optical bandpass microwave filter based on an electro-optic phase modulator," Optics Express, vol. 12, no. 16, pp. 3814-3819, Aug. 2004.

[10] F. Zeng and J. P. Yao, "Investigation of phase modulator based all-optical bandpass filter," J. Lightw. Technol., vol. 23, no. 4, pp.1721-1728, Apr. 2005.

3.3 A multi-tap all-optical microwave bandpass filter using an EOPM

In this Section, an all-optical microwave bandpass filter with multiple taps is experimentally implemented. Instead of using a single laser source to achieve single-tap microwave filter, as discussed in Sec. 3.2, we use a laser array with multiple wavelengths as the light source. By combining the laser array with the PM-IM module, an all-optical microwave bandpass filter with multiple taps is realized. The filter performances, including the mainlobe to sidelobe suppression ratio, the reconfigurability, tunability, and the dynamic range, are also investigated.

Investigation of phase-modulator-based all-optical bandpass microwave filter[2]

Fei Zeng, *Student Member, IEEE and OSA* and Jianping Yao, *Senior Member, IEEE, Member, OSA*

Microwave Photonics Research Laboratory
School of Information Technology and Engineering
University of Ottawa, Ottawa, Ontario, Canada
Email: jpyao@site.uottawa.ca

Abstract

Theoretical analysis and experimental implementation of an all-optical bandpass microwave filter are presented. Bandpass filtering is implemented using an electro-optic phase modulator combined with a dispersive device to eliminate the baseband resonance of a typical lowpass filter. In addition to bandpass operation, the proposed filter also provides an improved mainlobe-to-sidelobe ratio and a reduced mainlobe bandwidth compared to those of the conventional microwave filters with windowing. A four-tap bandpass microwave filter with a 3-dB mainlobe bandwidth of 2.65 GHz and a mainlobe-to-sidelobe ratio of 30-dB is demonstrated. The filter performances, including the reconfigurability, tunability and the dynamic range, are also discussed.

Index term: Bandpass filter, chromatic dispersion, mainlobe-to-sidelobe ratio, phase modulation, 1-dB compression point.

1. Introduction

The use of photonic devices to implement flexible filters for the processing of microwave and radiofrequency (RF) signals has been an interesting topic for a few years [1-2]. Compared with the conventional electronic microwave filters, the all-optical microwave filters have many advantages, such as broad bandwidth, low loss, light weight, large tunability and the immunity to electromagnetic interference. In addition, all-optical microwave filters are of particular interest for applications such as radio-over-fiber (RoF) systems and optically controlled phased

[2] Published in Journal of Lightwave Technology, vol. 23, no. 4, pp. 1721-1728, April 2005.

array antennas, where the signals can be processed directly in the optical domain without the need of optical/electrical (OE) and electrical/optical (EO) conversions.

Various configurations have been proposed for the implementation of all-optical microwave filters [3-8]. However, most reported approaches are based on incoherent operation, in which only the intensity of the optical signal can be manipulated and hence negative taps are difficult to obtain. This results in a severe limitation on the functionalities of the all-optical filters. For example, bandpass or highpass filtering cannot be implemented if only positive taps are available. Although in a coherent system optical phase can be manipulated to achieve negative coefficients [9-10], the implementation of such a coherent optical signal processor is hindered by the precise control of the optical phase, which is extremely sensitive to the environment variations. Moreover, the maximum time delay has to be shorter than the coherent length of the light source, which further imposes difficulties in the filter fabrication based on fiber optics. To overcome this limitation, several techniques have been proposed to realize negative coefficients and consequently achieve bandpass filtering using incoherent sources. One approach proposed by Sales et al. [11] is to use differential detection, which requires converting the optical signal to electrical signal at the cost of increased system complexity. Other approaches with negative coefficients include wavelength conversion based on cross-gain saturation modulation in a semiconductor optical amplifier (SOA) [12], and carrier depletion effect in a Fabry-Perot (FP) laser diode [13] or in a distributed-feedback (DFB) laser diode [14]. More recently, Capmany et al. [15] proposed a bandpass filter that employed two electro-optic modulators (EOMs). Negative coefficients were obtained by biasing the two EOMs at different operation points. Mora et al. [16] presented a simple approach to realizing transversal filters with negative coefficients. The negative taps were obtained by use of the transmission of a broadband source through uniform Bragg gratings. Chan et al. [17] presented a two-tap notch filter with one negative tap, in which a dual-output EOM was used. The EOM was connected in a way such that it undergoes a double-pass modulation. In these configurations, complicated structures or extra active or passive components are required.

In addition, the mainlobe-to-sidelobe ratio (MSR) and the mainlobe bandwidth are other two important issues that must be considered in the filter design. Although it is known from filter theory, uniform taps provide an MSR that increases linearly with the number of taps. This may

be insufficient for certain applications, where the available taps are limited. Different weighting functions have been proposed for the MSR improvement, either by adjusting the power of the optical sources [18, 19] or by controlling the attenuation/gain of the taps. However, for a fixed number of taps, the reduction of the MSR by use of appropriate window functions is achieved at the cost of an increased mainlobe bandwidth, which is usually unwanted for many applications.

Recently, we have proposed a method to implement all-optical microwave bandpass filters [20]. It is different from the negative-coefficient bandpass filters discussed in [12-17]; the proposed bandpass filter eliminates the baseband resonance of a typical lowpass filter by use of a phase modulator combined with a dispersive device. The fundamental concept was demonstrated based on a simple two-tap filter [20]. However, many issues such as the MSR, mainlobe bandwidth, tunability and dynamic range were not discussed in [20]. In this paper, we present a detailed theoretical and experimental investigation on these issues. A bandpass filter with four taps is implemented. We show that the proposed filter provides simultaneously a lower MSR and a narrower mainlobe bandwidth compared to the conventional negative-coefficient filters. The performances such as the reconfigurability, tunability and the dynamic range are also discussed in this paper.

This paper is organized as follows. In Section 2, the principle of the phase-modulation-based all-optical bandpass microwave filter is discussed. A theoretical model based on narrow-band phase modulation with intensity detection is developed. Issues such as the MSR, mainlobe bandwidth are discussed. In Section 3, experimental implementation of a four-tap bandpass microwave filter is performed to verify the theoretical analysis. Discussions on the filter tunability and the dynamic range are presented in Section 4. A conclusion is drawn in Section 5.

2. Theory

Consider a fiber link composed of a single-frequency laser source, an electro-optic phase modulator (EOPM), a dispersive device and a square-law photodetector. The diagram of the link is shown in Fig. 1, where the laser is fiber coupled to the phase modulator which is driven by a single-frequency sinusoidal electrical signal; the phase modulated optical signal is then applied to the dispersive device and the output is detected by the photodiode. The optical amplitude spectra at different points in the link are schematically shown in Fig. 1.

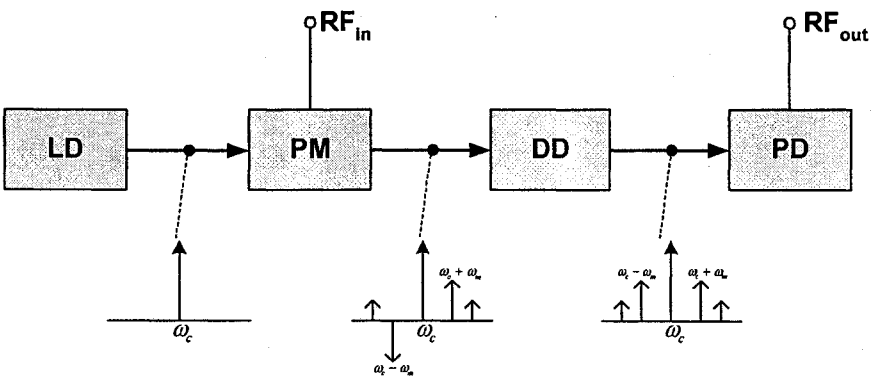

Fig.1 Diagram of narrow-band phase modulation with intensity detection. LD: laser diode, PM: phase modulator, DD: dispersion device, PD: photodetector.

The normalized amplitude of the phase modulated optical field $E(t)$ can be expressed in the form of

$$E(t) = \cos[\omega_c t + \Delta\varphi(t)] = \cos[\omega_c t + m_p \cdot V \cos(\omega_m t)], \quad (1)$$

where ω_c is carried angular frequency; ω_m is modulating angular frequency; $\Delta\varphi$ is the phase change of the carrier; V is the amplitude of modulating signal; and $m_p = \Delta\varphi_{\max} / V$ is the phase modulation index. Eq. (1) can be expanded in terms of Bessel functions of the first kind,

$$E(t) = \sum_{n=-\infty}^{\infty} J_n(m_p V) \cdot \cos[(\omega_c + n\omega_m)t + \frac{1}{2} n\pi], \quad (2)$$

where $J_n(\bullet)$ denotes the n-th order Bessel function of the first kind. To simplify, the argument ($m_p V$) will be omitted in the following text. From Eq. (2), we can see that the phase modulation process generates a series of sidebands with Bessel function amplitude coefficients. The power intensity of each sideband, plotted as the function of $m_p V$ in Fig. 2, is proportional to the square of the coefficient of the corresponding term in Eq. (2).

From Fig.2, we see that when $m_p V$ is small, only the first-order upper and lower sidebands can be considered; and higher-order sidebands are negligible. If $m_p V$ is relative large and the power levels of the higher-order sidebands are comparable to those of the carrier and the first-order

sidebands; the modulation is non-linear, which imposes a crucial limitation on the dynamic range of the proposed filter. The discussion on dynamic range will be presented in Section 4. Here, under small signal conditions, the phase modulation can be regarded as a narrow-band linear modulation. Eq. (2) can be further simplified as

$$E(t) = J_0 \cos(\omega_c t) + J_1 \cos[(\omega_c + \omega_m)t + \frac{\pi}{2}] + J_{-1} \cos[(\omega_c - \omega_m)t - \frac{\pi}{2}]. \quad (3)$$

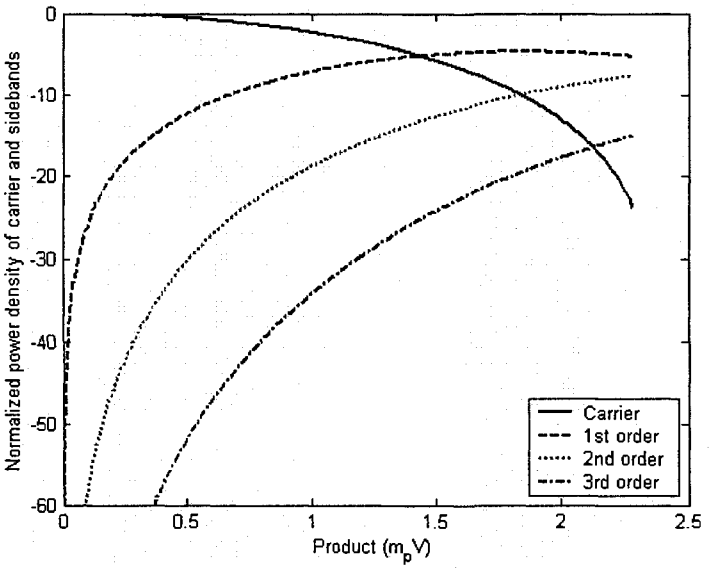

Fig. 2 Normalized power intensities of the carrier and the sidebands as the function of the product $m_p V$.

Based on the property of Bessel functions, we have

$$J_n = -J_{-n}, \text{ when n is odd.} \quad (4)$$

We can conclude that the two sidebands are π out of phase at the output of the phase modulator, which is different from an intensity modulation where the two sidebands are in phase. If this signal is directly detected using a photodiode, the RF signal cannot be recovered because the beating between the carrier and upper sideband exactly cancels the beating between the carrier and the lower sideband. However, as shown in Fig. 1, if the modulated optical signal passes through a dispersive device, the optical field can be expressed as

$$E(t) \propto J_0 \cos(\omega_c t + \varphi_0) + J_1 \cos[(\omega_c + \omega_m)t + \frac{\pi}{2} + \varphi_1] - J_1 \cos[(\omega_c - \omega_m)t - \frac{\pi}{2} + \varphi_2], \quad (5)$$

where φ_0, φ_1 and φ_2 are the phase delays of the spectral components ω_c, $\omega_c + \omega_m$ and $\omega_c - \omega_m$ induced by the chromatic dispersion of the dispersive device. Since the phase delays are different for the three components, which implies that the phase difference of the two sidebands can be effectively rotated to be totally or partially in phase; then the modulating RF signal may be recovered when this dispersed optical signal is fed to the photodetector.

It is well known that the phase delay can be given by an expansion in a Taylor series of the frequency dependent propagation constant $\beta(\omega)$ and light absorbed by the photodetector generates a current proportional to the square of the optical field [21-22]. Taking only the RF signal centered at the modulation frequency ω_m and ignoring the dc current and higher-order harmonics, we obtain the amplitude of the recovered RF signal

$$\begin{aligned} E_{RF}(t) &\propto \cos(\frac{\varphi_1 + \varphi_2}{2} - \varphi_0) \cdot \cos(\omega_m t + \frac{\varphi_1 - \varphi_2}{2}) \\ &= \cos(\frac{\pi \chi \lambda_0^2 f_m^2}{c} + \frac{\pi}{2}) \cdot \cos(\omega_m t + \theta) \end{aligned}, \quad (6)$$

where c is the optical wave propagation velocity in free space; χ is the accumulated dispersion of the dispersive device; λ_0 is the central wavelength of the carrier; f_m is the frequency of the modulation signal; and θ is the phase delay of the recovered microwave signal, which is also determined by χ and f_m. The frequency response of this narrow-band phase modulation and intensity-detection operation is shown in Fig. 3. As can be seen, a notch is observed at the dc frequency; the first peak and the second notch can be determined by letting $\pi\chi\lambda_0^2 f_m^2 / c = \pi/2$ and π, respectively.

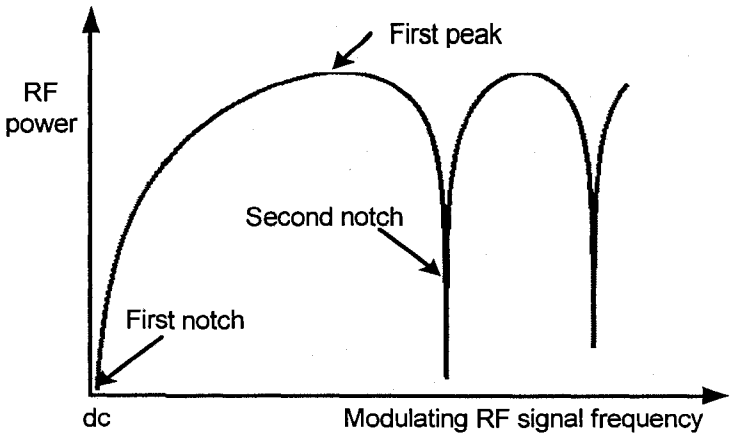

Fig. 3 Recovered RF power vs. RF frequency.

Now we use an array of N laser sources to replace the single laser source. Assume that the laser sources are not correlated. The central wavelengths are $\lambda_n\,(n=1,2,\cdots,N)$ and the output powers are $P_n\,(n=1,2,\cdots,N)$. As shown in Fig. 4, the combined outputs of the N wavelengths from the laser array are applied to the phase modulator, and the modulated optical signal passes through the dispersive device. The modulating RF signal is recovered at the photodetector, which can be expressed as the summation of resulting electrical signals from the N carriers

$$E_{RF}(t) \propto \sum_{n=1}^{N} \cos\left(\frac{\pi \chi_n \lambda_n^2 f_m^2}{c} + \frac{\pi}{2}\right) \cdot P_n \cdot \cos(2\pi f_m t + \theta_n), \tag{7}$$

where χ_n is the accumulated dispersion for the n-th carrier, and θ_n is the phase delay for the n-th recovered RF signal.

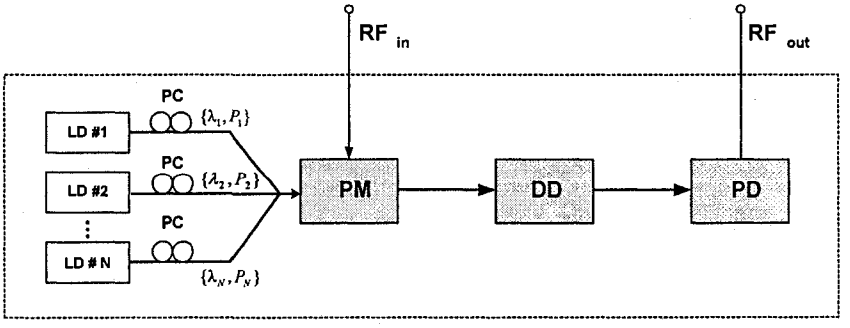

Fig. 4 Diagram of phase-modulator-based all-optical bandpass microwave filter. PC: polarization controller.

If the wavelength spacing between any adjacent laser diodes is identical and small, the first term on the right side of Eq. (7) can be considered identical for all the wavelengths. Then Eq. (7) can be rewritten as

$$E_{RF}(t) \propto \cos\left(\frac{\pi \overline{\chi_n} \cdot \overline{\lambda_n}^2 f_m^2}{c} + \frac{\pi}{2}\right) \cdot \sum_{n=1}^{N} P_n \cdot \cos[2\pi f_m t + \theta_1 + 2\pi f_m (n-1)T], \tag{8}$$

where $\overline{\chi_n}$ and $\overline{\lambda_n}$ denote the average accumulated dispersion and the mean value of carrier wavelength; $T = \overline{\chi_n} \cdot \Delta\lambda$ is the time interval between any two adjacent taps. Applying Fourier transform to both sides of Eq. (8), we get the frequency response

$$H(\omega) \propto \underbrace{\cos\left(\frac{\pi \overline{\chi_n \lambda_n}^2 f_m^2}{c} + \frac{\pi}{2}\right)}_{H_1(\omega)} \cdot \underbrace{\sum_{n=1}^{N} P_n \cdot \exp[j2\pi f_m (n-1)T]}_{H_2(\omega)}, \tag{9}$$

where $H_1(\omega)$ represents the dispersion-induced frequency response; and $H_2(\omega)$ is nothing but a frequency response of a typical transversal all-optical lowpass filter. The effective transfer function of this phase-modulation-based microwave filter can be expressed as the multiplication of these two responses, or in other words, a conventional lowpass response $H_2(\omega)$ with a free spectrum range (FSR) of $1/T$ is reshaped by the frequency response $H_1(\omega)$.

Based on the above theoretical analysis, a four-tap all-optical bandpass microwave filter is simulated, in which four carriers with $\overline{\lambda_n} = 1570$ nm and wavelength spacing $\Delta\lambda = 0.195$ nm are applied as the light sources. The accumulated dispersion $\chi = 425$ ps/nm at 1570 nm is chosen to ensure the second resonance peak of $H_2(\omega)$ located exactly at the same position of the first peak of $H_1(\omega)$. The frequency response of proposed microwave filter is shown in Fig. 5. As can be easily seen that the baseband resonance of the lowpass filtering function due to the conventional intensity-modulation direct-detection (IM-DD) scheme is eliminated; and an equivalent bandpass microwave filter is consequently achieved.

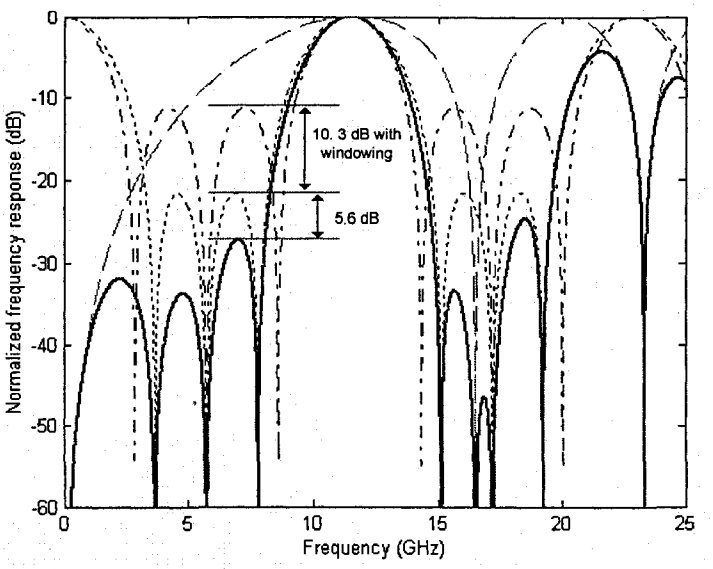

Fig. 5 Simulation results of a four-tap bandpass microwave filter. Dash-dot line: $H_2(\omega)$ based on a rectangular window {1,1,1,1}; dotted line: $H_2(\omega)$ based on a Kaiser window {0.54,1,1,0.54}; dashed line: dispersion effects induced $H_1(\omega)$; solid line: $H(\omega)$ based on the Kaiser window {0.54,1,1,0.54}.

A rectangular window of $\{P_n\} = \{1,1,1,1\}$ and a Kaiser window of $\{P_n\} = \{0.54,1,1,0.54\}$ are applied to show the MSR suppression due to different tap-weight apodization. Compared with the frequency response of a lowpass filter with uniform taps, 10.3 dB MSR improvement is obtained when the Kaiser window is applied, which is at the cost of a 0.4 GHz expansion of 3-dB passband width. However, by use of our approach, an MSR improvement of 15.9 dB can be achieved. Meanwhile, the expansion of the mainlobe bandwidth due to the application of the Kaiser window is only 0.1 GHz, which means that the presented approach makes it possible to improve the MSR and reduce the mainlobe bandwidth simultaneously.

3. Experiment

First, an experiment based on the configuration shown in Fig. 1 is carried to verify the dispersion effects in the phase modulated optical link. A tunable laser with a tunable range from 1520 nm to 1620 nm is used as the optical source. A 25-km standard SMF-28 fiber coil is employed as the dispersive device. The fiber shows a chromatic dispersion of 17.9 ps/(nm.km) at 1568 nm, which provides an accumulated dispersion of $\chi = 450$ ps/nm. The frequency

response at the output of the photodiode, shown in Fig. 6, is measured by a vector network analyzer by sweeping the modulating frequency from 45 MHz to 25 GHz at the same output power of 3 dBm.

An excellent agreement between the theoretical and experimental results is observed from Fig. 6(a). A quasi-periodic change of the RF power with a notch always at the dc is found. The first peak and the second notch are located at 11.2 GHz and 16.4 GHz respectively for $\lambda_0 = 1568.2$ nm. When the central wavelength is tuned around λ_0 by a few nanometers, no obvious change can be observed from the measured $H_1(\omega)$. This verifies the approximation in Section 2 that $H_1(\omega)$ can be considered identical for all the wavelengths. From Fig. 6(b), we can see that the plot of $H_1(\omega)$ is squeezed or stretched when the carrier wavelength is tuned from 1550 nm to 1620 nm or to 1520 nm respectively. This feature indicates that by varying the carrier frequency or the dispersion of the dispersive medium at large value, the frequency response $H_1(\omega)$ can be tuned. In Section 4, we will show that this feature can be used for filter tuning without introducing any filter response distortion.

The experimental setup of a four-tap all-optical bandpass microwave filter is shown in Fig. 7. Four tunable lasers emitting at wavelengths of $\lambda_1 = 1567.83$ nm, $\lambda_2 = 1568.03$ nm, $\lambda_3 = 1568.23$ nm and $\lambda_4 = 1568.42$ nm are fed to a high-speed electro-optic phase modulator via a star coupler. The pumping current and polarization state of each laser source are carefully adjusted to obtain a window function of {0.54, 1, 1, 0.54} at the output port of the phase modulator, as shown in Fig. 8(a). Same fiber coil is used as the dispersive device. The wavelength spacing between any two adjacent laser diodes is around 0.2 nm, which gives a time delay of 90 ps or an FSR of 11.1 GHz. This FSR ensures that the resonance peak of $H_2(\omega)$ is located at the same position as the first peak of $H_1(\omega)$.

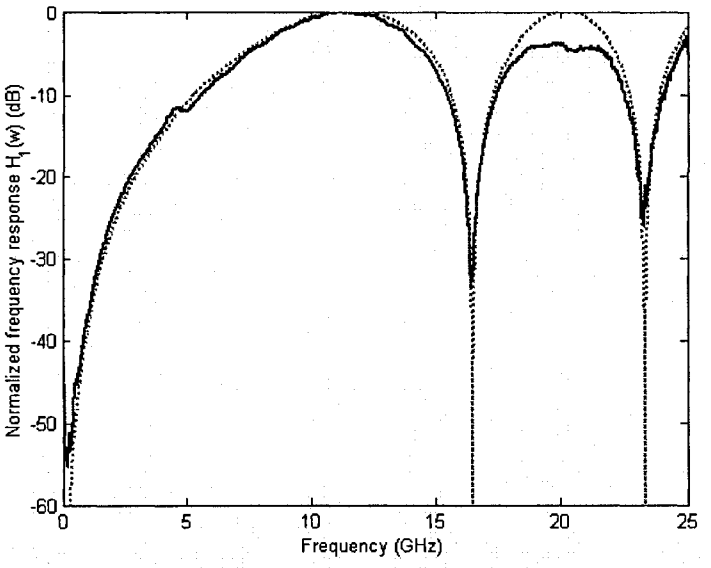

(a)

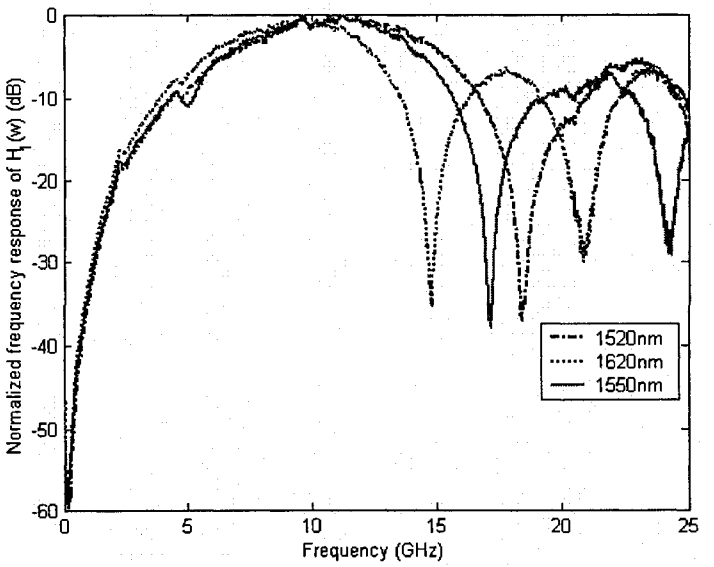

(b)

Fig. 6 Measured frequency response of $H_1(\omega)$. (a) Experimental $H_1(\omega)$ (solid) vs. theoretical $H_1(\omega)$ (dotted); (b) Experimental $H_1(\omega)$ at different carrier wavelengths.

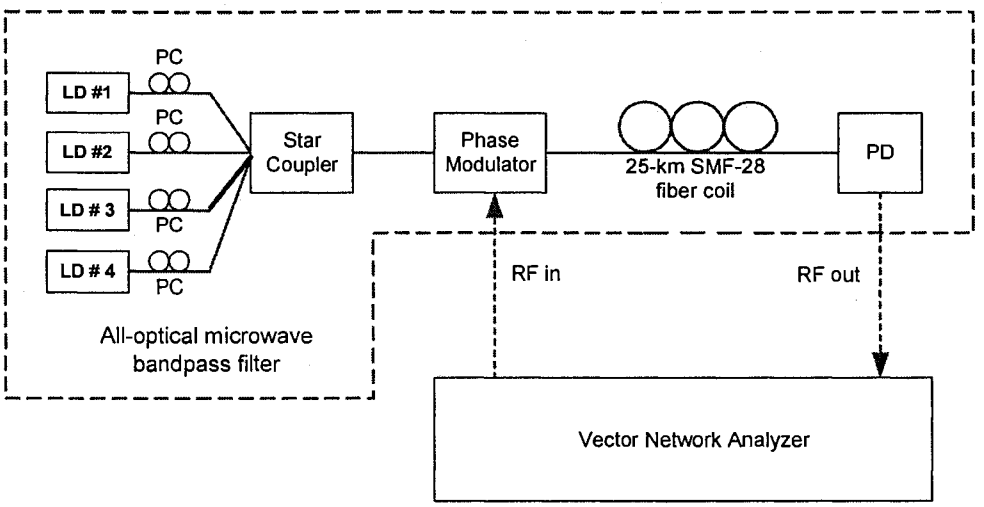

Fig. 7 Experimental setup of the proposed four-tap bandpass microwave filter.

The effective transfer function of the microwave filter $H(\omega)$, shown in Fig. 8(b), is measured using the same vector network analyzer, again an excellent agreement between the theoretical and experimental results are observed. Although the lowest measurement frequency is 45 MHz, it can be extrapolated that the filter response has a notch at the dc frequency and the baseband resonance of the conventional IM-DD based lowpass filter is eliminated, which indicates clearly the function of an equivalent bandpass filter. As expected, an additional MSR decrease of 4.7 dB and a 3-dB mainlobe bandwidth reduction of 0.4 GHz are obtained. The degradation of the magnitude response shown at higher frequencies is due to the unflat response of the phase modulator.

Another filter with different window function of $\{P_n\} = \{0.50, 1, 1, 0.49\}$ is also experimentally implemented to prove the reconfigurability of the proposed bandpass microwave filter. The measured optical power spectrum of the laser sources and the overall frequency response $H(\omega)$ are shown in Fig. 9(a) and Fig. 9(b). A bandpass filter with the passband centered at 11.2 GHz, a 3-dB mainlobe bandwidth of 2.65 GHz, and an MSR of 30 dB is demonstrated.

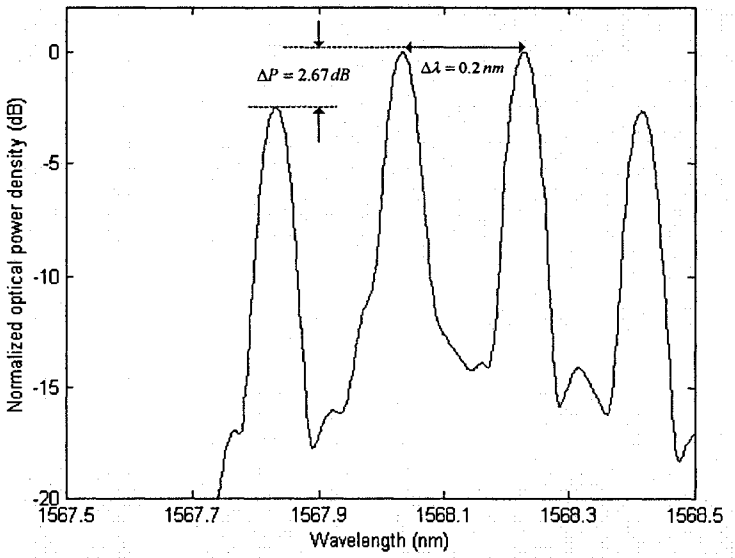

(a)

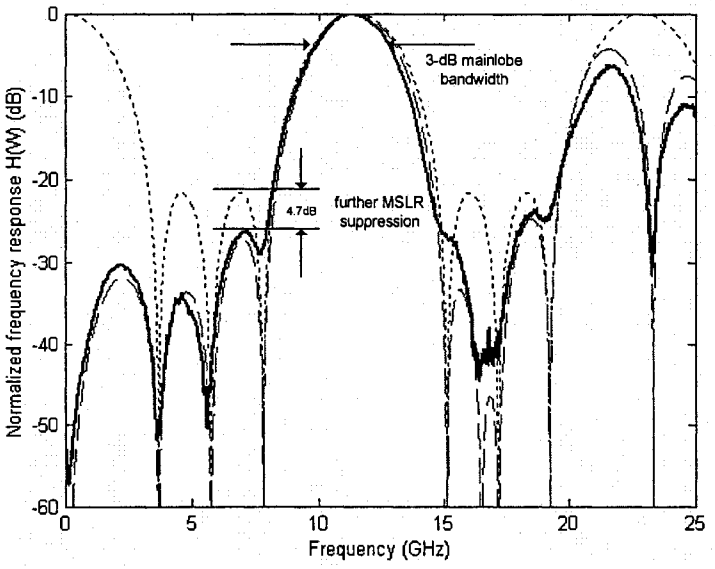

(b)

Fig. 8 Experimental results of the bandpass filter with a window function $\{P_n\} = \{0.54, 1, 1, 0.54\}$. (a) Optical spectrum of the laser array; (b) frequency responses: measured $H(\omega)$ (solid line), theoretical $H(\omega)$ (dashed line), theoretical $H_2(\omega)$ (dotted line).

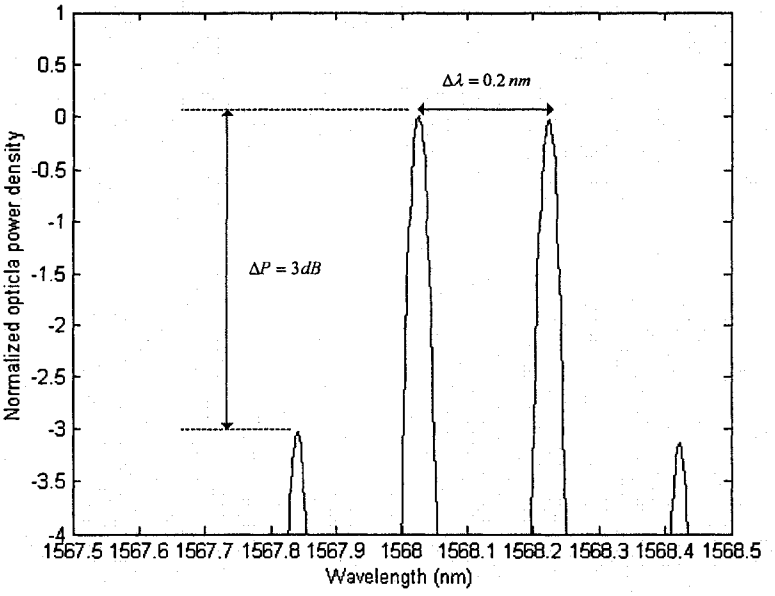

(a)

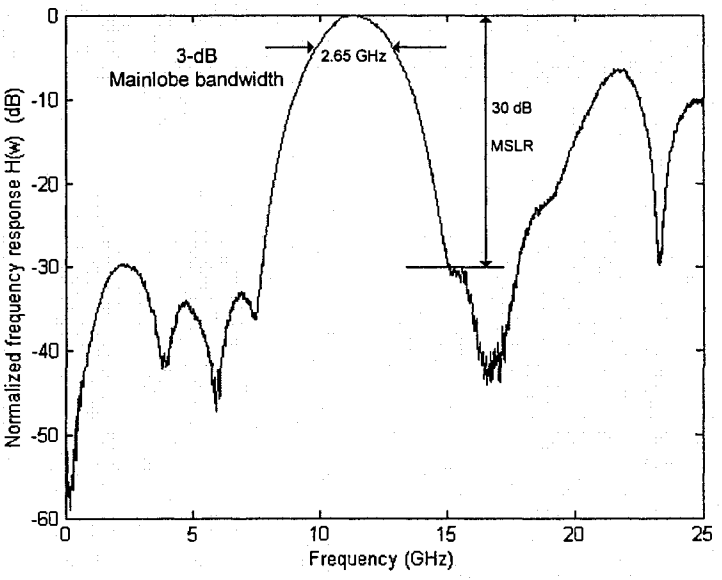

(b)

Fig. 9 Experimental results of the bandpass filter with a window function of $\{P_n\} = \{0.50, 1, 1, 0.49\}$. (a) Measured optical spectrum of the laser array; (b) Measured frequency response $H(\omega)$.

4. Further discussion

Tunability: For many applications, the filters are required to be tunable. In order to tune the frequency response of the filter, the time delay T between adjacent taps or the FSR has to be changed. In this approach, the immediate way to tune the filter is to tune the wavelength spacing of the laser array, since the time delay between any two adjacent taps is proportional to the wavelength spacing of these two taps. Fig. 10 shows the filter frequency response when the wavelength spacing between two adjacent laser source is tuned from 0.2 nm to 0.23 nm. We can see that the central frequency of the passband is changed from 11.2 GHz to 9.7 GHz. However, this tuning is at the cost of the shape distortion of the filter response. As shown in Fig. 10, when the passband is tuned towards a lower frequency, the left side MSR is further reduced but the right side MSR is degraded by about 7.5 dB. The reason is that the small change of wavelength spacing can only lead to the FSR change of $H_2(\omega)$, while $H_1(\omega)$ is almost kept unchanged. But as we discussed earlier, the overall frequency response is the multiplication of $H_1(\omega)$ and $H_2(\omega)$; and the second resonance peak of $H_2(\omega)$ must be located at the same position as the first peak of $H_1(\omega)$ in order to obtain a maximized MSR. So the MSR is degraded when only $H_2(\omega)$ is changed.

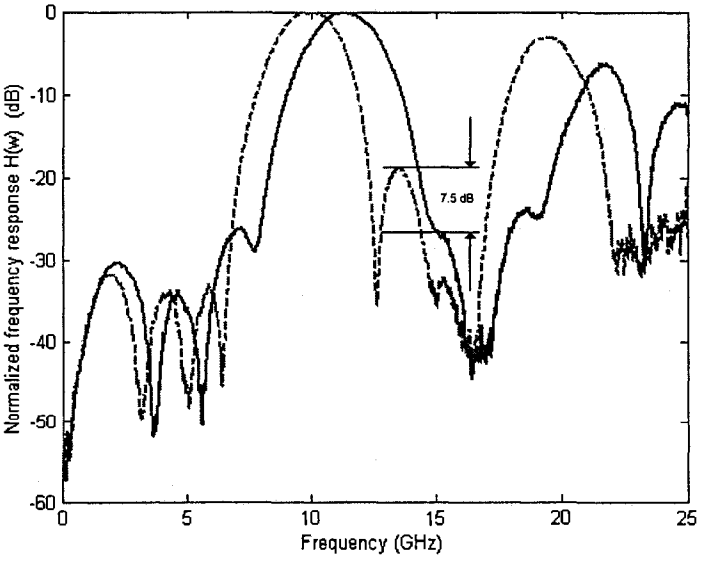

Fig. 10 Frequency responses of the bandpass filter for $\Delta\lambda = 0.2\,nm$ (solid) and $\Delta\lambda = 0.23\,nm$ (dashed).

The problem may be solved if a dispersive device with tunable dispersion is used, such as a chirped grating with tunable chirping [23]. By properly changing the dispersion of the dispersive device combined with the tuning of the wavelength spacing of the laser sources, the peak positions of the responses $H_1(\omega)$ and $H_2(\omega)$ can be maintained co-located at the same position; therefore the filter tuning without any MSR degradation can be achieved.

Dynamic range: Dynamic range is another important factor that needs to be addressed in the filter design. In the earlier analysis in Section 2, a small signal condition is applied to guarantee the linear modulation approximation, for which the second- or higher-order sidebands are neglected. However, as shown in Fig. 2, when the modulation depth becomes large the carrier power level decreases and the power levels of the sidebands increase quickly, which means for a large dynamic signal the second- and higher-order sidebands need to be considered. The dynamic range here is defined as the range from the minimum discernable signal (lower limit) to the maximum allowable signal (upper limit). The lower limit is determined by the system-induced noise, such as shot noise from the photodiode and the relative intensity noise from the laser array, which will not be discussed here. The upper limit is determined by the nonlinearity of the phase modulator. In this paper, 1-dB compression point is introduced to quantify the upper limit. In the analysis, the upper limit is found when the passband peak of the filter frequency response drops by 1 dB from the ideal value.

In general, the recovered RF signal at frequency ω_m can be expressed as the summation of the beatings between any adjacent sidebands [21],

$$E_{RF}(t) \propto \underbrace{J_0 J_1 \cos\left(\frac{1}{2}\chi_\omega \omega_m^2 + \frac{1}{2}\pi\right) \cdot \cos\left(\omega_m t + \omega_m \cdot \Delta\tau + \frac{1}{3}\dot{\chi}_\omega \omega_m^3\right)}_{\textit{beating between the 1st order sidebands and carrier}}$$
$$+ \underbrace{J_1 J_2 \cos\left(\frac{3}{2}\chi_\omega \omega_m^2 + \frac{1}{2}\pi\right) \cdot \cos\left(\omega_m t + \omega_m \cdot \Delta\tau + \frac{7}{3}\dot{\chi}_\omega \omega_m^3\right)}_{\textit{beating between the 1st and 2nd order sidebands}}, \qquad (10)$$
$$+ \cdots$$

where χ_ω denotes the accumulated dispersion in $s/radian$; $\dot{\chi}_\omega$ denotes the first-order derivation of χ_ω, and higher-order derivations of χ_ω are neglected; $\Delta\tau$ is the time delay of the

RF signal passing through the dispersive device. The beating between the first-order sidebands generates an RF signal at $2\omega_m$, which is not important because it can be filtered out. The Fourier transform of Eq. (10) gives the frequency response of $H_1(\omega)$. If $J_1J_2 << J_0J_1$, the second term on the right side of Eq. (10) can be neglected; then the frequency response $H_1(\omega)$ can be well approximated by Eq. (6) and has a frequency response that is independent of the input electrical signal power. When the product J_1J_2 increases, the power level of the recovered RF signal becomes non-linearly proportional to the power level of the modulating signal. In this case, the phase modulation cannot be approximated as a linear modulation, and the frequency response $H_1(\omega)$ is now power dependent.

Again, the 25-km SMF-28 fiber is used as the dispersion device, which has a dispersion profile given by

$$D_\lambda = \frac{S_0}{4}[\lambda - \frac{\lambda_0^4}{\lambda^3}]\, ps/(nm \cdot km), \tag{11}$$

where $\lambda_0 = 1310\, nm$ is the zero dispersion wavelength, and $S_0 \leq 0.092\, ps/(nm^2 \cdot km)$ is the zero dispersion slope. The phase modulator employed in the experiment has a modulation index m_p of $\pi / 4.8V$ at dc. Based on these parameters, the level at the passband peak of the filter frequency response as a function of the input signal power is plotted in Fig. 11.

From Fig. 11, we can see that the input power corresponding to the 1-dB compression point is about 10.3 dBm. This is the upper limit of the dynamic range of this filter. At this point, the product J_1J_2 is around 30 dB lower than J_0J_1, which means that the beating between the carrier and the first-order sidebands is dominant and the beating between the carrier and the higher-order sidebands are negligible. When the input signal power further increases, the filter frequency response at the passband peak decreases quickly; and the total frequency response of $H_1(\omega)$ distorts significantly as shown in Fig. 12.

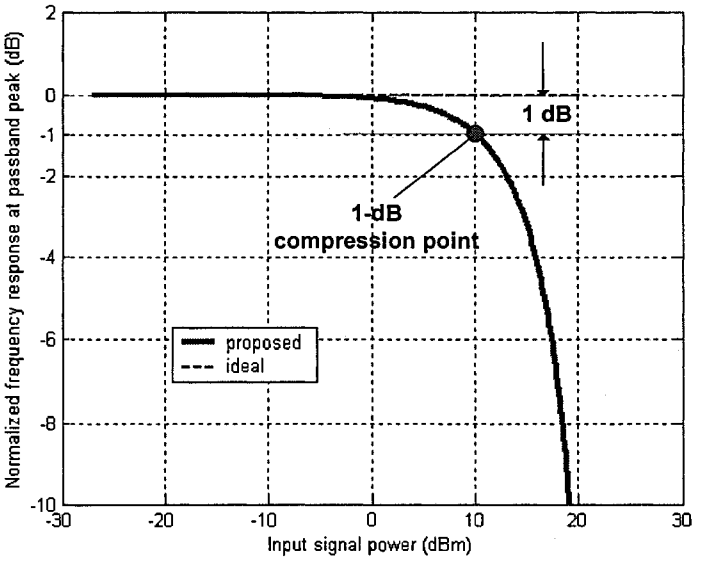

Fig. 11 Frequency response at the passband peak vs. input power.

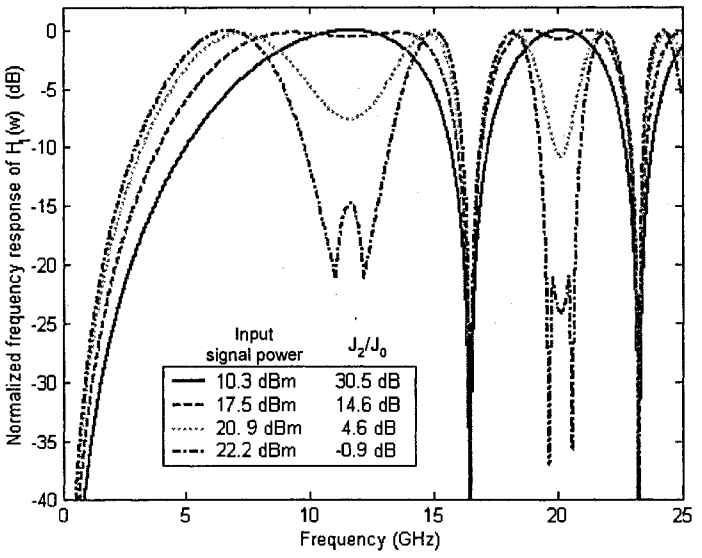

Fig. 12 Frequency responses of $H_1(\omega)$ for different input signal power levels at $m_p = \pi / 4.8V$.

In addition, if the input RF signal contains two frequency components ω_{m1} and ω_{m2}, the phase modulated optical field can be expressed as

$$E(t)=\sum_{n=-\infty}^{\infty}\sum_{k=-\infty}^{\infty}J_n(m_pV_1)\cdot J_k(m_pV_2)\cdot\cos[(\omega_c+n\omega_{m1}+k\omega_{m2})t+\frac{1}{2}n\pi+\frac{1}{2}k\pi], \qquad (12)$$

where V_1, V_2 represent the amplitudes of the modulating signal at frequency ω_{m1} and ω_{m2}, respectively. Inter-modulation products at $\omega_{m1}+\omega_{m2}$, $2\omega_{m1}+\omega_{m2}$, $\omega_{m1}+2\omega_{m2}$ as well as at the multiples of ω_{m1} and ω_{m2} may be generated. However, based on the earlier discussion if the power levels of the two signals are both below the 1-dB compression point, these components can be neglected, and the proposed bandpass microwave filter is linear.

5. Conclusions

Theoretical analysis and experimental implementation of an all-optical bandpass microwave filter were presented. In the proposed filter structure, an electro-optic phase modulator combined with a dispersive device was employed to eliminate the baseband resonance of a typical lowpass filter. In addition to the simple bandpass operation, the proposed filter has a better performance in terms of the MSR and the mainlobe bandwidth compared to the conventional microwave filters with windowing. A four-tap bandpass microwave filter with a 3-dB mainlobe bandwidth of 2.65 GHz and an MSR of 30-dB was demonstrated. Other issues, including the reconfigurability, tunability and upper limit of dynamic range, were also discussed. We should mention that thanks to the employment of a length of single mode fiber, the output of the proposed filter can be naturally distributed to a remote site, which provides an added advantage to the proposed filter, especially for radio-over-fiber applications. On the other hand, if the proposed filter is only used for local filtering, a dispersion-tunable linearly chirped fiber Bragg grating may be used to replace the fiber link as a dispersive device, the compactness of the proposed filter can be significantly improved.

References:

[1] K. Wilner and A. P. Van Den Heuvel, "Fiber-optic delay lines for microwave signal processing," Proc. IEEE, vol. 64, pp. 805-807, 1976.

[2] K. Jackson, S. Newton, B. Moslehi, M. Tur, C. Cutler, J. Goodman and H. J. Shaw, "Optical fiber delay-line signal processing," IEEE Trans. Microwave Theory Technol. vol. 33, pp. 193-204, Mar. 1985.

[3] S. Sampson, R. Griffin and D. Jackson, "Photonic CDMA by coherent matched filtering using time-address coding in optical ladder networks," J. Lightwave Technol., pp. 2001-2010, Nov. 1994.

[4] J. Capmany and J. Cascon, "Discrete time fiber-optic signal processors using optical amplifiers," J. Lightwave Technol., vol. 12, pp. 106-117, Jan. 1994.

[5] D. Norton, S. Johns, C. Keefer and R. Soref, "Tunable microwave filtering using high dispersion fiber time delays," IEEE Photon. Technol. Lett., vol. 6, pp. 831-832, Jul. 1994.

[6] D. B. Hunter, R. Minasian and P. A. Krug, "Tunable optical transversal filter based on chirped gratings," Electron. Lett., vol. 31, pp. 2207-2210, Dec. 1995.

[7] W. Zhang, J. A. R. Williams, and I. Bennion, "Polarization synthesized optical transversal filter employing high birefringence fiber gratings," IEEE Photon. Technol. Lett., vol. 13, pp. 523-525, May. 2001.

[8] V. Polo, B. Vidal, J. L. Corral, and J. Marti, "Novel tunable photonics microwave filter based on laser arrays and NxN AWG-based delay lines," IEEE Photon. Technol. Lett., vol. 15, pp. 584-586, Apr. 2003.

[9] K. Sasayama, M. Okuno and K. Habara, "Coherent optical transversal filter using silica-based waveguides for high-speed signal processing," J. Lightwave Technol., vol. 9, pp. 1225-1230, Oct. 1991.

[10] F. Coppinger, C. K. Madsen and B. Jalali, "Photonic microwave filtering using coherently coupled integrated ring resonators," Microwave Opt. Technol. Lett., vol. 21, pp. 90-93, Feb. 1999.

[11] S. Sales, J. Capmany, J. Marti, and D. Pastor, "Experimental demonstration of fiber-optic delay line filters with negative coefficients," Electron. Lett., vol. 31, pp. 1095-1096, Jul. 1995.

[12] F. Coppinger, S. Yegnanarayanan, P. D. Trinh, and B. Jalali, "All-optical RF filter using amplitude inversion in a semiconductor optical amplifier," IEEE Trans. Microwave Theory Tech., vol. 45, pp. 1473-1477, Aug. 1997.

[13] X. Wang and K. T. Chan, "Tunable all-optical incoherent bipolar delay-line filter using injection-locked Fabry-Perot laser and fiber Bragg gratings," Electron. Lett., vol. 36, pp. 2001-2002, Dec. 2000.

[14] S. Li, K. S. Chiang, W. A. Gambling, Y. Liu, L. Zhang, and I. Bennion, "A novel tunable all-optical incoherent negative-tap fiber-optic transversal filter based on a DFB laser diode and fiber Bragg gratings," IEEE Photon. Technol. Lett., vol. 12, pp. 1207-1209, Sept. 2000.

[15] J. Capmany, D. Pastor, A. Martinez, B. Ortega, and S. Sales, "Microwave photonics filters with negative coefficients based on phase inversion in an electro-optic modulator," Opt. Lett., vol. 28, pp. 1415-1417, Aug. 2003.

[16] J. Mora, M. V. Andres, J. L. Cruz, B. Ortega, J. Capmany, D. Pastor, and S. Sales, "Tunable all-optical negative multitap microwave filters based on uniform fiber Bragg gratings," Opt. Lett., vol. 28, pp. 1308-1310, Aug. 2003.

[17] E. H. W. Chan and R. A. Minasian, "Novel all-optical RF notch filters with Equivalent Negative Tap Response," IEEE Photon. Technol. Lett., vol. 16, pp. 1370-1372, May. 2004.

[18] D. B. Hunter and R. A. Minasian, "Microwave optical filters using in-fiber Bragg grating arrays," IEEE microwave. Guided Wave Lett., vol. 6, pp. 103-105, Feb. 1996.

[19] J. Capmany, D. Pastor and B. Ortega, "Efficient sidelobe suppression by source power apodization in fibre optic microwave filters composed of linearly chirped fibre grating by laser array," Electron. Lett., vol. 35, pp. 640-642, Apr. 1999.

[20] F. Zeng and J. P. Yao, "All-optical bandpass microwave filter based on an electro-optic phase modulator," Optics Express, vol. 12, pp. 3814-3819, Aug. 2004.

[21] G. J. Meslener, "Chromatic dispersion induced distortion of modulated monochromatic light employing direct detection," IEEE J. Quantum Electron., vol. 20, pp. 1208-1216, Oct. 1984.

[22] H. Schmuck, "Comparison of optical millimeter-wave system concepts with regard to chromatic dispersion," Electron. Lett., 1995, vol. 31, pp. 1848-1849, Nov. 1995.

[23] Y. Liu, J. P. Yao, X. Dong and J. Yang, "Tunable chirping of a fibre Bragg grating without center wavelength shift using simply supported beam," Optical Engineering, vol. 41, pp. 740-741, Apr. 2002.

3.4 A two-tap all-optical microwave bandpass filter with one negative tap

The filters discussed in Sec. 3.2 and Sec. 3.3 are microwave bandpass filters. The bandpass operation is realized by eliminating the baseband resonance with the dc notch of the transfer function of the PM-IM conversion. However, no negative taps are actually generated in the filters. Therefore, bandpass filtering with flat-top passband and larger mainlobe-to-sidelobe ratio is not possible. In this Section, we propose a novel method to realize an all-optical microwave bandpass filter with negative coefficients. Positive and negative coefficients are obtained through PM-IM conversion by reflecting the phase modulated optical carriers from linearly chirped fiber Bragg gratings with positive or negative dispersions. A two-tap transversal microwave filter with one negative coefficient is experimentally implemented.

All-optical microwave bandpass filter with negative coefficients based on an electro-optic phase modulator and linearly chirped fiber Bragg gratings[3]

Fei Zeng, *Student Member, OSA*, Jun Wang, and Jianping Yao, *Member, OSA*

Microwave Photonics Research Laboratory,
School of Information Technology and Engineering
University of Ottawa, Ottawa, Ontario, Canada.

Abstract

A novel all-optical microwave bandpass filter with negative coefficients is presented in this letter. Positive and negative coefficients are obtained through phase modulation to intensity modulation conversion, by passing the phase modulated optical carriers through chirped fiber Bragg gratings having group delay responses with positive and negative slopes. A two-tap transversal microwave filter with one negative coefficient is experimentally implemented.

All-optical microwave filters proposed in the last few years are mostly based on the incoherent manipulation of optical carriers with only positive taps and only lowpass filtering functionality can be realized. For many applications, such as radio-over-fiber systems, bandpass or flat-top filters are required. To overcome this limitation, several techniques [1-7] have been proposed in the last few years. Recently, we have reported a method to implement all-optical microwave bandpass filter with a simple structure [8], in which the baseband resonance of a typical lowpass filter is eliminated by using an electro-optic phase modulator (EOPM) combined with a dispersive device. In the proposed approach, the effective transfer function $H(\omega)$ is the multiplication of two frequency responses, i.e., a conventional lowpass frequency response $H_2(\omega)$ and a dispersion-induced phase modulation to intensity modulation (PM-IM) conversion $H_1(\omega)$. $H_1(\omega)$ has a notch at the dc frequency. Consequently, by carefully choosing the system parameters to let the second resonance peak of $H_2(\omega)$ locate exactly at the same position of the first peak of $H_1(\omega)$, one can ensure a frequency response equivalent to a

[3] Published in Optics Letters, vol. 30, no. 17, pp. 2203-2205, September 2005.

bandpass filter. It is different from the negative coefficient bandpass filters proposed in [2-7], however, no negative taps are actually generated in this approach. Therefore, bandpass filtering with flat-top passband and larger mainlobe-to-sidelobe ratio (MSR) is not possible with this approach. In this letter, we propose a novel method to realize an all-optical microwave bandpass filter with negative coefficients. Positive and negative coefficients are obtained through PM-IM conversion by reflecting the phase modulated optical carriers from linearly chirped fiber Bragg gratings (LCFBGs) with positive or negative dispersions.

The fundamental concept is shown in Fig. 1. Under small signal modulation condition, the phase modulated optical spectrum is illustrated on the left side of Fig. 1, which consists of an optical carrier (ω_o) and two first-order sidebands ($\omega_o - \omega_m, \omega_o + \omega_m$), where ω_m represents the modulating microwave frequency). At the output of the EOPM, the two sidebands are π out of phase. It is different from an IM where the two sidebands at the output of an intensity modulator are in phase. If the phase modulated signal is directly detected using a photodetector (PD), the modulating signal cannot be recovered and only a dc signal is observed because beating between the carrier and the upper sideband exactly cancels the beating between the carrier and the lower sideband. This behavior is expected since the PM does not alter the amplitude of the input optical carrier and the square-law PD works like an envelope detector. However, as shown in Fig. 1, if the modulated optical signal passes through a dispersive device, the phase relationship between any two optical frequency components will change due to the chromatic dispersion. When this dispersed optical signal is fed to a PD, the modulating signal can be recovered, which implies that the PM is converted to IM by the dispersive device. More interestingly, when $D = \partial\tau / \partial\omega > 0$ (the upper case in Fig. 1), the higher optical frequency component experiences more phase shift than that of the lower frequency component; and eventually the PM-IM conversion is fully achieved when all these three frequency components are exactly in phase. To the contrary, when $D = \partial\tau / \partial\omega < 0$ (the lower case in Fig. 1), the lower frequency component will experience more phase shift than the higher one, and the PM-IM conversion is fully obtained when the two sidebands have same phases but are π out of phase with the carrier. Consequently, the recovered RF signals from the different dispersive devices will have a π phase inversion, which can be directly applied to implement negative coefficients in an all-optical microwave filter.

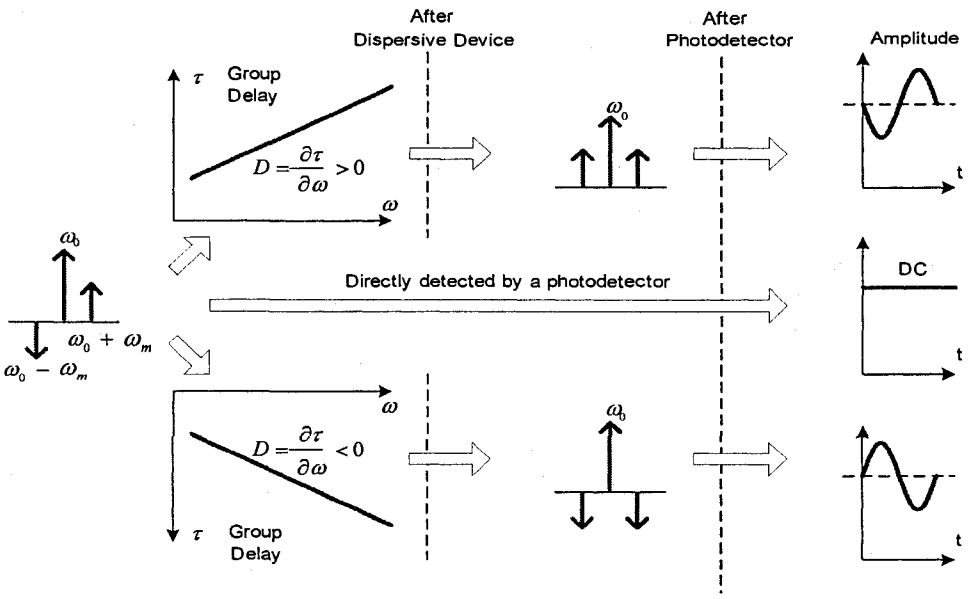

Fig. 1 Illustration of the recovered RF modulating signals that sustain a positive, zero or negative chromatic dispersion.

Mathematically, the recovered microwave signal from such a PM-IM conversion followed by a direct detection can be expressed by Eq. (1), which shows that the amplitude of the recovered RF signal, denoted as $E_{RF}(t)$, is the function of the system-induced dispersion as well as the modulating frequency [8],

$$E_{RF}(t) \propto \sin(\frac{1}{2} D\omega_m^2) \cdot \cos(\omega_m t + \varphi), \qquad (1)$$

where D is the chromatic dispersion of the dispersive device; and φ is the phase delay of the recovered microwave signal, which is also determined by D and ω_m. Based on Eq. (1), some important conclusions can be drawn to help us build a multi-tap microwave bandpass filter with negative coefficients. First, both positive and negative coefficients can be obtained by letting the phase modulated optical carriers experience chromatic dispersions with different signs, since $\sin(D\omega_m^2/2)$ is obviously an odd function. LCFBGs are a good candidate to be used as the dispersive devices since LCFBGs can provide very linear group delay (GD) profiles. The GD slope of an LCFBG can be easily reversed by connecting the optical input to the opposite port of the grating. Second, the PM-IM conversion efficiency reaches the maxima when

$\sin(D\omega_m^2/2) = \pm 1$, which implies that the free spectral range (FSR) of the proposed filter should be carefully designed to match the PM-IM conversion maxima; then an optimized filtering output can be obtained.

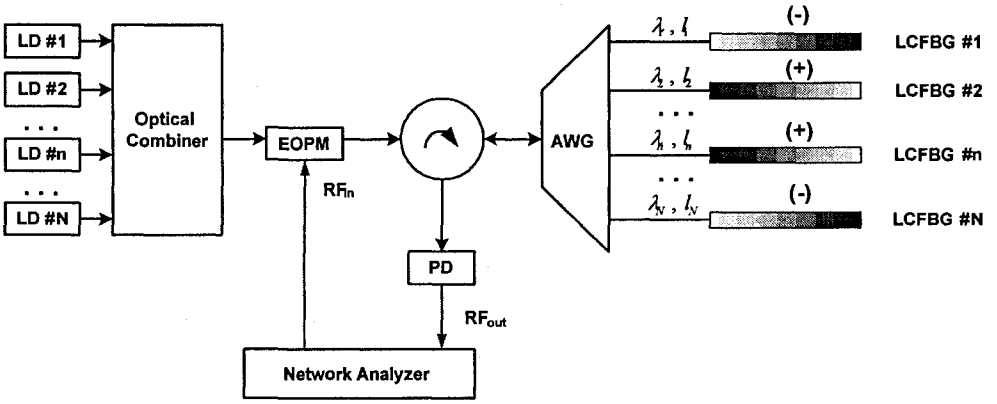

Fig. 2 System configuration of the proposed all-optical microwave bandpass filter with negative coefficients.

Based on the theoretical analysis, a fundamental architecture for the proposed filter is presented in Fig. 2. Optical carriers from an array of N laser diodes (LDs) emitting at $\lambda_1, \lambda_2, \cdots, \lambda_n, \cdots, \lambda_N$ are combined via an optical combiner and applied to an EOPM. Through an optical circulator, the modulated optical signals are de-multiplexed by an arrayed-waveguide grating (AWG) and fed to N LCFBGs via either the short wavelength or the long wavelength port, depending on whether the LCFBGs are employed to implement positive or negative taps. The reflected and dispersed optical signals are then multiplexed by the same AWG and sent to a PD to recover the modulating RF signal. The recovered RF signal can be expressed as a vector summation of the resulting electrical signals from the N carriers and the frequency response of the proposed all-optical microwave filter is then written as

$$H(\omega) \propto \sum P_n \cdot \sin(\frac{1}{2} D_n \omega_m^2) \cdot \exp[j\omega_m (n-1) \cdot \Delta\tau], \qquad (2)$$

where P_n and D_n represent the optical power of the n-th LD and the dispersion of the n-th LCFBG, respectively. Basically, P_n determines the weight of the n-th tap and the sign of D_n determines whether this tap is positive or negative. The length difference between any two

adjacent optical paths ($l_{n+1} - l_n = \Delta l,\ n = 1,2,\cdots,N-1$) determines the central frequency of the passband, i.e., $FSR = 1/\Delta\tau = c/2n_{eff} \cdot \Delta l$, where c is the optical wave propagation velocity in free space and n_{eff} is the effective refractive index. Although a multi-channel optical coupler can be used to replace the AWG, the use of AWG can reduce the system insertion loss and at the same time eliminate the inter-tap interference. The LCFBGs are required to have different central wavelengths corresponding to those of the LD array. The lengths and chirp rates of the LCFBGs should be identical to ensure that the dispersions of the LCFBGs are identical in magnitude. The small implementation error of the delay line length of the fiber link between the AWG and each LCFBG can be accurately compensated by slightly tuning the corresponding LD wavelength to be reflected at different positions in the LCFBG.

To prove the fundamental concept of this approach, a two-tap microwave filter with one negative coefficient is experimentally implemented. Two LCFBGs are fabricated through one linearly chirped phase mask. By applying different tension to the fiber during the UV exposing process, a central wavelength shift of 0.7 nm is achieved. A Gaussian apodization profile is applied to flatten and smooth the reflectivity response and the group delay ripples. Both gratings have a length of 8 cm. The measured GD and reflectivity responses for both gratings, one is measured at the short wavelength port (denoted as LCFBG#1) and the other one is measured at the long wavelength port (denoted as LCFBG#2), are shown in Fig. 3, from which the average dispersion of LCFBG#1 and LCFBG#2 are calculated to be 1350 ps/nm and -1327 ps/nm, respectively.

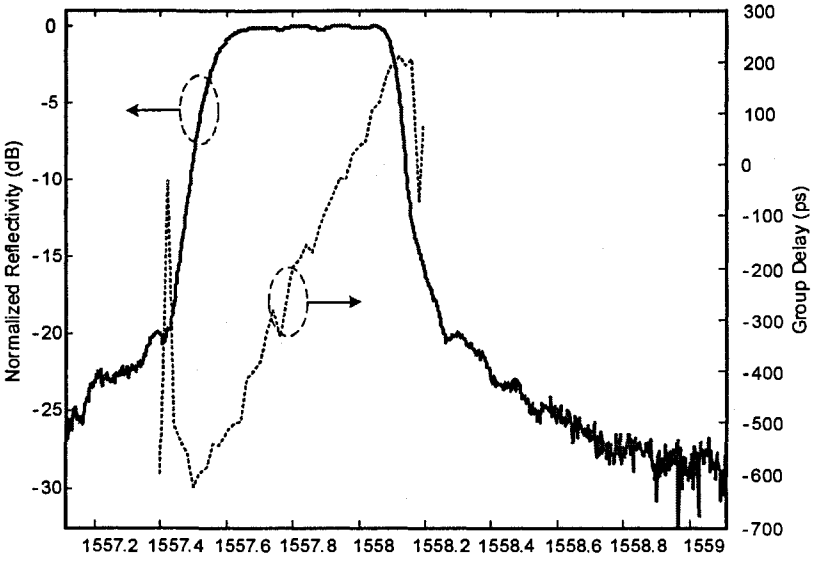

(a)

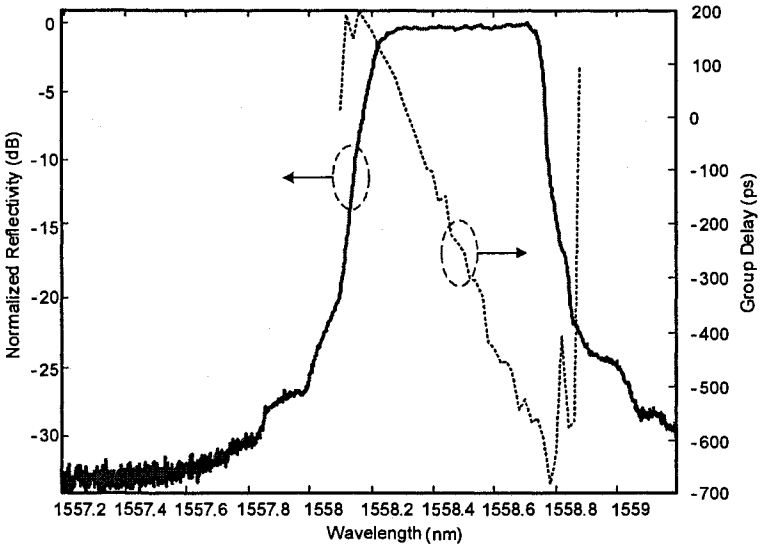

(b)

Fig. 3 Measured reflectivity and GD responses of (a) LCFBG#1 and (b) LCFBG#2.

Two tunable LDs emitting at λ_1 and λ_2 with identical output power levels and typical linewidth of 150-KHz are applied as the light sources. Since no AWG is available at the time of experiment, a 3-dB coupler is used replacing the AWG. First, the wavelengths of the two LDs are tuned to be reflected by LCFBG#1 via the same port, as shown in Fig. 4(a), in which these two phase-modulated optical signals are reflected from different positions of LCFBG#1 but the experienced dispersions are identical thanks to the linearity of the GD profile. The frequency

response of the implemented filter observed from the network analyzer is shown in Fig. 4(b). The measured FSR is about 2.4 GHz, corresponding to a time interval of 417 ps. Comparing the measured frequency response with the simulated lowpass response $H_2(\omega)$, it is clearly seen that the baseband resonance of the lowpass filter is eliminated due to the PM-IM conversion. This situation is the same as our approach demonstrated in [8], which can be considered as an equivalent bandpass filter with all positive coefficients. However, by keeping λ_1 fixed while λ_2 is tuned to be reflected by LCFBG#2, as shown in Fig. 5(a), which has a reversed GD slope with respect to that of LCFBG#1. The measured frequency response of the proposed microwave filter is shown in Fig. 5(b). In this case, the FSR is 2.25 GHz, corresponding to a time interval of 444 ps. It is observed from Fig. 5(b) that $H_2(\omega)$ has a transfer function corresponding to a bandpass filter and a negative coefficient is indeed obtained. By comparing the frequency responses in Fig. 4(b) and in Fig. 5(b), we can see that the lowpass resonance of the bandpass-equivalent filter is only partially suppressed by the dc notch generated by the PM-IM conversion, a relatively high sidelobe at the low frequency is observed. For the frequency response in Fig. 5(b), since it is a true bandpass filter with a negative tap, no lowpass resonance exists in the frequency response; a frequency response with higher MSR (15 dB improvement) is obtained.

In conclusion, a novel approach to implementing all-optical microwave bandpass filter with negative coefficients were proposed and demonstrated. The proposed filter has a very simple structure with positive or negative coefficients obtained through PM-IM conversion by reflecting the phase modulated optical carriers from the regular LCFBGs with positive or negative GD slopes. A two-tap microwave bandpass filter with one negative tap was demonstrated, it has a better MSR compared to the bandpass-equivalent filter with all-positive taps. More taps with either positive or negative weights can be easily realized by simply adding more LCFBGs, which provides the possibility to implement microwave bandpass filters with flat-top response and high MSR. For practical applications, the proposed filter can be miniaturized by using matured DWDM light sources. The size can be further reduced with better performance if the chirped gratings can be integrated with the AWG on a single substrate.

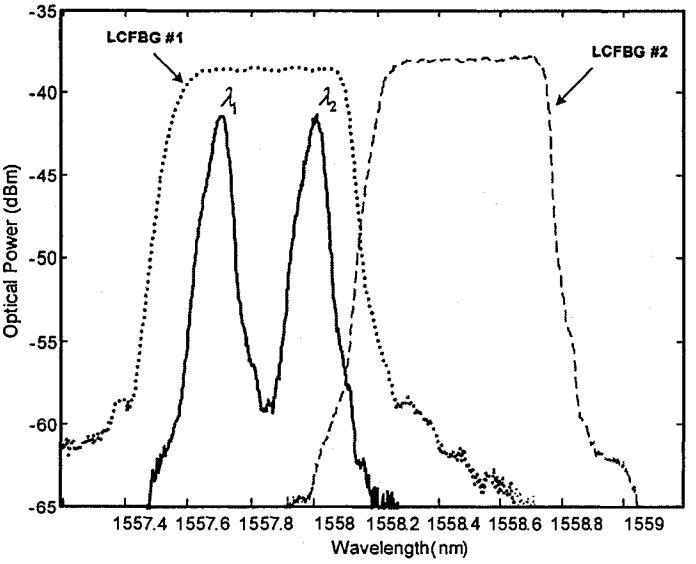

(a)

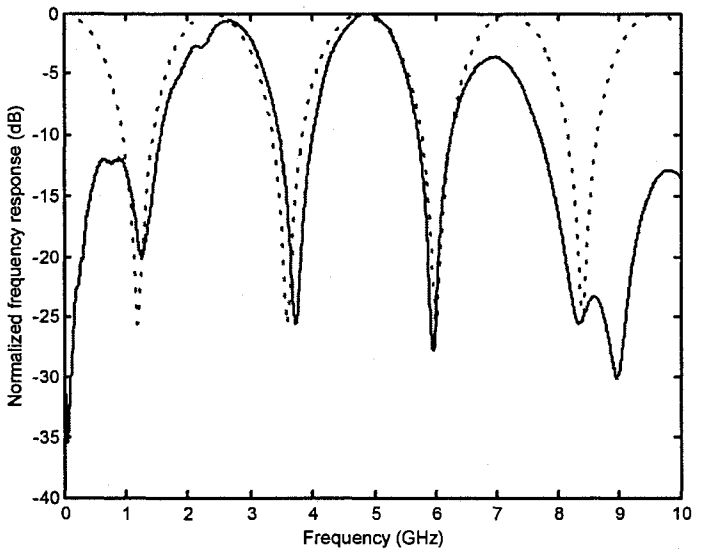

(b)

Fig. 4 Experimental results of the implemented filter with two positive taps. (a) Measured optical spectrum (solid line) before the PD when both LDs are reflected from the same port of LCFBG#1; (b) frequency responses: measured $H(\omega)$ (solid line) and simulated $H_2(\omega)$ (dotted line) which shows a lowpass filtering.

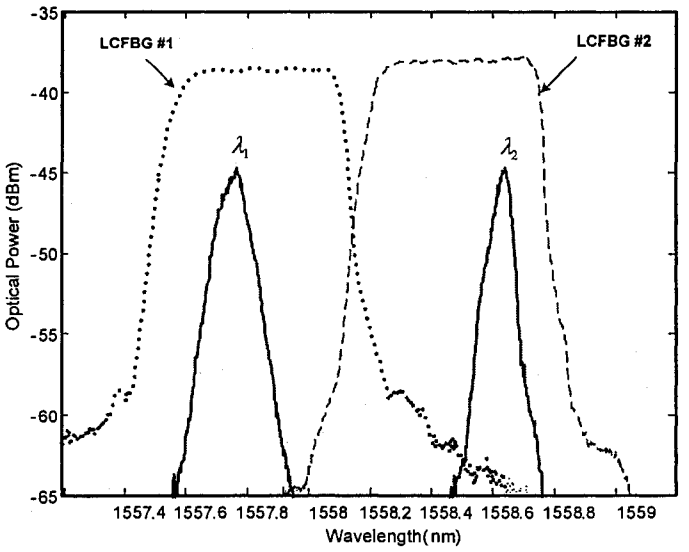

(a)

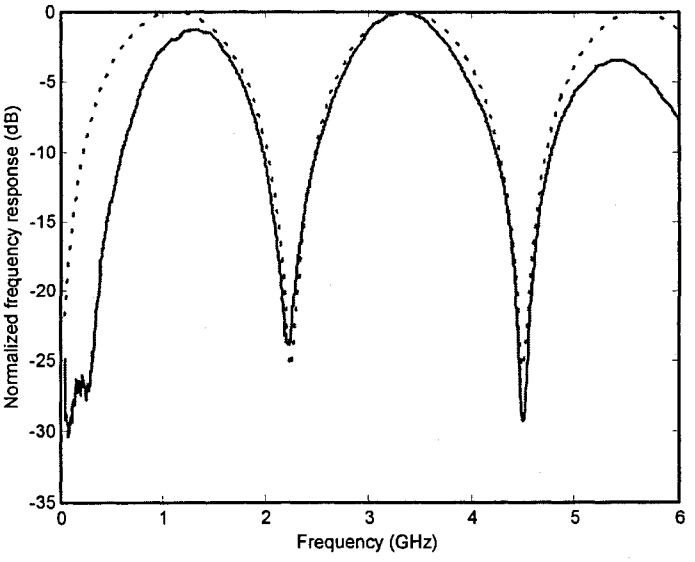

(b)

Fig. 5 Experimental results of the two-tap filter with one negative coefficient. (a) Measured optical spectrum (solid line), when λ_1 is reflected by LCFBG#1 from the short wavelength port and λ_2 is reflected by LCFBG#2 from the long wavelength port; (b) frequency responses: measured $H(\omega)$ (solid line) and simulated $H_2(\omega)$ (dotted line) which shows a bandpass filtering with one negative tap.

References:

[1] S. Sales, J. Capmany, J. Marti, and D. Pastor, Electron. Lett. 31, 1095 (1995).

[2] F. Coppinger, S. Yegnanarayanan, P. D. Trinh, and B. Jalali, IEEE Trans. Microwave Theory Tech. vol. 45, 1473 (1997).

[3] X. Wang and K. T. Chan, Electron. Lett. 36, 2001 (2000).

[4] S. Li, K. S. Chiang, W. A. Gambling, Y. Liu, L. Zhang, and I. Bennion, IEEE Photon. Technol. Lett. 12, 1207 (2000).

[5] J. Capmany, D. Pastor, A. Martinez, B. Ortega, and S. Sales, Opt. Lett. 28, 1415 (2003).

[6] E. H. W. Chan and R. A. Minasian, IEEE Photon. Technol. Lett. 16, 1370 (2004).

[7] J. Mora, M. V. Andres, J. L. Cruz, B. Ortega, J. Capmany, D. Pastor, and S. Sales, Opt. Lett. 28, 1308 (2003).

[8] F. Zeng and J. P. Yao, Opt. Express 12, 3814 (2004), http://www.opticsexpress.org.

CHAPTER 4

ALL-OPTICAL MICROWAVE MIXING AND FILTERING

In addition to all-optical microwave bandpass filtering, the use of an EOPM can also perform all-optical microwave frequency mixing. As we have discussed in Chapter 2, if the phase modulation depth is large, the higher-order harmonics and inter-modulation products of the modulating signal will be obtained after a proper PM-IM conversion and a direct detection. For example, if a two-tone (f_1 and f_2) microwave signal is applied to an EOPM, besides the signals at f_1 and f_2, their higher-order harmonics ($2f_1$, $2f_2$, $3f_1$, $3f_2$ ...) and inter-modulation terms ($|f_1 \pm f_2|$, $|2f_1 \pm f_2|$, $|f_1 \pm 2f_2|$, ...) will also be generated. Microwave frequency mixing can find applications for subcarrier up- and down-conversion in radar and radio communication systems. However, usually only the up-converted signal at $f_1 + f_2$ or the down-converted signal at $f_2 - f_1$ (assume $f_2 > f_1$) is desired, proper bandpass filtering must be performed to suppress the unwanted frequency components.

In this chapter, an electrooptic phase modulation based all-optical signal processor that can perform both microwave mixing and bandpass filtering simultaneously in a radio-over-fiber link will be presented. First, in Sec. 4.1, a prove-of-concept experiment to up convert a subcarrier frequency from 3 GHz to 11.8 GHz using an EOPM-based signal processor with a local oscillator frequency of 8.8 GHz in a 25-km SMF link is carried out. Then, in Sec. 4.2, a further investigation of subcarrier frequency up conversion with data modulation is performed. The system performance is also studied.

4.1 All-optical microwave mixing and bandpass filtering

In this Section, an all-optical microwave signal processor that can perform microwave mixing and bandpass filtering simultaneously in a radio-over-fiber link is proposed and demonstrated. The system consists of a multiwavelength laser source, an EOPM, a length of SMF, and a PD. Two microwave tones ($f1$ and $f2$) are mixed in the EOPM and the mixed optical signals after the EOPM are then applied to the SMF link that serves as a dispersive device as well as a transmission medium. The up-converted microwave tone ($f1 + f2$) is obtained at the output of the PD located at the end of the fiber span. Other unwanted mixing products are rejected.

All-optical microwave mixing and bandpass filtering in a radio-over-fiber link[4]

Fei Zeng, *Student Member, IEEE* and Jianping Yao, *Senior Member, IEEE*

Microwave Photonics Research Laboratory
School of Information Technology and Engineering
University of Ottawa, Ottawa, Ontario, Canada
Email: jpyao@site.uottawa.ca

Abstract

An all-optical signal processor that performs both microwave mixing and bandpass filtering in a radio-over-fiber link is proposed and demonstrated. The key device in the processor is an electro-optic phase modulator which performs all-optical microwave mixing. The microwave bandpass filtering is realized by passing the mixed microwave signals through a length of single mode fiber, which acts as a dispersive device. Up- or down-converted microwave signal is obtained and other unwanted frequency components are rejected at the end of the fiber span. The use of the proposed signal processor to perform an up-conversion of a microwave signal from 3 GHz to 11.8 GHz in a 25-km fiber link is demonstrated.

Index terms: Electro-optic phase modulation, chromatic dispersion, all-optical microwave mixing, all-optical microwave filtering, bandpass filter, radio-over-fiber.

1. Introduction

Radio-over-fiber technologies are of great interest for many potential applications such as broadband wireless access networks, sensor networks, radar and satellite communication systems, and have been extensively studied in the last few years. The key function of a radio-over-fiber network is to distribute microwave and millimeter-wave signals over optical fiber to take the advantages of the low loss, low dispersion and large bandwidth of optical fiber links. On the other hand, it is also highly desired that the distributed signals can be processed directly in the fiber link without optical/electrical (O/E) and electrical/optical (E/O) conversions, such as

[4] Published in IEEE Photonics Technology Letters, vol. 17, no. 4, pp. 899-901, April 2005.

all-optical microwave mixing and filtering. Many papers have been published in the last two decades for all-optical microwave mixing [1-4] and filtering [5-9]. However, to the best of our knowledge, no approaches have been proposed to implement simultaneously all-optical microwave mixing and all-optical microwave filtering over a fiber link. In this paper, we propose an approach to perform both all-optical microwave mixing and bandpass filtering in a radio-over-fiber link using an electro-optic phase modulator (EOPM) and a length of single mode fiber (SMF). The first function of the EOPM is to perform all-optical microwave mixing. The mixed signals at the output of the EOPM are then fed to the SMF link, which acts as a dispersive device for bandpass filtering, and distributes the mixed signal to a remote site. The combination of the EOPM, a multiwavelength laser source and the SMF link forms an all-optical microwave bandpass filter [10], which can be designed to have a passband located at the up- or down-converted microwave frequency. Frequency components other than the up-converted or down-converted frequency component will be rejected. In addition to achieving bandpass filtering, the use of an EOPM has some other advantages over an intensity modulator, which include a lower insertion loss, no bias control and simpler system design. Experiments are performed to evaluate the effectiveness of the proposed signal processor. The results show that an up-conversion of a microwave signal from 3 GHz to 11.8 GHz is achieved while other unwanted signal components are rejected at the end of the fiber link of 25 km.

2. Principle

The block diagram of the proposed signal processor is shown in Fig. 1. The signal processor consists of a multiwavelength laser source, an EOPM and a length of SMF. The light from the multiwavelength laser source is applied to the EOPM through a polarization controller (PC). A microwave signal at frequency f_S is to be up-converted to $f_S + f_{LO}$, where f_{LO} is the frequency of the local oscillator signal. Both signals are applied to one port of the phase modulator via a power combiner. The other port of the phase modulator is terminated in a load. The mixed optical signals after the EOPM are then applied to the SMF link serving as a dispersive device as well as a transmission medium. The up-converted (or down-converted) electrical signal is obtained at the output of a photodetector located at the end of the fiber link.

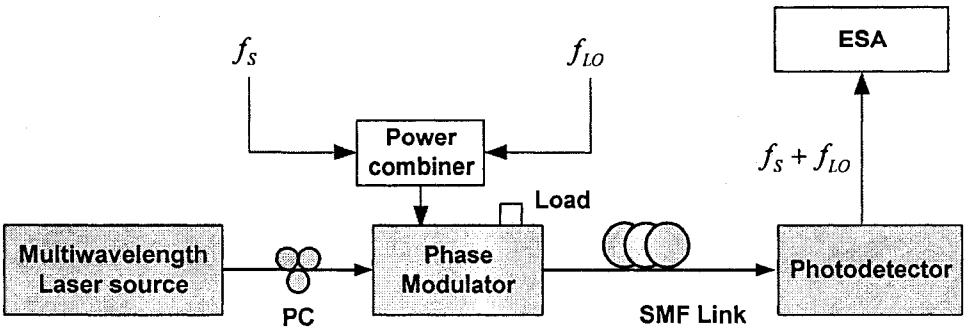

Fig. 1 Block diagram of the proposed all-optical microwave signal processor.
ESA: electrical spectrum analyzer.

The electrical signals applied to the EOPM have two frequencies at f_S and f_{LO}, the phase modulated optical field can be expressed in terms of Bessel functions of the first kind,

$$E(t)=\sum_{i=1}^{I}\sum_{n=-\infty}^{+\infty}\sum_{k=-\infty}^{+\infty}J_n[m_p(\omega_S)V_S]\cdot J_k[m_p(\omega_{LO})V_{LO}]\cdot\cos[(\omega_{c,i}+n\omega_S+k\omega_{LO})t+\frac{1}{2}n\pi+\frac{1}{2}k\pi] \tag{1}$$

where $\omega_{c,i}$ is the angular frequency of the i-th optical carrier; $m_p(\omega)$ represents the effective phase modulation index, which is a function of the microwave frequency; V_S and V_{LO} are the amplitudes of the modulating microwave signals applied to the input port of the phase modulator at frequencies of ω_S and ω_{LO}, respectively; n and k are integers representing the orders of the harmonics; and $J_n[\bullet]/J_k[\bullet]$ denotes the n-th/k-th order Bessel function of the first kind. To simplify, the argument $(m_p(\omega)V)$ will be omitted in the remainder of the paper. From Eq. (1), we can find that the phase modulated optical field consists of multiple carriers and a series of sidebands with amplitudes determined by the Bessel functions. For each carrier, the corresponding sidebands have frequency deviations from the carrier of $\pm\omega_S$, $\pm\omega_{LO}$, $\pm 2\omega_S$, $\pm 2\omega_{LO}$, ..., and $\omega_{LO}\pm\omega_S$, $2\omega_S\pm\omega_{LO}$, $2\omega_{LO}\pm\omega_S$, $\cdots$. Meanwhile, based on the property of the Bessel function of the first kind,

$$\begin{aligned} &J_n=-J_{-n}, J_k=-J_{-k}, \quad \textit{when } n,\ k \textit{ are odd} \\ &J_n=J_{-n}, J_k=J_{-k}, \quad \textit{when } n,\ k \textit{ are even} \end{aligned}, \tag{2}$$

we can see that the odd-order sidebands (when $|n+k|$ is odd) of each pair is π out of phase. If this phase-modulated optical signal is directly detected (DD) using a photodiode, no microwave signal but a dc can be obtained. This behavior is expected since the PM does not alter the amplitude of the input optical carrier, and the square-law photodetector works like an envelope detector. However, if the phase modulated optical signal passes through a dispersive device, for example, a section of SMF, the phase relationship between any two optical frequency components will be changed due to the chromatic dispersion of the SMF. When this dispersed optical signal is fed to a photodetector, microwave signals with different frequencies may be obtained, which indicates that the PM is converted to IM by the dispersive SMF and a microwave mixing function is achieved.

Furthermore, since here we use a multiwavelength laser source and assume each lasing wavelength is independent; eventually the output RF signal at each mixing frequency is a vector summation of all the corresponding electrical signals carried by the different wavelengths with different delays. This summation may be constructive or destructive depending on the frequency of the mixing product and the dispersion of the SMF: a transversal microwave filtering function is also achieved. The frequency response can be approximated as [10]

$$H(\omega) \propto \underbrace{\cos\left(\frac{\pi \overline{\chi_i \lambda_i}^2 f^2}{c} + \frac{\pi}{2}\right)}_{H_1(\omega)} \cdot \underbrace{\sum_{i=1}^{I} P_i \cdot \exp[j 2\pi f (i-1) T]}_{H_2(\omega)}, \tag{3}$$

where $\overline{\chi_i}$ and $\overline{\lambda_i}$ denote the average accumulated dispersion and the mean value of the optical carrier wavelengths; P_i represents the power of the i-th optical carrier; $T = \overline{\chi_i} \cdot \Delta\lambda$ is the time interval between any two adjacent taps; $H_1(\omega)$ represents the effects of PM-IM conversion, which has a quasi-periodic frequency response with a notch at the dc frequency and the first resonance peak at $f_1 = \sqrt{c/2\overline{\chi_i \lambda_i}^2}$ (let $H_1(\omega) = -1$); and $H_2(\omega)$ is a typical frequency response of an all-optical transversal lowpass filter, which has a periodic frequency response with the first resonance peak at the dc and the second resonance peak at $f_2 = 1/T = 1/(\overline{\chi_i} \cdot \Delta\lambda)$ (it is also the FSR of $H_2(\omega)$). The effective transfer function $H(\omega)$ of the proposed filter is

expressed as the multiplication of these two responses. By choosing proper $\overline{\chi_i}$, $\overline{\lambda_i}$, and $\Delta\lambda$ to make $f_1 = f_2$, an equivalent bandpass filter is achieved, because the baseband resonance of $H_2(\omega)$ is eliminated by the notch of $H_1(\omega)$ at dc.

Based on the above analysis, if the passband peak of the proposed microwave bandpass filter is located at the frequency of the desired mixing product, the proposed system can perform simultaneously all-optical microwave mixing and bandpass filtering.

3. Experiment and results

The signal processor based on the block diagram shown in Fig. 1 is built. The experiment is carried in four steps.

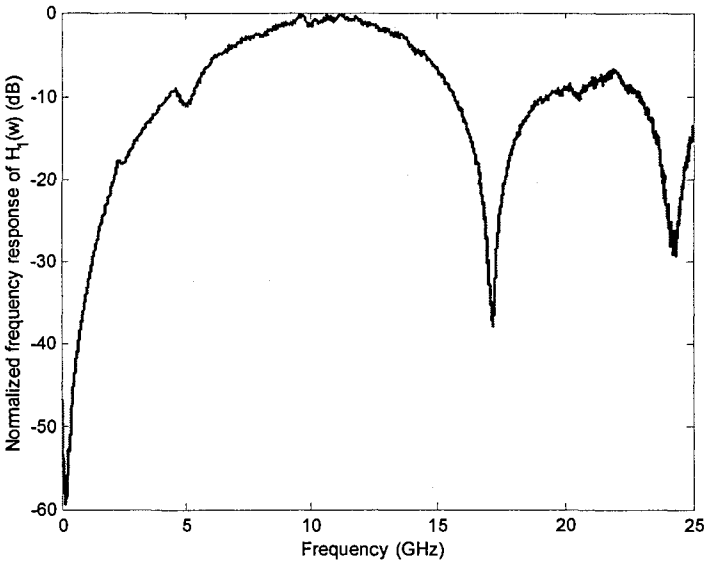

Fig. 2 Frequency response of the PM-IM conversion. A notch is observed at the dc frequency.

Step 1: *PM-IM conversion.* Instead of using a multiwavelength laser, a single-wavelength laser diode (LD) with a wavelength of 1550 nm is used as the light source. A 25-km standard SMF-28 fiber is employed as the dispersive device. The SMF-28 fiber has a chromatic dispersion of $17ps/nm \cdot km$ at 1550 nm. 25 km of this fiber has an accumulated dispersion of $\chi = 425ps/nm$. To experiment the PM-IM conversion, a single microwave signal is applied to the phase modulator. By sweeping the modulating frequency from 45 MHz to 25 GHz while

keeping the same output power of 3 dBm, we obtain the recovered microwave signal at the output of the photodetector. The output signal power versus the microwave frequency is shown in Fig. 2. We can see that the PM-IM conversion has a quasi-periodic frequency response with a notch at the dc frequency.

Step 2: *Microwave Mixing*. Keeping the LD as the light source, instead of using a single microwave signal, we use two microwave signals operating at frequencies of $f_S = 3$ GHz and $f_{LO} = 8.8$ GHz to drive the phase modulator. The power level for both signals is 17 dBm. The recovered microwave signals which consist of different frequency components are monitored using an ESA. As can be seen in Fig. 3, a series of microwave signals which correspond to the different frequency components of the mixing product are observed. Note that the power levels of the signals at f_S and f_{LO} are higher than the up-converted signal $f_S + f_{LO}$, Also the power levels of the higher-order harmonics ($2f_S$, $3f_S$, $2f_{LO}$, $\cdots$) and other unwanted inter-modulation products ($f_{LO} - f_S$, $2f_{LO} - 2f_S$, $2f_{LO} - f_S$, $2f_S + f_{LO}$, $3f_S + f_{LO}$, $\cdots$) are comparable to that of the $f_S + f_{LO}$ component. Therefore, a bandpass filter with narrow passband and high mainlobe to sidelobe ratio (MSR) must be used to suppress the unwanted frequency components.

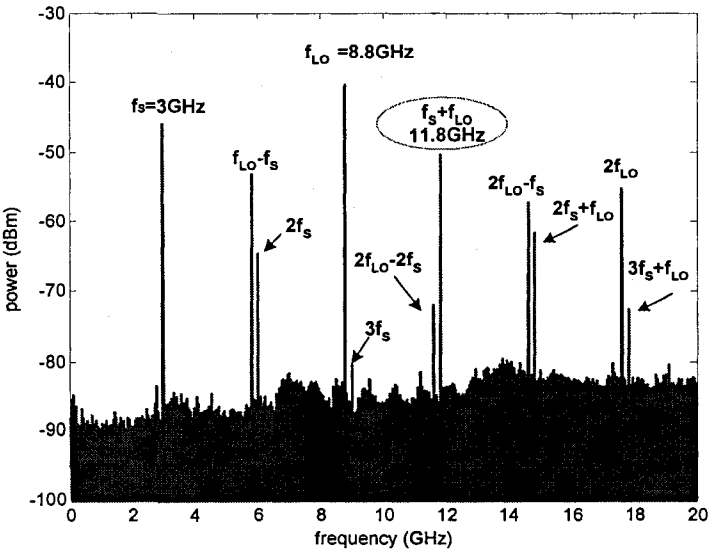

Fig. 3 Electrical spectrum of the signal at the output of the mixer, which consists of different mixing frequency components.

Step 3: *All-optical microwave bandpass filtering.* To achieve microwave filtering with very narrow bandwidth, the number of taps must be large. Many taps can be realized by using an array of LDs, but with a complicated and costly system. To simplify the signal processor, in the experiment instead of using an array of LDs, we use a multiwavelength fiber ring laser with about 30 wavelengths and a wavelength spacing of 0.2 nm proposed recently by us [11]. The key problem to be solved for achieving multiwavelength lasing with small wavelength spacing at room temperature is the homogeneous line broadening, which leads to cross gain saturation. Different wavelengths are competing for the gain, no stable lasing is possible. To achieve stable multiwavelength lasing at room temperature, in the laser cavity, a semiconductor optical amplifier (SOA) is incorporated in the ring cavity with a low-voltage low-frequency sinusoidal signal applied to the SOA. The SOA is operating as a phase modulator, which suppresses significantly the homogeneous line broadening. Stable multiwavelength lasing up to 30 wavelengths with wavelength spacing of 0.2 nm at room temperature is achieved. The output power spectrum of the multiwavelength laser is shown in Fig. 4.

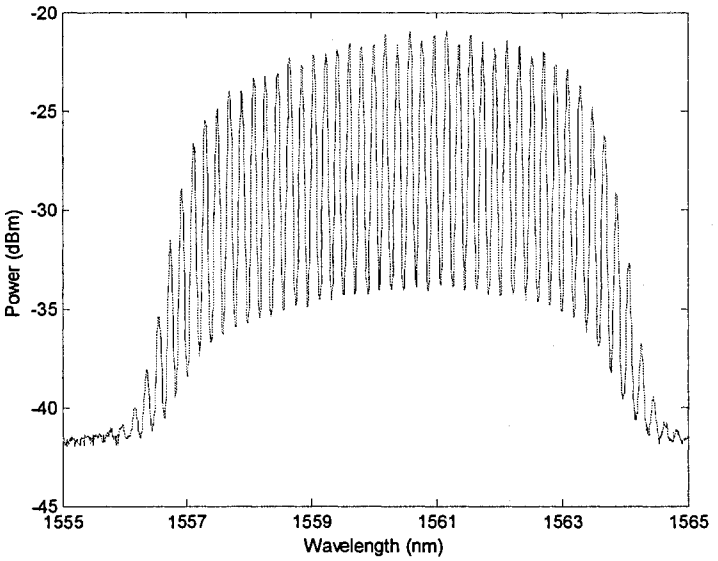

Fig. 4 Output power spectrum of the multiwavelength fiber laser

Using this multiwavelength laser as the light source and sweeping the modulating frequency from 45 MHz to 25 GHz, we obtain the frequency response of the proposed signal processor, as shown in Fig. 5. It can be seen that that the baseband resonance of the conventional IM-DD based all-optical microwave lowpass filter is eliminated. A bandpass filter with a 3-dB

mainlobe bandwidth of 330 MHz and an MSLR of 30 dB is achieved. The RF frequency at the peak of the passband is of 11.8 GHz and is determined by the wavelength spacing of the multiwavelength light source and the accumulated dispersion of the 25-km SMF link, which agrees well with the theoretical value (11.9 GHz) calculated from Eq. (3).

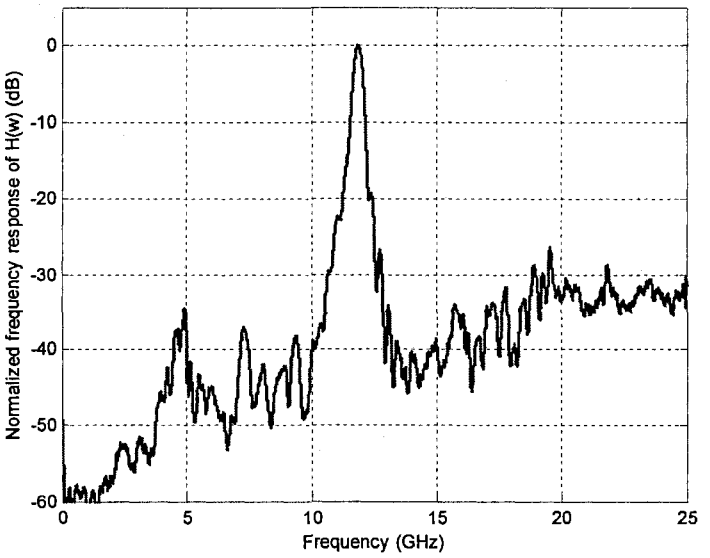

Fig. 5 Frequency response of the bandpass filter.

Step 4: *All-optical microwave mixing and bandpass filtering.* Using the multiwavelength fiber ring laser as the light source, and applying the two signals ($f_S = 3$ GHz and $f_{LO} = 8.8$ GHz) to the phase modulator, we obtain the up-converted microwave signal at the output of the photodetector. As can be seen from Fig. 6, only the up-converted component at $f_S + f_{LO}$ is obtained while other frequency components are efficiently suppressed. The zoom-in spectrum with a span of 30 KHz at $f_S + f_{LO}$ is also shown as an insert in Fig. 6, which exhibits a high quality up-converted signal. Compared with the results shown in Fig.3, a good rejection (better than 40 dB) of the unwanted frequency components is achieved. We should also note that thanks to the use of the SMF link as the dispersive device, the up-converted signal can be naturally distributed to a remote station over a 25 km span, which provides an added advantage of the proposed system. If further dispersion management is applied, the microwave distribution distance will be flexible. It should be mentioned here that due to the poor efficiency of the O/E and E/O conversions, a large RF conversion loss of about 70 dB is observed in our experimental

implementation. However, we believe that this problem can be mitigated by applying either a photodetector with a better responsivity, or a phase modulator with a smaller half-wave voltage $V_\pi(f)$. The insertion loss can also be compensated by using an erbium doped fiber amplifier (EDFA).

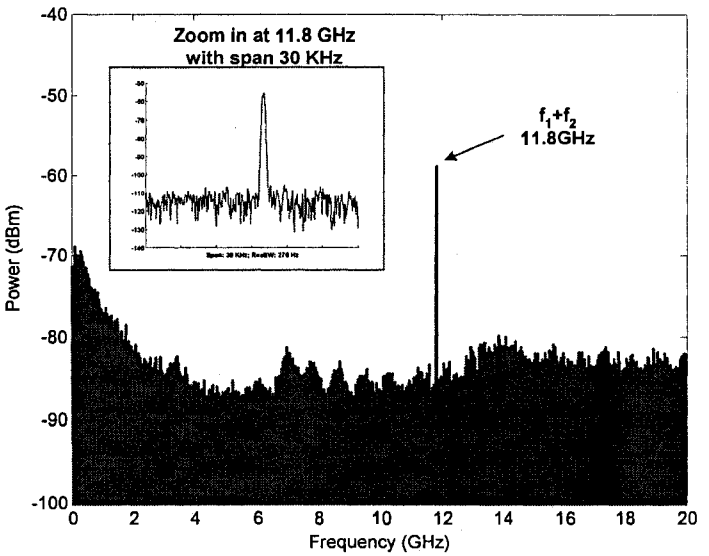

Fig. 6 Power spectrum at the output of the photodetector. Only the up-converted signal at 11.8 GHz is obtained and other frequency components are rejected.

4. Conclusion

In this paper, we demonstrated a novel all-optical signal processor that performed simultaneously all-optical microwave mixing and bandpass filtering in a radio-over-fiber link. Since a length of SMF was used in the system as a dispersive device, the up-converted microwave signal was generated at a remote site. Experimental results showed the up-converted signal was obtained at the remote site with a high rejection of other unwanted frequency components. The proposed signal processor can be used for frequency up-conversion or down-conversion and the converted signal can be distributed to a desired distance by properly designing the wavelength spacing of the multiwavelength laser and properly managing the dispersion of the fiber link, which will find many interesting applications in radio-over-fiber systems.

References:

[1] G. K. Gopalakrishnan, W. K. Burns and C. H. Bulmer, "Microwave-optical mixing in $LiNbO_3$ modulators," IEEE Trans. Microwave Theory Tech., vol. 41, no. 12, pp. 2383-2391, Dec. 1993.

[2] J. L. Corral, J. Marti and J. M. Fuster, "General expressions for IM/DD dispersive analog optical links with external modulation or optical up-conversion in a Mach-Zehnder electrooptical modulator," IEEE Trans. Microwave Theory Tech., vol. 49, no. 10, pp. 1968-1976, Oct. 2001.

[3] G. Maury, A. Hilt, T. Berceli, B. Cabon and A. Vilcot, "Microwave-frequency conversion methods by optical interferometer and photodiode," IEEE Trans. Microwave Theory Tech., vol. 45, no. 8, pp. 1481-1485, Aug. 1997.

[4] J. Marti, F. Ramos, V. Polo, J. M. Fuster and J. L. Corral, "Millimeter-wave generation and harmonic upconversion through PM-IM conversion in chirped fibre gratings," Electron. Lett., vol. 35, no. 15, pp. 1265-1266, Jul. 1999.

[5] K. P. Jackson, S. A. Newton, B. Moslehi, M. Tur, C. C. Cutler, J.W. Goodman and H. J. Shaw, "Optical fiber delay line signal processing," IEEE Trans. Microwave Theory Tech., vol. MTT-33, pp. 193-209, Mar. 1985.

[6] D. B. Hunter, R. Minasian and P. A. Krug, "Tunable optical transversal filter based on chirped gratings," Electron. Lett., vol. 31, no. 25, pp. 2207-2210, Dec. 1995.

[7] G. Yu, W. Zhang, and J. A. R. Williams, "High-performance microwave transversal filter using fiber Bragg grating arrays," IEEE Photon. Technol. Lett., vol. 12, no. 9, pp. 1183-1185, Sep. 2000.

[8] J. Capmany, D. Pastor, A. Martinez, B. Ortega, and S. Sales, "Microwave photonics filters with negative coefficients based on phase inversion in an electro-optic modulator," Opt. Lett., vol. 28, pp. 1415-1417, Aug. 2003.

[9] E. H. W. Chan and R. A. Minasian, "Novel all-optical RF notch filters with Equivalent Negative Tap Response," IEEE Photon. Technol. Lett., vol. 16, no. 5, pp. 1370-1372, May. 2004.

[10] F. Zeng and J. P. Yao, "All-optical bandpass microwave filter based on an electro-optic phase modulator," Optics Express, vol. 12, no. 16, pp. 3814-3819, Aug. 2004.

[11] J. Yao and J. P. Yao, Z. Deng and J. Liu, "Stable multiwavelength erbium-doped fiber ring laser," Proc. SPIE Photonics North 2004, vol. 5577, Ottawa, Canada, Sep. 2004

4.2 Performance investigation of subcarrier frequency up conversion

In Sec. 4.1, a subcarrier frequency at 3 GHz was successfully up converted to 11.8 GHz, with other unwanted frequency components being rejected by an all-optical microwave bandpass filter. In that experiment, no baseband information was carried by the subcarrier. The work to be reported in this Section is a continuation of the work presented in Sec. 4.1, to investigate the performance of the proposed signal processor when a digital baseband signal is carried by the microwave tone (the subcarrier).

Demonstration of a Phase-Modulator-Based All-optical Microwave Mixing and Filtering System for Radio-Over-Fiber Applications[5]

Fei Zeng, Jianping Yao,

Microwave Photonics Research Laboratory,
School of Information Technology and Engineering,
University of Ottawa, 800 King Edward Avenue, P.O. Box 450, Stn. A,
Ottawa, ON, Canada, K1N 6N5

Abstract

In this paper an all-optical signal processor that performs both microwave mixing and bandpass filtering in a radio-over-fiber link is proposed and demonstrated. The frequency mixing is achieved by applying a local oscillator frequency and a BPSK modulated subcarrier to an electrooptic phase modulator. The mixed signals at the output of the electrooptic phase modulator are then fed to a single mode fiber link, which acts as a dispersive device for bandpass filtering and distributes the mixed signal to a remote site. The combination of the phase modulator, a multiwavelength laser source and the SMF link forms an all-optical microwave bandpass filter to suppress the levels of unwanted mixing products. A subcarrier frequency up-conversion from 3.25 GHz and 3.5 GHz to 11.7 GHz performed over a 25 km fiber link is experimentally demonstrated, in which BPSK modulation formats with data rates of 172 Mb/s and 344 Mb/s are applied. Eye diagrams are measured at the receiver end after demodulation, demonstrating a good up-conversion is achieved.

Keywords: All-optical microwave mixing, up-conversion, all-optical microwave filtering, radio-over-fiber, phase modulation to intensity modulation (PM-IM) conversion.

1. Introduction

Radio-over-fiber technologies are of great interest for many potential applications such as broadband wireless access networks, sensor networks, radar and satellite communication

[5] Published in Proceedings of SPIE, vol. 5971, 59711Q, September 2005.

systems, and have been extensively studied in the last few years [1]-[3]. The key function of a radio-over-fiber network is to distribute microwave and millimeter-wave signals over optical fiber to take the advantages of low loss, low dispersion and large bandwidth of optical fiber links. On the other hand, it is also highly desired that the distributed signals can be processed directly in the fiber link without optical/electrical and electrical/optical conversions, such as all-optical microwave mixing and filtering.

In order to efficiently use the transmission bandwidth, the baseband information is usually modulated on a low frequency subcarrier and up-converted to a high frequency by mixing the low frequency subcarrier with a local oscillator signal. The up-converted high frequency signal is then delivered to an antenna. Many papers have been published in the last two decades for all-optical microwave mixing [4]-[7]. All-optical mixing of microwave signals at a laser diode (LD) has been intensively investigated in [4]. However, since the modulation frequency of an LD is usually limited to less than 10 GHz, it is not suitable for next-generation broadband wireless access networks, in which the subcarrier frequencies would be in the millimeter-wave range. To solve this problem, high speed external electrooptic modulators can be applied. The use of two cascaded intensity modulators [5] and the use of an LD together with an intensity modulator [6] have been proposed to implement all-optical microwave mixing. However, these approaches suffer from chromatic dispersion of the optical fiber which limits the bandwidth of the radio-over-fiber systems. All-optical microwave mixing can also be realized based on the non-linearity of semiconductor optical amplifiers, but special care must be given to suppress the inter-modulation distortion [7].

Before sending the frequency up-converted microwave signal to an antenna, an adequate filtering, either in the optical domain or the electrical domain, is required to reject the unwanted mixing products to avoid the possible interference to other radiation frequency bands. According to the current microwave technologies, it is difficult to implement bandpass filter at ultrahigh frequency range with narrow bandwidth and large tunability. To solve this problem, all-optical microwave filters with the advantageous features of broad bandwidth and large tunability are highly desirable for broadband radio-over-fibre applications. Many approaches have been proposed in the last two decades to realize all-optical microwave filtering [8]-[11]. To the best of our knowledge, few approaches have been proposed to implement simultaneously

microwave mixing and all-optical microwave filtering over a fiber link. Recently, we have proposed an approach to perform both all-optical microwave mixing and bandpass filtering in a radio-over-fiber link using an electrooptic phase modulator in combination with a length of single mode fiber (SMF) [12]. The phase modulator performs all-optical microwave mixing and the mixed signals at the output of the modulator are then fed to the SMF link, which acts as a dispersive device to perform PM-IM conversion and at the same time distributes the mixed signal to a remote site. The filtering function is realized by combining the phase modulator with a multiwavelength laser source and the SMF link. The passband can be designed to be located at the up-converted microwave frequency. In our earlier study [12], a continuous subcarrier signal at 3 GHz was successfully up-converted to 11.8 GHz, with other unwanted frequency components rejected by the all-optical bandpass filter. In that experiment, no baseband information was carried by the subcarrier. The work reported in this paper is a continuation of our earlier work, to investigate the performance of the phase-modulator-based all-optical microwave processor when digital baseband signal is carried by the subcarrier. In the next section, a review of microwave mixing using an electrooptic phase modulator and PM-IM conversion using a length of SMF is presented, followed by a mathematical expression of the transfer function of the phase-modulator-based all-optical microwave filter. In Section 3, we report the experimental study of the proposed all-optical microwave processor when a baseband signal is carried by a subcarrier at 3.5 GHz. The frequency of the subcarrier is then up-converted to 11.7 GHz. The baseband signal has a BPSK modulation format with two different data rates of 172 Mb/s and 344 Mb/s. A conclusion is drawn in Section 4.

2. All-optical subcarrier frequency up-conversion and filtering

The block diagram of the all-optical subcarrier frequency up-conversion and microwave filtering system is shown in Fig. 1. The system consists of a multiwavelength laser source, an electrooptic phase modulator, a length of SMF and a photodetector. A subcarrier at a low microwave frequency ω_{SC} and a local oscillator frequency ω_{LO} are applied to the phase modulator via a power combiner. All-optical mixing of the microwave signals is implemented at the phase modulator. The output signal from the phase modulator is then sent to a remote site via the SMF, which also acts as a dispersive device to convert the phase modulated signal to an intensity modulated signal. The up-converted electrical signal is obtained at the output of the

photodetector located at the other end if the fiber link, where frequency components other than the up-converted frequency $\omega_{SC}+\omega_{LO}$ will be rejected.

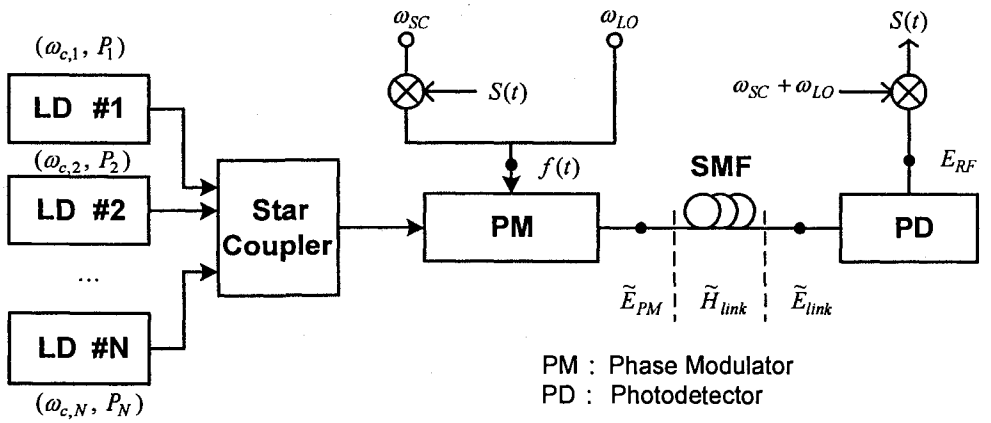

Fig. 1 Schematic diagram of phase-modulator-based all-optical microwave mixing and filtering system.

A. Phase-modulator-based all-optical microwave mixing

Assume the electrical signal applied to the phase modulator is

$$f(t)=A_{SC}\sin(\omega_{SC}t)\cdot s(t)+A_{LO}\sin(\omega_{LO}t), \tag{1}$$

where A_{SC} and A_{LO} represent the amplitudes of the subcarrier with a frequency ω_{SC} and local oscillator with a frequency ω_{LO} respectively, $s(t)$ is the BPSK baseband signal used to modulate the subcarrier. Usually the bandwidth of $s(t)$ is much smaller than the subcarrier frequency ω_{SC}. To simplify the mathematical derivation, we still consider the baseband signal modulated subcarrier as a single frequency sinusoidal signal. Then the optical field with optical frequency $\omega_{c,n}$ for the n-th optical carrier at the phase modulator output is

$$\tilde{E}_{PM,n}=\sqrt{2P_n\cdot(1-t_{ff})}\cdot[e^{j\omega_{c,n}t}]\cdot[e^{j\beta_{SC}\sin(\omega_{SC}t)}]\cdot[e^{j\beta_{LO}\sin(\omega_{LO}t)}], \tag{2}$$

where P_n is the optical power of the n-th LD, t_{ff} is the insertion loss of the phase modulator, β_{SC} and β_{LO} represent the phase modulation depths for the subcarrier and the local oscillator, respectively.

Using the following properties of trigonometric functions,

$$\begin{cases} \cos(\beta \cdot \sin \omega t) = J_0(\beta) + 2\sum_{k=1}^{\infty} J_{2k}(\beta) \cdot \cos 2k\omega t \\ \sin(\beta \cdot \sin \omega t) = 2\sum_{k=1}^{\infty} J_{2k-1}(\beta) \cdot \sin(2k-1)\omega t \\ e^{jx} = \cos(x) + j\sin(x), \end{cases} \tag{3}$$

we can rewrite Eq. (2) as

$$\begin{aligned} \tilde{E}_{PM,n} &= \sqrt{2P_n \cdot (1-t_{ff})} \cdot [e^{j\omega_{c,n}t}] \cdot [\sum_{k=-\infty}^{\infty} J_k(\beta_{SC}) \cdot e^{jk\omega_{SC}t}] \cdot [\sum_{l=-\infty}^{\infty} J_l(\beta_{LO}) \cdot e^{jl\omega_{LO}t}] \\ &= \sqrt{2P_n \cdot (1-t_{ff})} \cdot \sum_{k=-\infty}^{\infty} \sum_{l=-\infty}^{\infty} J_k(\beta_{SC}) \cdot J_l(\beta_{LO}) \cdot e^{j(\omega_{c,n}+k\omega_{SC}+l\omega_{LO})t}, \end{aligned} \tag{4}$$

where k and l are integers representing the orders of the harmonics; and $J_k[\bullet]/J_l[\bullet]$ denote the k-th/l-th order Bessel functions of the first kind. From Eq. (4), we can find that the two-frequency phase modulation will generate various optical sidebands. The frequency derivation from the optical carrier $\omega_{c,n}$ are $\pm\omega_{SC}$, $\pm\omega_{LO}$, $\pm 2\omega_{SC}$, $\pm 2\omega_{LO}$, ..., and $\omega_{SC} \pm \omega_{LO}$, $2\omega_{SC} \pm \omega_{LO}$, $\omega_{SC} \pm 2\omega_{LO}$, ... However, based on the property of the Bessel function of the first kind,

$$\begin{cases} J_k = -J_{-k}, when \quad k \quad is \quad odd, \\ J_k = J_{-k}, when \quad k \quad is \quad even, \end{cases} \tag{5}$$

we can conclude that if this phase-modulated optical signal is directly detected using a photodiode, no microwave signal can be recovered because all the odd-order sidebands are π out of phase at the output of the electrooptic phase modulator, which leads to a cancellation of all microwave signals except a dc. This behavior is expected since the phase modulation does not alter the amplitude of the input optical carrier, and the square-law photodiode works as an envelope detector.

B. PM-IM conversion using a dispersive device

In order to obtain the modulating signals and their mixing products by using direct detection, the phase-modulated signal should be converted to an intensity-modulated signal. In our proposed system, the phase-modulated optical signal passes through a length of SMF which acts as a dispersive device; the phase relationship between all spectral lines will be changed thanks to the chromatic dispersion of the fiber. Such a dispersive link can be modeled with a frequency response with respect to optical frequency ω as

$$\widetilde{H}_{link}(\omega)=\left|\widetilde{H}_{link}(\omega)\right|\cdot e^{j\theta_{link}(\omega)}=\frac{1}{\sqrt{L}}\cdot e^{j[\theta_{0,n}+(\omega-\omega_{c,n})\cdot\tau_n+\frac{D}{2}\cdot(\omega-\omega_{c,n})^2]}, \tag{6}$$

where L is the optical power loss of the dispersive link, $\theta_{o,n}$ and τ_n are the insertion phase and group delay induced by the fiber link at $\omega=\omega_{c,n}$, respectively, and $D=\partial\tau/\partial\omega$ is the first-order dispersion term. From Eq. (6) we see that the frequency response of the dispersive link is assumed to be flat in magnitude and parabolic in phase because the second-order and higher dispersion terms are ignored.

As the optical signal at the output of the phase modulator passes through the fiber link with a frequency response described by Eq. (6), the optical field at the end of the link is

$$\widetilde{E}_{link,n}(t)=\sqrt{\frac{2P_n\cdot(1-t_{ff})}{L}}\cdot[e^{j(\omega_{c,n}t+\theta_{0,n})}]\cdot\left\{\sum_{k=-\infty}^{\infty}\sum_{l=-\infty}^{\infty}J_k(\beta_{SC})\cdot J_l(\beta_{LO})\times e^{j[(k\omega_{SC}+l\omega_{LO})\cdot(t+\tau_n)+\frac{D}{2}(k\omega_{SC}+l\omega_{LO})^2]}\right\}. \tag{7}$$

As the optical signal is detected by an ideal photodetector with a responsivity $\Re$, the temporal expression of the detected current can be calculated from the envelope of the incident optical signal. In general, the expression of the recovered RF signal at frequency ω_{RF} (can be ω_{SC}, ω_{LO}, $\omega_{SC}+\omega_{LO}$, ...) is the sum of different beatings of the optical frequency components which are separated by ω_{RF}. For example, by assuming that the modulation depth is small, frequency conversion at $\omega_{SC}+\omega_{LO}$ mainly comes from the beatings of the spectral lines $\omega_{c,n}+\omega_{SC}$ with

$\omega_{c,n}-\omega_{LO}$, $\omega_{SC}+\omega_{LO}$ with $\omega_{c,n}-\omega_{SC}$, $\omega_{c,n}+\omega_{SC}+\omega_{LO}$ with $\omega_{c,n}$, and $\omega_{c,n}-\omega_{SC}-\omega_{LO}$ with $\omega_{c,n}$, which can be expressed as

$$\begin{aligned} E_{RF,n}(t) \cong & \frac{\Re \cdot P_n \cdot (1-t_{ff})}{L} \cdot [J_0(\beta_{SC})J_0(\beta_{LO})J_1(\beta_{SC})J_1(\beta_{LO})] \\ & \times \left\{ -2\cos[\frac{D}{2} \cdot (\omega_{SC}^2 - \omega_{LO}^2)] \cdot \cos[(\omega_{SC}+\omega_{LO})t + (\omega_{SC}+\omega_{LO})\tau_n] \right. \\ & \left. +2\cos[\frac{D}{2} \cdot (\omega_{SC}+\omega_{LO})^2] \cdot \cos[(\omega_{SC}+\omega_{LO})t + (\omega_{SC}+\omega_{LO})\tau_n] \right\}. \end{aligned} \tag{8}$$

The proposed PM-IM conversion has a frequency response with respect to the up-converted frequency $\omega_{SC}+\omega_{LO}$ as

$$\begin{aligned} H_{PM-IM}(\omega_{SC}+\omega_{LO}) &\propto -\cos[\frac{D}{2}(\omega_{SC}^2 - \omega_{LO}^2)] + \cos[\frac{D}{2} \cdot (\omega_{SC}+\omega_{LO})^2] \\ &= -2\sin[\frac{D}{2}(\omega_{SC}^2 + \omega_{SC} \cdot \omega_{LO})] \cdot \sin[\frac{D}{2}(\omega_{LO}^2 + \omega_{SC} \cdot \omega_{LO})]. \end{aligned} \tag{9}$$

Recall the PM-IM conversion induced frequency response when a single-frequency small signal modulation is applied, we have [13]

$$H_{PM-IM}(\omega_{RF}) \propto \cos(\frac{D}{2}\omega_{RF}^2 + \frac{\pi}{2}) = -\sin\frac{D}{2}\omega_{RF}^2, \tag{10}$$

which is different from the frequency response described by Eq. (9). The simulated frequency responses corresponding to Eq. (9) and Eq. (10) are shown in Fig. 2. The solid line shows the PM-IM conversion when a single frequency ω_{RF} is applied, while other curves show the PM-IM conversion as the function of the up-converted frequency $\omega_{SC}+\omega_{LO}$ when two frequencies are applied to the phase modulator. It indicates that the PM-IM conversion induced frequency responses vary with frequencies of different mixing products, which should be taken into account to optimize the mixing performance.

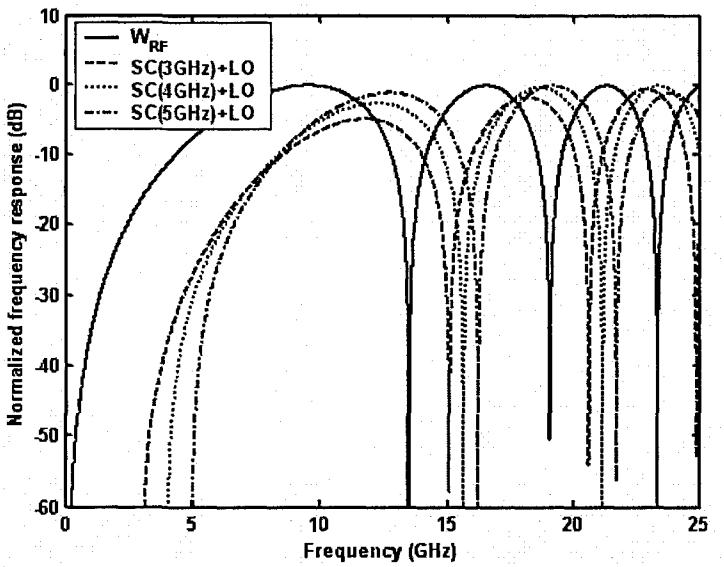

Fig. 2 Recovered microwave signal vs. microwave frequency.

C. All-optical microwave filtering

Since in the proposed system we use a multiwavelength laser source and assume each lasing wavelength is independent; eventually the output microwave signal at each mixing frequency is a vector summation of all the corresponding electrical signals carried by the different wavelengths with different time delays. This summation may be constructive or destructive depending on the frequency of the mixing product and the dispersion of the SMF. Then a microwave filtering function is achieved. The frequency response of the proposed all-optical microwave filtering can be written as [13]

$$\tilde{H}_{filter}(\omega_{RF}) = \sum_{n=1}^{N} P_n \cdot e^{j\omega_{RF}\tau_n} . \tag{11}$$

When the frequency spacing $\Delta\omega$ between any two adjacent optical carriers is identical, $\tau_n = D \cdot \Delta\omega$ is a constant and $\tilde{H}_{filter}(\omega_{RF})$ is a typical frequency response of a lowpass filter with a frequency spectral range (FSR) of $1/\tau_n$.

Based on the previous theoretical analysis, we can see that the overall effective transfer function with respect to the microwave frequency of the proposed system is expressed as the

multiplication of $\tilde{H}_{filter}(\omega_{RF})$ and $H_{PM-IM}(\omega_{RF})$. To obtain an optimized mixing performance, i.e., maximum power of the up-converted product together with higher rejection of the fundamentals, ω_{SC}, ω_{LO} and the FSR of the proposed all-optical microwave filter should be carefully selected to meet the following rules: 1) resonance peak of the overall frequency response should be coincide with the un-converted frequency; 2) fundamental frequency components, ω_{SC} and ω_{LO}, usually have high power levels and should be located at or close to the notches of the system frequency response; 3) other unwanted mixing products should be located far away the up-converted frequency to avoid defiling the demodulated baseband signal at the receiver.

3. Experiment

Based on the schematic diagram shown in Fig. 1, a testbed is built in our laboratory. The experimental system is implemented in two steps.

First, instead of using a multiwavelength laser, a single-wavelength LD is used as the light source and the all-optical subcarrier up-conversion is experimentally implemented. A 25-km standard SMF-28 fiber is employed as the dispersive device, which has a chromatic dispersion of $17 ps/nm \cdot km$ at 1550 nm and an accumulated dispersion of 425 ps/nm. A 3.25 GHz microwave signal with 0 dBm power is applied to a $LiNbO_3$ strait-line phase modulator. To up-convert the subcarrier frequency, an 8.45 GHz local oscillator signal with an output power of 17 dBm is applied to the same phase modulator. Two pseudo random bit sequence (PRBS) 2^7-1 BPSK signals of data rates of 172 Mb/s and 344 Mb/s are respectively used to modulate the subcarrier.

Fig. 3(a) shows the optical power spectrum at the output of the phase modulator. The electrical spectrum at the output of the photodetector is shown in Fig. 3(b), in which a strong frequency up-converted subcarrier at 11.7 GHz is observed. Note that other frequency components, including the subcarrier, the local oscillator and some unwanted mixing products are also observed. Especially, the power levels of the signals at ω_{SC} and ω_{LO} are higher than the up-converted signal $\omega_{SC}+\omega_{LO}$; also the power levels of some higher-order harmonics and inter-modulation products are comparable to that of the up-converted signal. Fig. 3(c) and Fig. 3(d)

shows the baseband spectrum and eye diagram after demodulating the up-converted BPSK signal with an 11.7 GHz local oscillator at the receiver. Fig. 3(e) shows another eye diagram when a 344 Mb/s PRBS signal is applied. Both the eye diagrams are clear and widely opened, indicating that an effective up-conversion is reached.

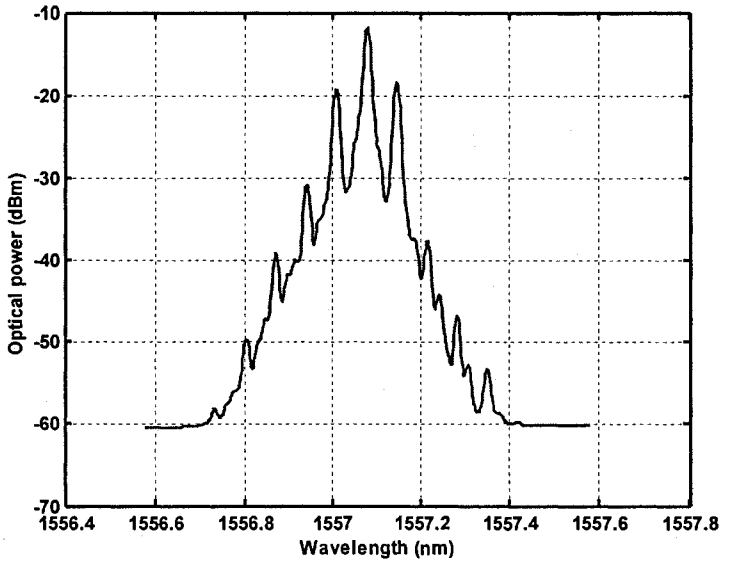

(a)

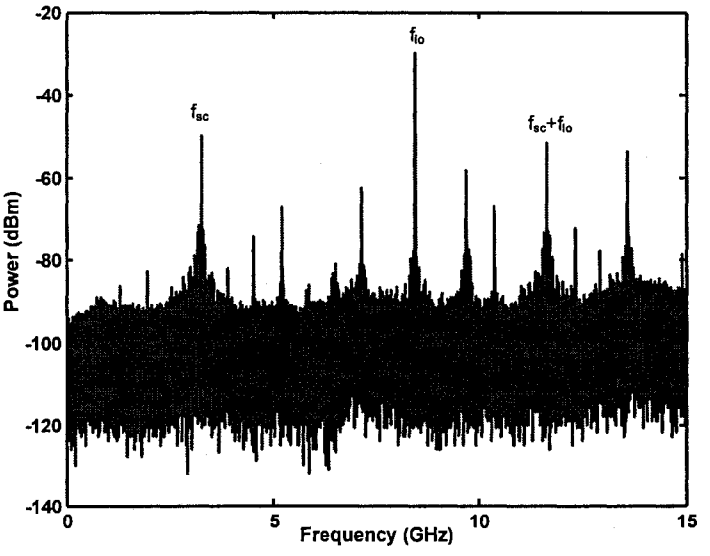

(b)

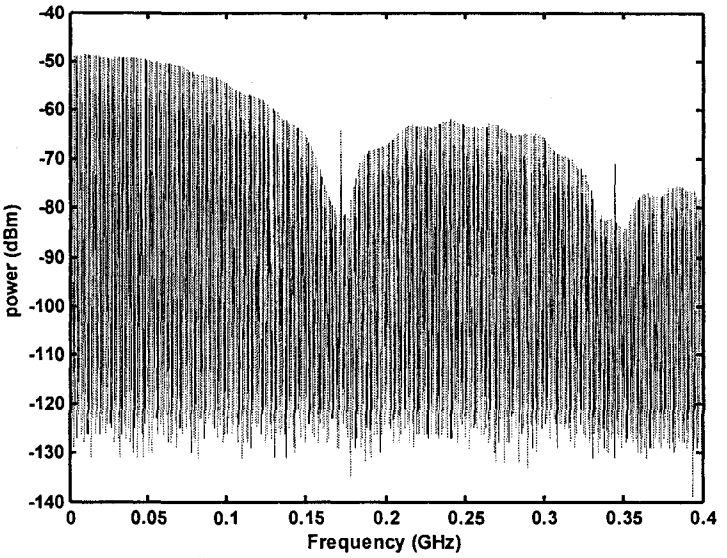

(c)

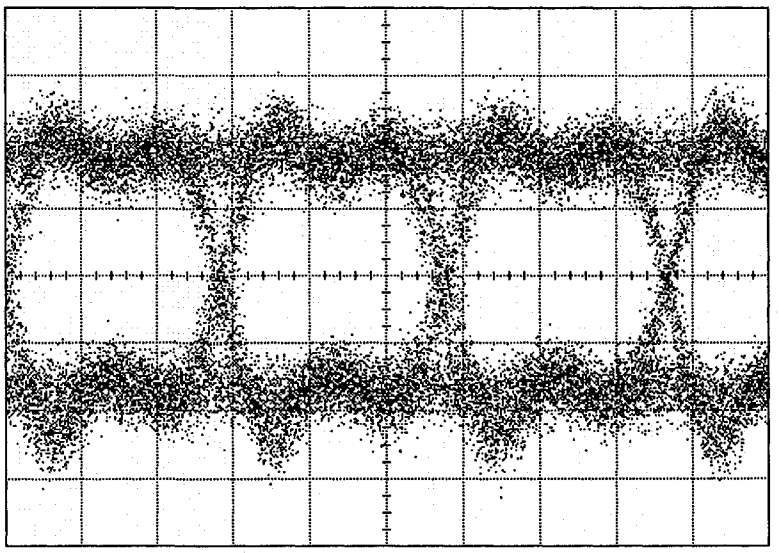

X axis: 2ns/div

(d)

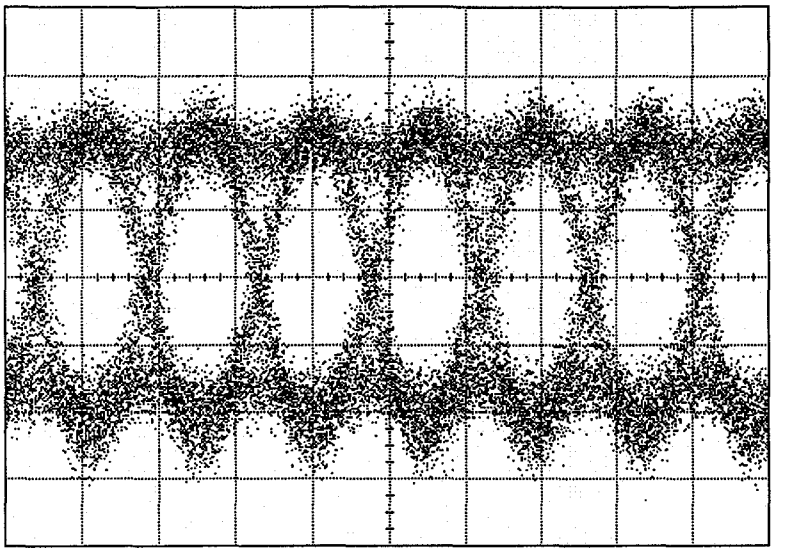

X axis: 2ns/div

(e)

Fig. 3 Experimental results when a light source with a single wavelength is used: (a) measured optical spectrum at the output of the phase modulator, (b) measured electrical spectrum at the output of the photodetector, (c) measured baseband signal spectrum after demodulation, (d) measured eye diagram at the receiver when a 172 Mb/s PRBS 2^7-1 signal is applied, and (e) measured eye diagram at the receiver when a 344 Mb/s PRBS 27-1 signal is applied.

In the second step of the experiment, we use a light source that has two wavelengths generated from two LDs with a wavelength spacing of 0.75 nm. A two-tap notch filter is thus implemented. Again, the optical power spectrum at the output of the phase modulator is shown in Fig. 4(a). The corresponding frequency response of the proposed all-optical microwave filter is measured by using a network analyzer and sweeping the modulating frequency from 45 MHZ to 15 GHz, as shown in Fig. 4(b). The FSR is around 3 GHz, which is determined by the wavelength spacing of the two LDs (0.75 nm) and the accumulated dispersion induced by the SMF link. In the experiment, the frequencies of the subcarrier and the local oscillator are at 3.5 GHz and 8.25 GHz, respectively. The electrical spectrum at the output of the photodetector is shown in Fig. 4(c). Compared with that in Fig. 3(b), the power level difference between the local oscillator and the up-converted signal is about 10 dB, which is much smaller than that value (22 dB) when no filtering is applied. Meanwhile we can see that the power levels of other unwanted inter-modulation products are also significantly suppressed. Fig. 4(d) shows the eye diagram of the demodulated 172 Mb/s PRBS 2^7-1 signal, which is clear and widely opened, demonstrating that an excellent up-conversion is achieved.

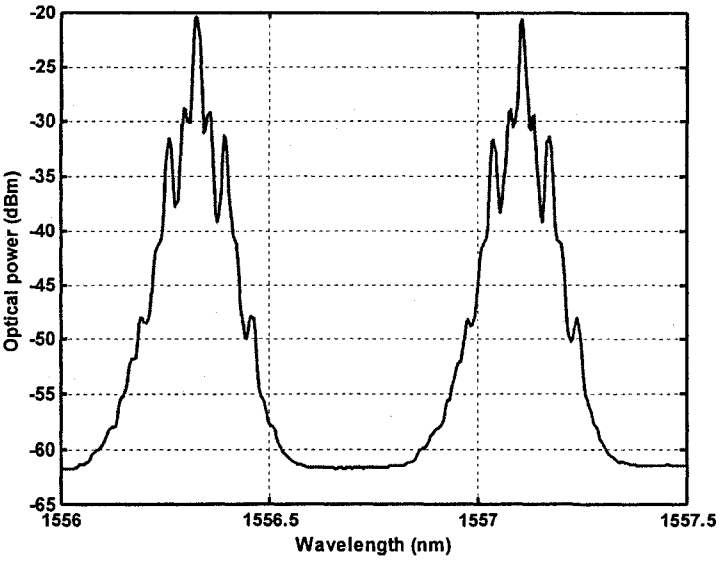
-20
-25
-30
-35
-40
-45
-50
-55
-60
-65
Optical power (dBm)
1556
1556.5
1557
1557.5
Wavelength (nm)

(a)

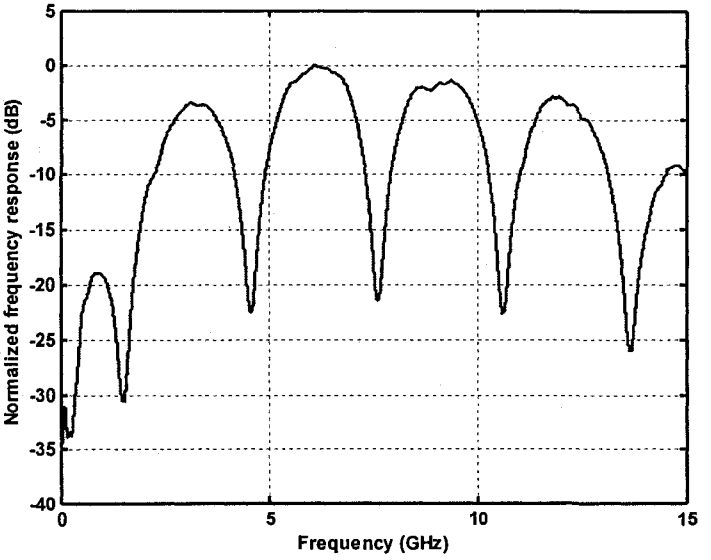
5
0
-5
-10
-15
-20
-25
-30
-35
-40
Normalized frequency response (dB)
0
5
10
15
Frequency (GHz)

(b)

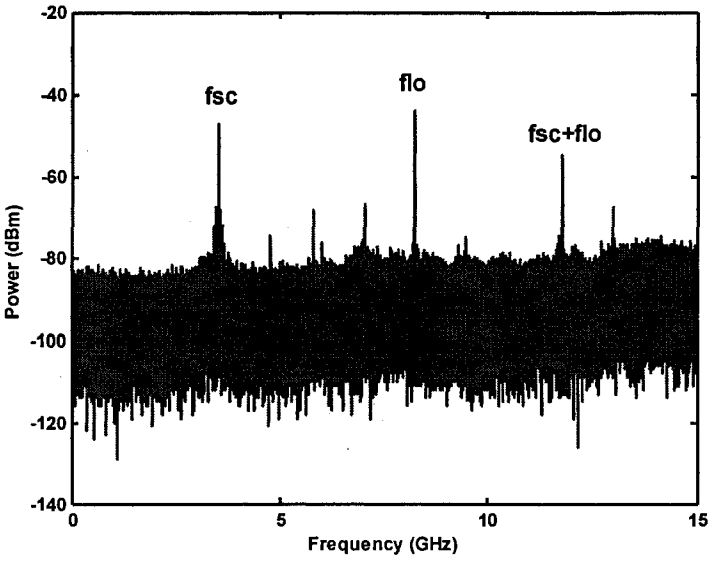

(c)

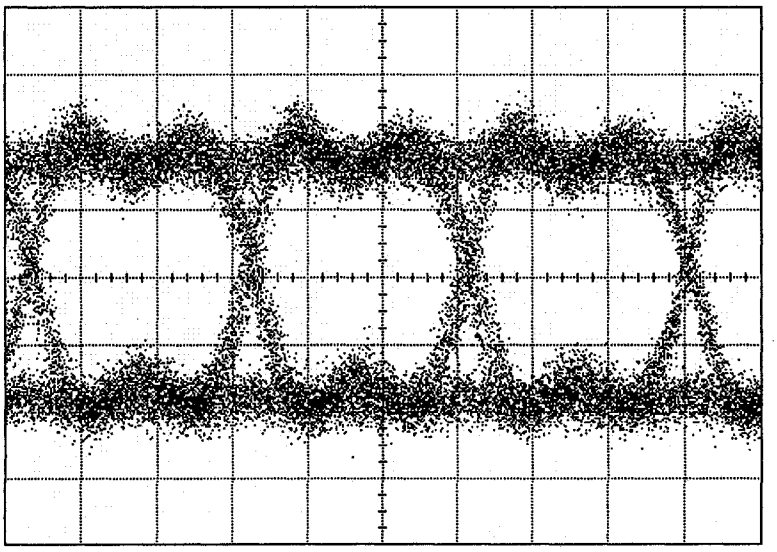

X axis: 2ns/div

(d)

Fig. 4 Experimental results when the light source has two wavelengths generated from two LDs: (a) measured optical spectrum at the output of the phase modulator, (b) measured frequency response of the proposed all-optical microwave filtering, (c) measured electrical spectrum at the output of the photodetector, and (d) measured eye diagram at the receiver when 172 Mb/s PRBS 2^7-1 signal is applied.

4. Conclusions

The work presented here is a continuation of our earlier work, to investigate the performance of the phase-modulator-based all-optical microwave mixing and filtering system when a digital baseband signal was carried by the subcarrier. In our experimental investigation, the system using one optical wavelength without the filtering functionality and using two optical wavelengths with the filtering functionality were performed. In both cases, a frequency up-converted microwave signal was obtained at the output of the photodetector after 25-km transmission. It was demonstrated that when two optical wavelengths were used, a filtering function equivalent to a microwave notch filter was observed, which helped to reduce the unwanted frequency components at the output of the SMF span. Experiments on the system performance with data modulation for both one- and two-wavelength cases were performed. Although from the eye diagrams, we could not see a significant performance improvement in data recovery, the unwanted frequency components were significantly reduced when two optical wavelengths were employed in the system. We believe that when more optical wavelengths are used, a microwave filter with much narrower passband would be realized, which could further reduce the unwanted frequency components, a system with significantly improved performance would thus be realized.

References

[1] H. Ai-Raweshidy and S. Komaki, *Radio over fiber technologies for mobile communications networks*, Artech House, Boston, 2002.

[2] L. A. Johansson and A. J. Seeds, "36-GHz 140-Mb/s radio-over-fiber transmission using an optical injection phase-lock loop source," IEEE Photon. Technol. Lett., vol. 13, no. 8, pp. 893-895, Aug. 2001.

[3] D. Wake, M. Webster, G. Wimpenny, K. Beacham, and L. Crawford, "Radio over fiber for mobile communications," 2004 IEEE Int. Topical Meeting on Microwave Photonics, pp. 157-160, Oct. 2004.

[4] G. Maury, A. Hilt, B. Cabon, V. Girod, and L. Degoud, "Remote up-conversion in microwave fiber-optic links employing an unbalanced Mach-Zehder interferometer," SPIE 44th Annual Meeting, International Symposium on Optical Science, Engineering, and Instrumentation, vol. 3795, pp. 468-476, Denver, USA, Jul. 1999.

[5] C. K. Sun, R. J. Orazi, and S. A. Pappert, "A photonic link millimeter-wave mixer using cascaded optical modulators and harmonic carrier generation," IEEE Photon. Technol. Lett., vol. 8, no. 9, pp. 1166-1168, Sept. 1996.

[6] J. L. Corral, J. Marti, and J. M. Fuster, "Optical up-conversion on continuously variable true time delay lines based on chirped fiber gratings for millimeter-wave optical beamforming networks," IEEE Trans. Microwave Theory Technol., vol. 47, pp. 1315-1320, Jul. 1999.

[7] J. H. Seo, Y. K. Seo, and W. Y. Choi, "Spurious free dynamic range characteristics of the photonic up-converter based on a semiconductor amplifier," IEEE Photon. Technol. Lett., vol. 15, no. 11, pp. 1591-1593, Nov. 2003.

[8] K. P. Jackson, S. A. Newton, B. Moslehi, M. Tur, C. C. Cutler, J. W. Goodman, and H. J. Shaw, "Optical fiber delay line signal processing," IEEE Trans. Microwave Theory Technol., vol. MTT-33, pp. 193-209, Mar. 1985.

[9] D. B. Hunter, R. Minasian, and P. A. Krug, "Tunable optical transversal filter based on chirped gratings," Electron. Lett., vol. 31, no. 25, pp. 2207-2210, Dec. 1995.

[10] G. Yu, W. Zhang, and J. A. R. Williams, "High-performance microwave transversal filter using fiber Bragg grating arrays," IEEE Photon. Technol. Lett., vol. 12, no. 9, pp. 1183-1185, Sept. 2000.

[11] J. Capmany, D. Pastor, A. Martinez, B. Ortega, and S. Sales, "Microwave photonics filters with negative coefficients based on phase inversion in an electro-optic modulator," Opt. Lett., vol. 28, pp. 1415-1417, Aug. 2003.

[12] F. Zeng and J. P. Yao, "All-optical microwave mixing and bandpass filtering in a radio-over-fiber link," IEEE Photon. Technol. Lett., vol. 17, no. 4, pp. 899-901, Apr. 2005.

[13] F. Zeng and J. P. Yao, "Investigation of phase modulator based all-optical bandpass filter," J. Lightw. Technol., vol. 23, no. 4, pp.1721-1728, Apr. 2005.

CHAPTER 5

FBG-BASED PM-IM CONVERSION AND ITS APPLICATIONS

The approaches presented in Chapter 3 and Chapter 4 are mainly dealing with dispersive-device-based PM-IM conversions and their applications for microwave bandpass filtering and mixing. As we have discussed in Sec. 2.2 of Chapter2, however, PM-IM conversion can also be achieved by us of an optical filter that performs as an optical frequency discriminator. Same as the dispersion-based PM-IM conversion, optical-filter-based PM-IM conversion also plays a very important role in all-optical microwave signal processing. Different optical filters can be used to implement frequency discrimination, such as an asymmetric MZI, a Michelson interferometer, or a fiber Sagnac filter. Although it is relatively simple to design, all these filters have a large high-order harmonic distortion due to their sinusoidal-type transfer functions, which would limit the dynamic range. Fabry-Perot resonator has also been investigated in the role of frequency discriminator to improve the linearity. However, the lens system must be carefully adjusted to overcome the effects of non ideal mode matching in free space operation.

FBGs have been widely used for all-optical signal processing due to the many advantages over other optical filters. First, similar to a Fabry-Perot resonator, an FBG can be considered as a multi-tap optical filter having a very high Q value, which gives an improved linearity and dynamic range compared to those of a two-tap filter (MZI, Michelson interferometer or Sagnac-loop). Second, very different and sophisticated filter frequency responses can be achieved by manipulating the implementation parameters of a single FBG or an FBG array during the synthesis and fabrication processes. Third, the interaction wavelength can be further tuned via changing the grating pitch by applying strain or variable heating. In addition, no free space to fiber coupling is required because the FBG is fabricated within the optical fiber. All these features make the synthesis of wideband and tunable frequency discriminator possible.

In this Chapter, we will focus on the investigation of FBG-based frequency discrimination and its applications for all-optical microwave signal processing. First, in Sec. 5.1, PM-IM conversion by use of an FBG-based frequency discriminator is presented. Both the frequency and phase responses of the FBG are taken into account to build a numerical model in the frequency domain. Gaussian-apodized FBGs are fabricated to carry out the experiments. In Sec. 5.2, by using the FBG-based frequency discriminator, a novel approach to implementing unipolar-bipolar phase-time encoding/decoding in an optical CDMA system is presented. Two FBG arrays are employed to perform en/de coding. It is demonstrated that the proposed scheme is equivalent to a sequence inversion keyed (SIK) direct-sequence CDMA, which would provide an improved performance compared to the conventional incoherent scheme using optical orthogonal codes. The FBG-based frequency discriminator can also be used to generate UWB pulses. In Sec. 5.3, two approaches to generating UWB pulses are proposed and experimentally demonstrated. The use of the proposed all-optical signal processor to implement UWB pulse polarity and pulse shape modulation is also discussed which provides the potential for fully exploiting the advantages provided by UWB-over-fiber networks.

5.1 Frequency domain analysis of FBG-based PM-IM conversion

In this Section, PM-IM conversion implemented using an FBG-based frequency discriminator is presented. Both the frequency and phase responses of the FBG are taken into account to build a numerical model in the frequency domain. A Gaussian-apodized FBG is fabricated to carry out the experiments. PM-IM conversion based on the Gaussian-apodized FBG is experimentally implemented. The results confirm the theoretical analysis.

Frequency Domain Analysis of Fiber Bragg Grating Based Phase Modulation to Intensity Modulation Conversion[6]

Fei Zeng, Jianping Yao,

Microwave Photonics Research Laboratory,
School of Information Technology and Engineering,
University of Ottawa, 800 King Edward Avenue, P.O. Box 450, Stn. A,
Ottawa, ON, Canada, K1N 6N5

Abstract

In this paper, optical phase modulation to intensity modulation by the use of a fiber Bragg grating (FBG) based frequency discriminator is proposed and experimentally demonstrated. In the proposed approach, the optical carrier frequency is placed at the quadrature point of the positive or negative slope of the reflection response of the FBG. The phase modulated light reflected from the two opposite slopes will have a π phase difference, which makes bipolar operation possible in an all-optical microwave signal processor or an optical code division multiple-access system. Both the frequency and phase responses of the FBG are taken into account to build a theoretical model in a frequency domain. Phase modulation to intensity modulation conversion based on a Gaussian apodized FBG is experimentally implemented. The results confirm the theoretical analysis.

Keywords: Microwave photonics, bipolar operation, fiber Bragg grating, phase modulation, intensity modulation, frequency discriminator.

1. Introduction

The distribution of microwave or millimeter-wave signals over fiber is of great interest for applications such as next generation broadband wireless access networks, radar, and satellite communications, by taking the advantages of low loss, large bandwidth and immunity to electromagnetic interference over traditional microwave links using copper cables. Radio-over-

[6] Published in Proceedings of SPIE, vol. 5971, 59712B, September 2005.

fiber systems employing intensity modulation (IM) and direct detection (DD) have been intensively investigated over the last few years. However, in many instances it is more desirable that the information is carried in the optical phase instead of amplitude. Such communication systems employing phase modulation (PM) or frequency modulation (FM) have advantages over IM systems which are well known for radio communications. In addition, In an optical communication system using PM or FM, the intensity of the optical carrier remains constant which is highly tolerant to non-linear effects, such as self-phase modulation (SPM), cross-phase modulation (XPM) or cross-gain modulation (XGM) [1].

There are in general two methods to detect a PM or FM signal. In the first method, a PM or FM signal can be detected using a coherent detection scheme [2], [3], in which the optical signal is mixed with a local oscillator light. The merit of the coherent optical transmission system is the reduction in detection noise. However, the construction of a local oscillator with high frequency and phase stability is difficult at present. In addition, the temperature and mechanical vibrations in the transmission line will result in phase and polarization fluctuations of the transmitted light, which would appear as noise at the receiver. Phase-locking techniques, such as light injection locking [4] and optical phase lock loop [5] can be applied to get rid of the phase noise, but this increases the system complexity. Alternatively, one can use a simple DD scheme with a frequency discriminator [6], [7]. This is typically an optical filter in which the optical carrier is placed on the steep slope of the filter spectral response, where the transmission or reflection is a function of frequency. The steepness of the slope determines the overall gain of the proposed system, while its linearity determines the devices dynamic range. Thus the frequency discriminator is a crucial device in the RF photonic system.

Frequency discriminator can also be used to characterize unwanted frequency or phase derivation imparted onto the optical carrier [8], [9], which is induced by some active components like laser diodes or external electrooptical modulators. For example, in a communication system using an intensity modulated DFB laser, the frequency chirp imparted onto the optical carrier can far exceed the actual signal bandwidth and therefore would limit the data rate due to fiber chromatic dispersion. Then an accurate characterization of the frequency chirp as a function of injection current is required to achieve an optimum system performance.

Frequency discriminators based on a variety of optical filters have been studied. The most widely used technique to implement FM/PM to IM conversion is to use an asymmetric Mach-Zehnder interferometer (MZI) [8] that is biased at the phase quadrature. While it is relatively simple to design and fabricate, MZI has a large higher-order harmonic distortion due to its sinusoidal transfer characteristics. This gives a limited dynamic range when a high conversion gain is desired. Other two-arm interferometers, such as Michelson interferometer [9] and fiber Sagnac filter [10], can also be used to achieve the same results but also suffer from the same problem. Fabry-Perot resonator [11] has also been investigated in the role of frequency discriminator to improve its linearity. However, the lens system must be carefully adjusted to overcome the effects of non ideal mode matching in free space operation.

In this paper, we propose a scheme for FM/PM to IM conversion based on a uniform fiber Bragg grating (FBG). There are many advantages of using FBGs for FM/PM to IM conversion [12]. First, since the FBG is fabricated within the fiber, no free space to fiber coupling is required. Second, very different and sophisticated filter frequency responses can be achieved by manipulating the fabrication parameters during the FBG writing processes. In addition, the interaction wavelength can be further tuned via changing the grating pitch by applying strain or variable heating. All these features make the synthesis of wideband and tunable frequency discriminator possible.

This paper is organized as follows. In Section 2, a theoretical model of uniform FBG-based PM-IM converter is presented, which describes the relationship between the system transfer function and the characteristics of the employed FBG. Based on this model, simulations are carried out to evaluate the performance of the proposed system. The results show that FBGs with proper apodization profiles and short lengths are preferred to achieve linear operation and high dynamic range. Experimental implementation is carried out in Section 3. The results agree well with the theoretical analysis. Both the theoretical analysis and experimental verification described in this paper are commonly referred to as a frequency domain network analysis. A conclusion is drawn in Section 4 with further discussions on future applications.

2. Theory

Let us consider an optical carrier which is phase modulated by a single frequency electrical signal. The normalized amplitude of the optical field $E(t)$ can be expressed in the form of

$$E(t) = \cos[\omega_c t + \Delta\varphi(t)] = \cos[\omega_c t + \Delta\varphi_{\max} \cos(\omega_m t)], \quad (1)$$

where ω_c is angular frequency of the optical carrier; ω_m is modulating angular frequency; $\Delta\varphi(t)$ is the modulation-induced phase change of the carrier; and $\Delta\varphi_{\max}$ is the maximum phase shift. Eq. (1) can be expanded in terms of Bessel functions of the first kind,

$$E(t) = \sum_{n=-\infty}^{\infty} J_n(\Delta\varphi_{\max}) \cdot \cos[(\omega_c + n\omega_m)t + \frac{1}{2}n\pi], \quad (2)$$

where $J_n(\bullet)$ denotes the n-th order Bessel function of the first kind. To simplify, the argument $(\Delta\varphi_{\max})$ will be omitted in the following text. From Eq. (2), we can see that the PM process generates a series of sidebands with Bessel function amplitude coefficients. The power intensity of each sideband is proportional to the square of the coefficient of the corresponding term in Eq. (2).

Under small signal conditions, only the first order sidebands need to be considered and Eq. (2) can then be simplified as

$$E(t) = J_0 \cos(\omega_c t) + J_1 \cos[(\omega_c + \omega_m)t + \frac{\pi}{2}] + J_{-1} \cos[(\omega_c - \omega_m)t - \frac{\pi}{2}]. \quad (3)$$

Based on the property of Bessel functions we have $J_n = -J_{-n}$ when n is odd. We can therefore conclude that the two sidebands are π out of phase at the output of the phase modulator, which is different from an IM where the two sidebands are in phase. If this signal is directly detected using a photodiode, the RF signal cannot be recovered because the beating between the carrier and upper sideband exactly cancels the beating between the carrier and the lower sideband. As we have demonstrated earlier [13], to achieve PM-IM conversion, we can pass the phase modulated optical signal through a dispersive device. Subsequently the two sidebands can be

effectively rotated to be totally or partially in phase; and then the modulating RF signal can be recovered using DD.

In fact, introducing any imbalance to the PM signal spectrum will result in a certain degree of PM-IM conversion. In this paper, we propose to use an FBG to implement the PM to IM conversion. Fig. 1 shows the proposed the system which consists of an FBG-based frequency discriminator and a square-law detector.

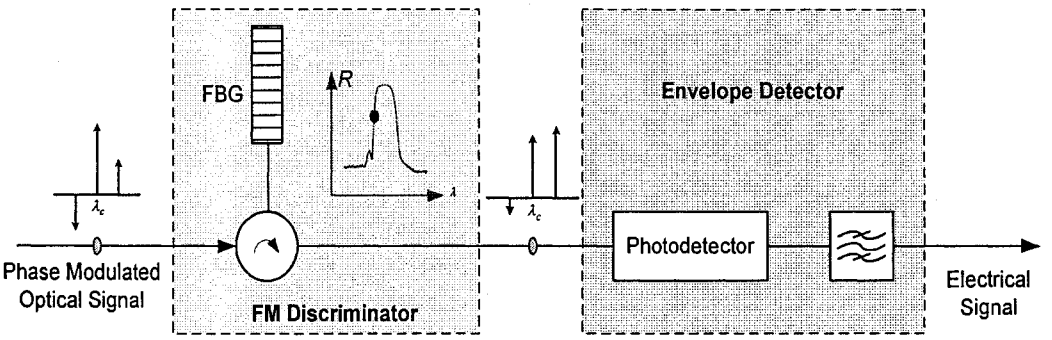

Fig. 1 Schematic diagram of the proposed PM-IM converter.

An ideal frequency discriminator should have a linear frequency response as well as a linear phase response. Its transfer function can be written as

$$H_d(j\omega) = |H_d(j\omega)| \cdot \angle H_d(j\omega) = |K| \cdot \omega \cdot \exp[-j\omega\tau_d], \tag{4}$$

where K is the slope steepness factor of the magnitude response, and $\tau_d = d[H_d(j\omega)]/d\omega$ is the group delay induced by the frequency discriminator.

A photodetector functions as a square-law detector, i.e., the output photocurrent is proportional to $|E_d(t)|^2$, where $E_d(t)$ represents the output optical field of the frequency discriminator. Taking only the RF signal centered at the modulating frequency ω_m, and ignoring the dc and higher-order harmonics (by using a bandpass filter), the recovered electrical signal can be expressed as

$$E_{out}(t) \propto K^2 \cdot \omega_m \cdot \cos[\omega_m(t-\tau)], \tag{5}$$

where τ is the total group delay induced by the PM-IM converter.

Recall the Fourier transform pair

$$\Im\{f'(t-\tau)\} = \underbrace{j\omega \cdot e^{-j\omega\tau}}_{H(j\omega)} \cdot \underbrace{F(j\omega)}_{\Im\{f(t)\}}, \tag{6}$$

where $\Im\{\bullet\}$ denotes the Fourier transform, and compare Eq. (6) with Eq. (5), we find that the recovered RF signal is a delayed differential version of the modulating signal.

In our proposed PM-IM converter, the two slopes of the FBG reflection spectrum are employed to implement frequency discrimination. Based on the above theoretical analysis, we know that the steepness and width of the slopes determines the overall conversion efficiency and operational signal bandwidth, while both the reflectivity and phase response at the slopes should be linear and any nonlinearity will introduce distortion to the recovered electrical signal. Therefore, to improve the performance, the FBG should be optimized. In the design, the fabrication parameters, such as grating length, refractive index modulation depth, and apodization profile, are properly decided to find out the best compromise between system operation dynamics and linearity.

To evaluate the performance of the proposed frequency discriminator, FBGs with different lengths and apodization profiles, i.e., uniform, hyperbolic tangent, and Gaussian profiles with different taper parameters, are simulated based on standard coupled mode equations [14]. Each grating is divided into short segments and the fundamental matrices for each segment were multiplied to obtain its overall characteristic. The results show that if no apodization is applied, the wings of the grating will act like a Fabry-Perot cavity and strong resonance will result in rapid fluctuation of reflectivity and phase response. Employing Gaussian apodization can highly suppress these effects. A Gaussian profile can be expressed as below

$$A(z) = \exp\{-\ln 2 \cdot \left[\frac{2 \cdot (z - L/2)}{s \cdot L}\right]^2\}, \tag{7}$$

where $A(z)$ represents the average index change along the grating length L as the function of the propagation distance z along the fiber, and s is the taper parameter. Fig. 2 shows the

amplitude reflectivity and phase response of an FBG with a length of 10 mm, an average index change of 0.0002, and a Gaussian taper factor of 0.25. The zoom in response on the left slope is shown as Fig. 2(b), in which the reflection spectrum shows a significant suppression of sidelobes and very smooth rolling off slopes. Meanwhile the phase response is considerable linear as well.

Using the chosen FBG, the normalized overall responses of the proposed PM-IM converter are calculated and shown in Fig. 3. Thanks to the optimization of the FBG, both the magnitude (Fig. 3(a)) and phase responses (Fig. 3(b)) indicate a good linearity with respect to the modulating frequency. It should be noticed that in order to evaluate the system tolerance to optical carrier detuning, some different work points on the reflection slope are chosen. The results show that regarding to the linearity and steepness, no significant changes is observed. If both the reflection and transmission of the FBG are used to construct a balanced detection, the residual amplitude noise induced by the carrier frequency detuning can be further rejected [9], [15].

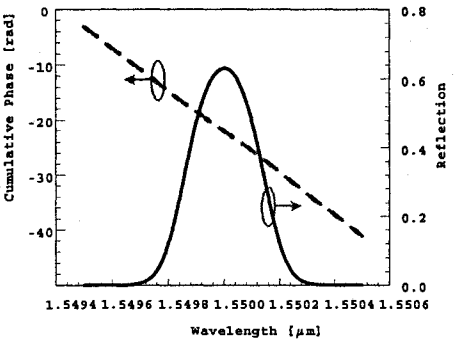

(a)

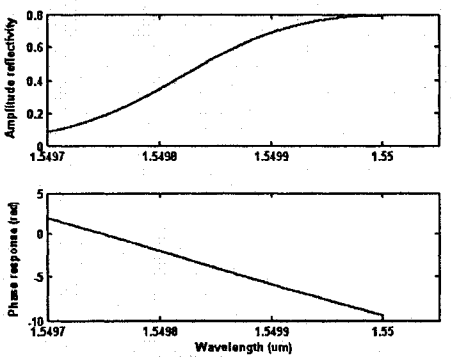

(b)

Fig. 2 Simulated reflectivity and phase response of a Gaussian apodized FBG:
(a) whole reflection band, and (b) zoom-in left slope.

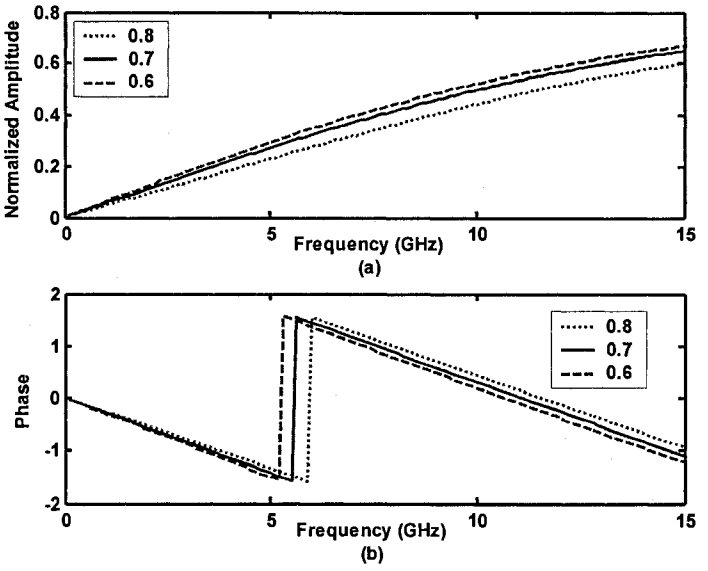

Fig. 3 (a) Normalized overall magnitude and (b) phase responses of the proposed PM-IM converter, employing the FBG shown in Fig.2. Optical carrier is placed at three different locations on the FBG reflection slope, where the amplitude reflectivity is 60% (dashed line), 70% (solid line) and 80% (dotted line) of the maximum amplitude reflectivity, respectively.

3. Experiment

Based on the theoretical analysis in Sec. 2, an FBG is fabricated and a PM-IM converter based on the fabricated FBG is experimentally implemented. The FBG has a length of 10 mm, a peak power reflectivity of 90% and is Gaussian apodized with $s = 0.45$. Additional inverse apodization is applied during the FBG fabrication process to further suppress the sidelobes on short-wavelength side. Its reflectivity spectrum is shown in Fig. 4, which has a central wavelength at 1536.12 nm and a 3-dB bandwidth of 0.23 nm.

A tunable laser with typical linewidth of 150 KHz is applied as the light source. The single frequency RF signal is generated using an Agilent signal generator (E8254A). PM is performed by using a LiNbO3 straight-line phase modulator. An Agilent spectrum analyzer (E4448A) is used to monitor the output of a photodetector. An erbium-doped fiber amplifier is used to compensate for the power loss in the system.

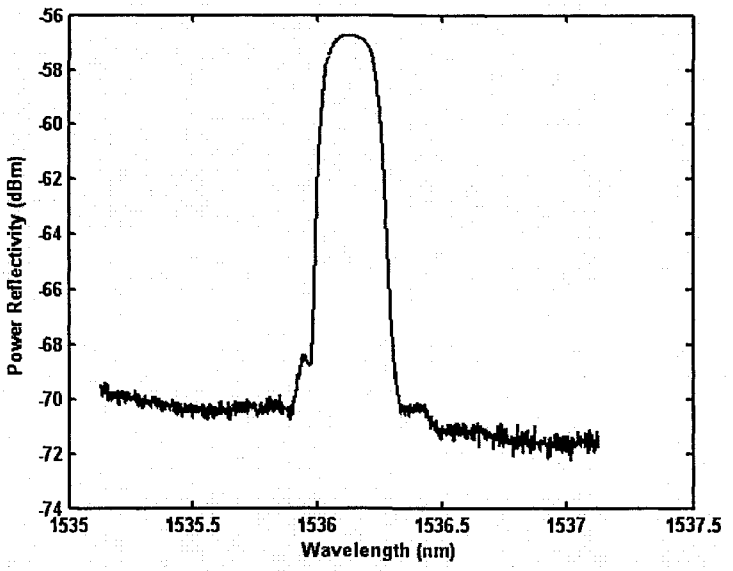

Fig. 4 Measured power reflection spectrum of the FBG used in the experiment.

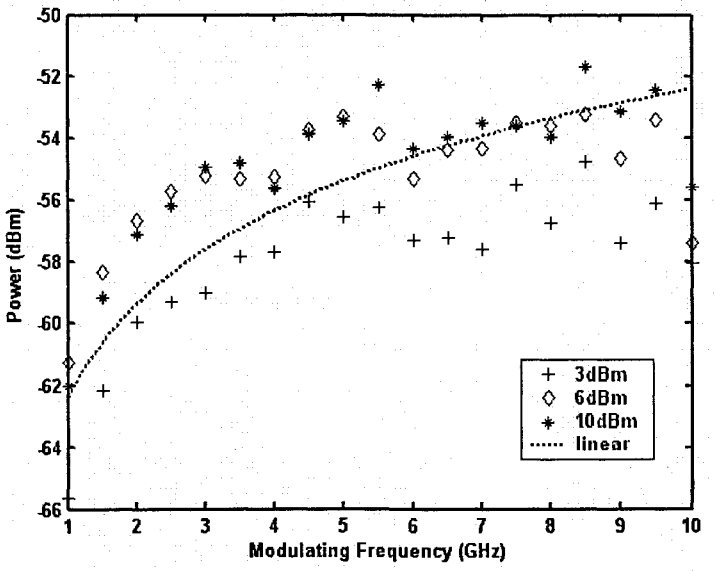

Fig. 5 Measured frequency responses of the proposed PM-IM converter when different modulating signal power levels are applied.

At first, the carrier wavelength is tuned at of 1536.00 nm, which lies on the left slope of the FBG. Sweeping the modulating signal from 1 to 10 GHz while keeping the power level at a specific value, we obtain a frequency response of the proposed PM-IM converter. The measurements are performed three times with the power level of 3 dBm, 6 dBm and 10 dBm,

respectively. The corresponding frequency responses are shown in Fig. 5. Comparing with an ideal linear response which is plotted as a reference on the same figure, a good agreement between the measured and the ideal frequency responses is observed. The residual variations are due to the non-linearity of the FBG slope response. In addition, the unflat responses of the phase modulator and the photodetector also contribute to these errors. When the modulating signal power level is increased from 6 to 10 dBm, we cannot obtain an expected 4 dB output increasing. The reason is that when the modulation depth becomes higher, more modulating power is transferred to the higher-order harmonics, which implies that the dynamic range of the proposed system is limited by the PM depth as well.

To further verify the theoretical analysis presented in Sec. 2, we tune the carrier wavelength and make it be reflected at different locations of the grating reflection spectrum, i.e., the left slope, the middle, and the right slope. In this experiment, an oscilloscope is used to observe the waveforms of the recovered signal. Modulating frequency is set at 4 GHz, which is limited by the bandwidth of the oscilloscope. Fig. 6(a) shows the reflection spectra for different carrier wavelengths and Fig. 6(b) shows the waveforms of the corresponding electrical outputs. It is interesting to notice that when the carrier wavelengths are located at the opposite slopes of the FBG reflection spectrum, the detected RF signals will have a π phase difference, and no RF signal can be recovered if the carrier is located at the center of the reflection band. These interesting features can be directly applied to achieving bipolar operation in all-optical signal processing, e.g., synthesis of all-optical microwave filters with negative coefficients.

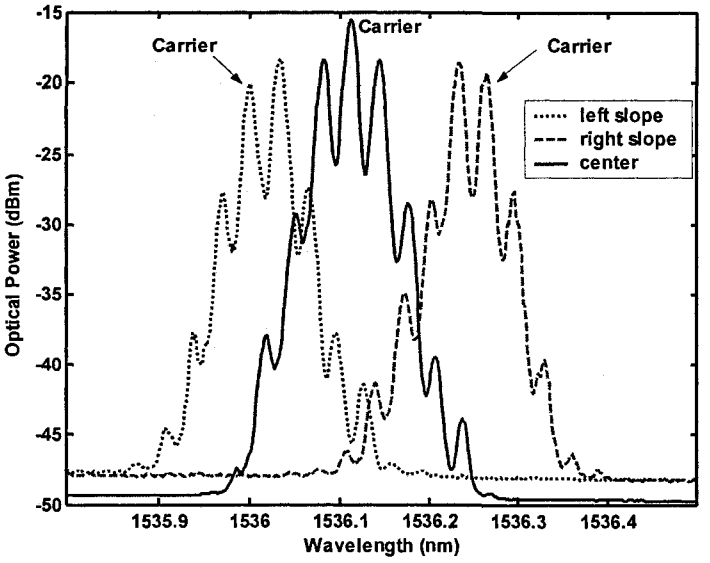

(a)

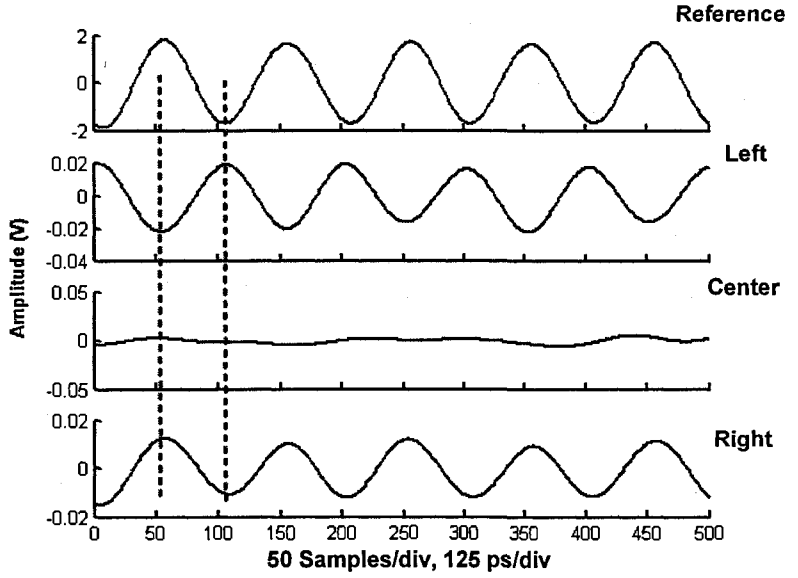

(b)

Fig. 6 (a) Measured spectra of the phase modulated optical signals reflected at different points, solid line: center of the reflection band; dotted line: left slope; dashed line: right slope. (b) Measured waveforms of the electrical outputs corresponding to different optical spectra shown in (a).

4. Conclusions

A PM-IM converter was proposed by the use of an FBG based frequency discriminator, in which the optical carrier frequency is placed on the slope of the reflection response of the FBG. A frequency domain theoretical analysis showed that using an FBG with proper Gaussian apodization can realize relatively high linearity and wideband operation, but at the cost of lower conversion gain. An experiment was carried out and the experimental results showed a good agreement with the theoretical analysis. In addition, by locating the carrier wavelength at the opposite slopes of the FBG reflection spectrum, the detected RF signals will have a π phase difference, which makes bipolar operation possible in all-optical microwave signal processing and optical code division multiple-access system. For further considerations when a high performance frequency discriminator is required, the combination of transmitted and reflected signals in a balanced detection scheme may be an appealing solution.

References

[1] A. Yariv, Optical Electronics in Modern Communications, Fifth ed. London, U.K.: Oxford Univ. Press, 1997.

[2] T. Chikama, S. Watanabe, H. Onaka, T. Kiyonaga, Y. Onoda, H. Miyata, M. Suyama, M. Seino, and H. Kuwahara, "Modulation and demodulation techniques in optical heterodyne PSK transmission systems," J. Lightw. Technol., vol. 8, pp. 309-322, Mar. 1990.

[3] A. H. Gnauck and P. J. Winzer, "Optical phase-shift-keyed transmission," J. Lightw. Technol., vol. 23, pp. 115-130, Jan. 2005.

[4] J. Genest, M. Chamberland, P. Tremblay, and M. Tetu, "Microwave signals generated by optical heterodyne between injection-locked semiconductor lasers," IEEE J. Quantum Elec., vol. QE-33, pp. 989-998, Jun. 1997.

[5] L. G. Kazovsky, and D. A. Atlas, "A 1320-nm experimental optical phase-locked loop: performance investigation and PSK homodyne experiments at 140 Mbps and 2 Gbps," J. Lightw. Technol., vol. 8, pp. 1414–1425, Sept. 1990.

[6] S. Saito, Y. Yamamoto, and T. Kimura, "Semiconductor laser FSK modulation and optical direct discrimination detection," Electron. Lett., vol. 18, pp. 468-470, 1982.

[7] Q. S. Xiang, Y. Zhao, and F. S. Choa, "A high performance RF lightwave transmitter for analog fiber links," In Proc. LEOS 2000. 13th Annu. Meeting, vol. 1, pp. 138-139.

[8] W. V. Sorin, K. W. Chang, G. A. Conrad, and P. R. Hernday, "Frequency domain analysis of an optical FM discriminator," J. Lightw. Technol., vol. 10, pp. 787-793, Jun. 1992.

[9] E. Goobar, "A Michelson interferometer with balanced detection for the characterization of modulation and noise properties of semiconductor lasers," IEEE J. Quantum Elec., vol. QE-29, pp. 1116-1130, Apr. 1993.

[10] G. Chen, J. U. Kang, and J. B. Khurgin, "Frequency discriminator based on ring-assisted fiber Sagnac filter," IEEE Photon. Technol. Lett., vol. 17, pp. 109-111, Jan. 2005.

[11] P. Tremblay and R. Ouellet, "Frequency response of a Fabry-Perot interferometer used as a frequency discriminator," IEEE Trans. Instrum. and Meas., vol. IM-40, pp. 204-207, Apr. 1991.

[12] K. O. Hill and G. Meltz, "Fiber Bragg grating technology fundamentals and overview," J. Lightw. Technol., vol. 15, pp. 1263-1276, Aug. 1997.

[13] F. Zeng and J. P. Yao, "All-optical bandpass microwave filter based on an electro-optic phase modulator," Optics Express, vol. 12, pp. 3814-3819, Aug. 2004.

[14] T. Erdogan, "Fiber grating spectra," J. Lightw. Technol., vol. 15, pp. 1277-1294, Aug. 1997.

[15] I. P. Kaminow, "Balanced optical discriminator," Appl. Opt., vol. 3, pp. 507-510, Apr. 1964.

5.2 Unipolar-Encoding/Bipolar-Decoding for Optical CDMA

In this Section, a novel approach to implementing unipolar-bipolar phase-time encoding/decoding in an optical CDMA system using the FBG-based frequency discriminator is proposed and demonstrated. Two FBG arrays are employed to perform the encoding and decoding. The proposed scheme is equivalent to a sequence inversion keyed (SIK) direct-sequence CDMA, which would provide an improved performance compared to the conventional incoherent scheme using optical orthogonal codes.

Unipolar-Encoding/Bipolar-Decoding for Optical CDMA Using an Electro-optical Phase Modulator and Fiber Bragg Grating Arrays[7]

Fei Zeng and Jianping Yao,

Microwave Photonics Research Laboratory,
School of Information Technology and Engineering,
University of Ottawa, 800 King Edward Avenue, P.O. Box 450, Stn. A,
Ottawa, ON, Canada, K1N 6N5

Abstract

In this paper, we propose a novel approach to implementing unipolar-bipolar phase-time encoding/decoding for optical code division multiple access (CDMA) networks. In the proposed approach, an electrooptic phase modulator and two fiber Bragg grating (FBG) arrays are employed to perform En/De coding. At the transmitter, a low-bit-rate data sequence modulates the optical phase and is then mapped to a high-bit-rate optical sequence via the encoder FBG array in a unipolar way. At the receiver, an identical FBG array that functions as a matched filter is used. Bipolar decoding is achieved by locating the optical carriers on either the positive or the negative slopes of the reflection responses of the decoder FBG array. The proposed encoding/decoding scheme is equivalent to a sequence inversion keyed direct sequence CDMA, which can provide an improved performance compared with the conventional incoherent scheme using optical orthogonal codes. In addition, compared with bipolar decoder applying balanced detection, this approach has a simpler architecture. A proof-of-principle experiment is demonstrated.

Keywords: Code division multiple-access (CDMA), phase modulation, sequence inversion keying (SIK), fiber Bragg grating (FBG), matched filter.

1. Introduction

[7] Published in Proceedings of SPIE, vol. 5971, 59712A, September 2005.

In a local-area network (LAN) environment where the traffic is usually bursty, an efficient multiple access protocol that allows many users to access the network asynchronously at all times is essential. In contrast to contention-based protocols, such as token passing or carrier sense multiple access with collision detection (CSMA/CD), code division multiple access (CDMA) permits a destination receiver to capture a packet rather than the whole communication bandwidth [1, 2]. In addition, a system employing CDMA offers better security than a system using other multiple access schemes.

CDMA is one of the spreading spectrum techniques that transmits data signal over a much larger bandwidth than a conventional transmission system, thus it is particularly suited for optical fiber transmission networks where bandwidth is no longer a limited resource. However, for this resource to be utilized effectively, all-optical processing, such as all-optical encoding and decoding, is desired, to avoid electrical to optical conversions. In addition, optical networks using all-optical processing can maintain a high data rate, which could eliminate electrical processing bottlenecks.

Optical CDMA can be implemented based on incoherent or coherent operation. For an incoherent optical CDMA, unipolar codes are utilized, with matched filtering and direct detection [3-5]. These so-called incoherent implementations provide the impetus for the development of unipolar pseudo-orthogonal codes (0, 1). Compared with conventional electronic bipolar codes (-1, +1) such as Gold sequences, the cross-correlation function of unipolar codes is high and the number of codes in the family is very low. Thus, long, sparse codes and narrower pulses have to be employed to support a larger number of users and higher transmission capacities, which is traded off against the complexity of the implementation. In a coherent optical CDMA, both channel and reference sequences are required to be mapped to a bipolar format, signal processing elements that are capable of distinguishing phase information should be used, . The systems using coherent matched filters to manipulate optical phase have been reported by some researchers [6-8]. Foschini and Vannucci [6] proposed to achieve optical phase encoding and decoding using a pair of electrooptic phase modulators; one is at the transmitter and the other is at the receiver. However, the sequences employed to drive the modulators have to be electrically generated; therefore, the maximum achievable bit rate is limited by the speed of the electronic circuitry. Simpson et al [7] proposed a coherent temporally

coded optical CDMA system based on ladder encoder/decoder. Limited by the geometry of ladder encoders, few codes are available. Encoding and decoding of femtosecond pulses has also been reported for the implementation of coherent ultra-high-speed CDMA networks [9, 10]. In these approaches, basically, an ultrashort light pulse is spatially decomposed by a diffraction grating and pseudorandom phase shifts for the diffracted spectral components are induced to achieve the encoding. At the destination receiver, decoding is performed by a similar arrangement that induces the complex conjugate phase shifts of the encoder. The major disadvantage of the coherent approaches is the environmental influence and the polarization drift, rendering the coherent approach difficult to implement.

A new family of optical CDMA systems based on bipolar modulation/balanced detection has been developed to improve a signal-to-noise ratio (SNR) [11-14]. Basically, the bipolar operation is realized by separating a bipolar sequence into two complementary unipolar sequences which is performed unipolar-unipolar correlation in a pair of parallel correlators. The optical output of each correlator is differenced at the detector by a balanced photodiode receiver. Although such a scheme can perfectly cancel out the multiple-access interference (MAI) under an ideal situation, it brings a challenging implementation issue: additional complexity and cost at both the transmitter and receiver.

In this paper, we propose a novel approach to implementing optical CDMA encoding/decoding using an electrooptic phase modulator, a photodetector and two identical FBG arrays. At the transmitter, a low-bit-rate data sequence modulates the optical phase and is then mapped to a high-bit-rate optical sequence via an FBG-array encoder. At the receiver an identical FBG array that is reversely connected functions as a matched filter. The bipolar decoding is achieved by placing the optical carriers at either the positive or the negative slopes of the reflection responses of the decoder FBG array. Since the encoding is unipolar and the decoding is bipolar, the proposed scheme is equivalent to a sequence inversion keying (SIK) CDMA. Theoretical analysis and experimental results show that this approach has the potential to provide better performance than an incoherent implementation, and a simpler architecture than bipolar modulation/balanced detection scheme. In the next section, the principle and performance comparison of optical CDMA systems using different encoding/decoding schemes are presented, followed by a discussion of our proposed approach. In Section 3, a proof-of-principle

experiment using a single FBG to achieve phase modulation to intensity modulation (PM-IM) conversion is presented. Finally, Section 4 summarizes the findings of this study.

2. Principles

A. Coherent and incoherent CDMA systems

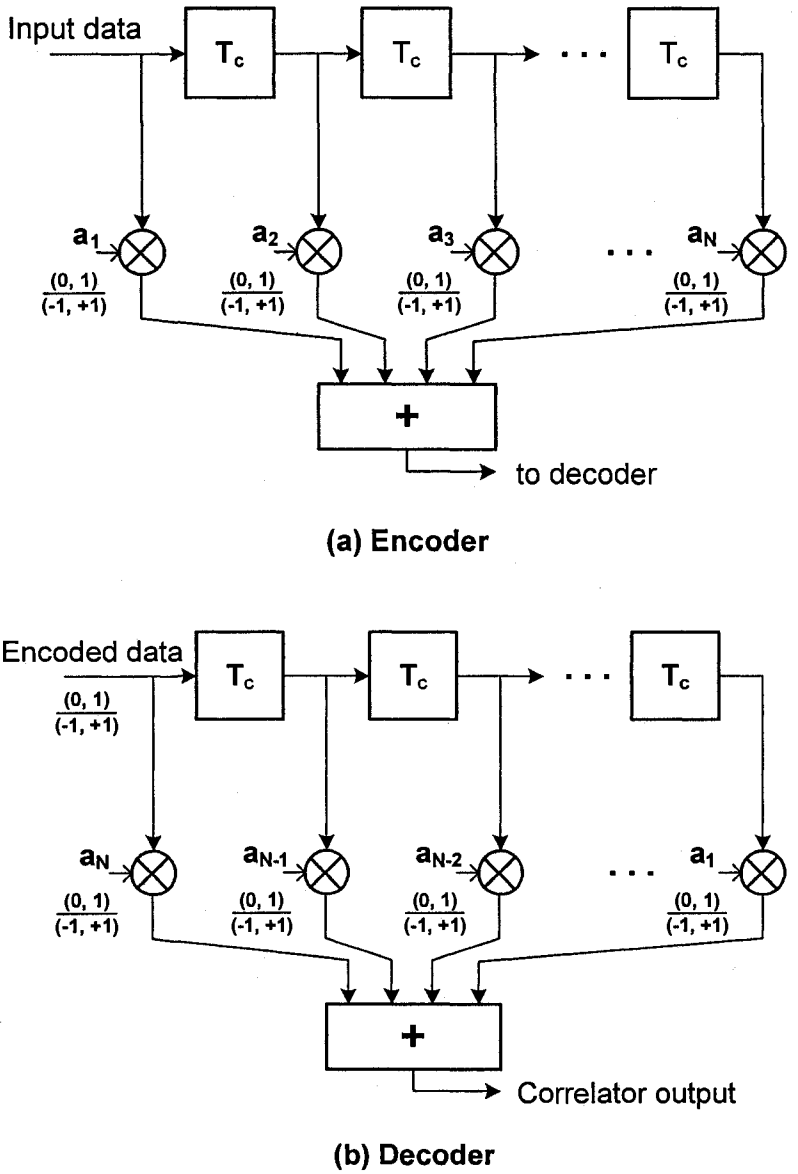

Fig. 1 Schematic diagram of an encoder/decoder pair. (a) An encoder, (b) a decoder. T_c is the chip width. Coefficients a_n can be either 1 or 0 for a unipolar correlator and -1, or +1 for a bipolar correlator.

To clearly distinguish the difference between a bipolar operation and a unipolar operation, the fundamental structures of an encoder and a decoder are shown in Fig. 1. At the transmitter, the encoder typically maps a low-bit-rate electrical signal to a high-bit-rate sequence, either in a bipolar way that pseudo randomly shifts the phase of the optical carrier, or in a unipolar way that alters the intensity of the optical carrier. At the receiver, a correlation is performed by a delay line matched filter which has an impulse response that is the time reversed complex conjugate of the input sequence. The resulting signal is then threshold detected for auto-correlation peaks. In traditional radio or copper-based direct-sequence CDMA systems, detection is achieved via coherent correlation of a bipolar channel sequence (-1, +1) with a bipolar reference sequence (-1, +1). It takes into account phase information in the sequence since the receiver is able to track the phase information. However, in an optical CDMA system, typically an intensity modulator, fiber-optic delay line matched filters, and a square-law photodetector are utilized, both encoding and decoding are constrained to be unipolar. Although optical CDMA with bipolar encoding and decoding can be implemented, the systems are usually very complicated and costly. As a compromise, a scheme called sequence inversion keying (SIK) is proposed. In the SIK scheme, a unipolar channel sequence (0, 1) is correlated with a bipolar reference sequence (-1, +1), which provides better performance than an incoherent CDMA system, but with a simpler architecture than a coherent CDAM system.

To compare the correlation performance of these three schemes, Gold codes of length 31 are employed since they are a popular choice in conventional CDMA systems. As shown in Fig. 2(a), two orthogonal Gold sequences are generated from a pair of maximum-length sequences. Fig. 2(b) shows the auto-correlation and cross-correlation functions obtained for coherent, SIK, and incoherent system respectively. From Fig. 2(b), we can see that the difference between the auto- and cross-correlation peaks for a unipolar-unipolar system is much smaller than that obtained in the bipolar-bipolar system. Although sparse optical orthogonal codes (OOCs) can be applied to reduce that difference, they are only pseudo-orthogonal and long code length and small code weight must be utilized, which reduces the spectral efficiency of the systems. SIK scheme shows a scaled-down version of those obtained by bipolar-bipolar system with an offset depending on the number of simultaneous users, which is a good compromise between the system complexity and performance.

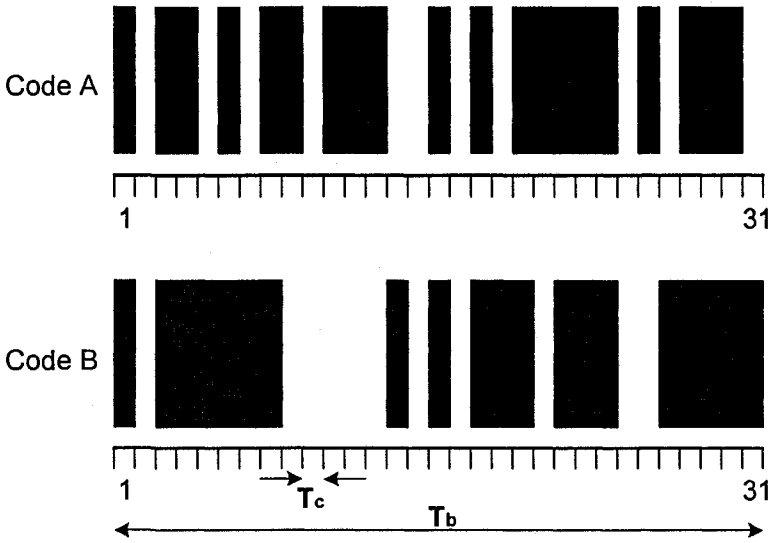

(a)

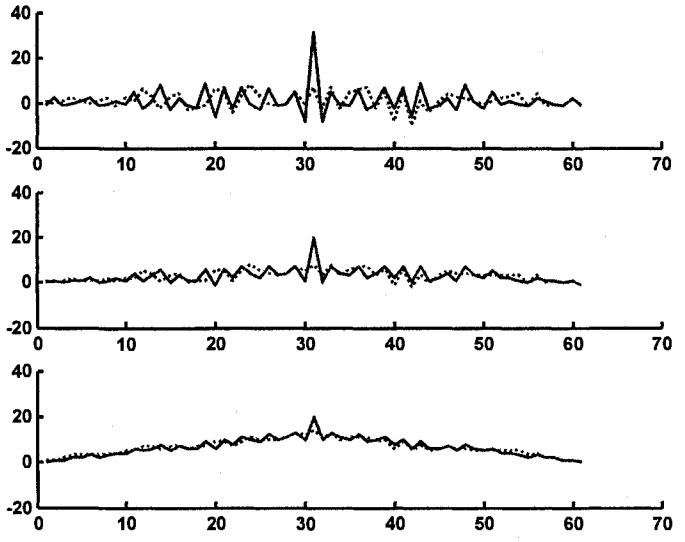

(b)

Fig. 2 Performance comparison among the three optical CDMA schemes (a) Two Gold sequences of length 31: Code A and Code B. (b) Comparison of auto- (solid line) and cross-correlation (dotted line) functions for the two Gold codes. Upper: in a bipolar-bipolar system; middle: in a unipolar-bipolar system (SIK); lower: in a unipolar-unipolar system.

B. FBG based PM-IM conversion

Before introducing the proposed unipolar-bipolar CDMA encoder and decoder, we first discuss the principle of an FBG based PM-IM converter proposed by us [15], which is the key element in

the proposed CDMA system. In the proposed PM-IM converter, PM-IM conversion is achieved by using a uniform FBG serving as a frequency discriminator and a photodetector. In [15], a frequency domain analysis was carried out under a small-signal single-frequency modulation condition. In this situation, only three frequency components, i.e., the optical carrier and the two first-order sidebands were taken into account. We also showed that the reflection slopes of a properly designed FBG can be considered having a linear frequency response with a linear phase response. By using the properly designed FBG and a photodetector, a signal which is the delayed first order derivative of the modulating signal could be obtained. In addition, by locating the optical carrier at the opposite slopes of the FBG reflection spectrum, the detected electrical signals had a π phase difference. Note that no signal could be recovered if the carrier was located at the centre of the reflection band. However, in a digital communication system, the modulating signal is no longer a single frequency sinusoidal tone, but a mapping of binary data sequence to analog waveforms, e.g., square waves. In this case, the modulating signal $s(t)$ can be expressed as

$$s(t) = \sum_{l=-\infty}^{\infty} b_l \cdot P_T(t - l \cdot T), \tag{1}$$

where b_l is the binary data sequence that takes on 0 or 1 for each l, and $P_T(t)$ is a rectangular pulse of duration T. We know that such a signal can be considered as a summation of infinite frequency components and it will be very difficult to do the frequency domain analysis, because when this multi-frequency signal is used to phase modulate an optical carrier, the number of the cross-modulation products is usually very large. Instead, a time domain analysis can be easily executed.

The normalized modulated optical field can be written in a general form of

$$E_{PM}(t) = \cos[\omega_c t + \Delta\varphi(t)] = \cos[\omega_c t + \beta_{PM} \cdot s(t)], \tag{2}$$

where ω_c is the angular frequency of the optical carrier; $\Delta\varphi(t)$ is the modulation-induced phase change of the carrier; and β_{PM} is the phase modulation index. After passing the optical signal described in Eq. (2) through an ideal frequency discriminator having an impulse response

of $\delta'(t)$, where $\delta(t)$ is the unit impulse and $\delta'(t)$ is its first-order derivative, we obtain the differential optical field

$$E_{FD}(t) = K_{FD} \cdot E'_{PM}(t) = -K_{FD} \cdot [\omega_c + \beta_{PM} \cdot s'(t)] \cdot \sin[\omega_c t + \beta_{PM} \cdot s(t)], \quad (3)$$

where $E_{FD}(t)$ represents the optical field at the output of the frequency discriminator, $E'_{PM}(t)$ and $s'(t)$ represent the first-order derivatives of $E_{PM}(t)$ and $s(t)$ respectively. K_{FD} is the slope steepness factor of the frequency discriminator.

A square-law photodetector functions as an envelope detector having an output proportional to $|E_{FD}(t)|^2$, then the recovered electrical signal can be expressed as

$$r(t) \propto \omega_c^{\,2} + 2\omega_c \cdot \beta_{PM} \cdot s'(t) + [\beta_{PM} \cdot s'(t)]^2, \quad (4)$$

where the first term on the right side, $\omega_c^{\,2}$, represents a dc and can be eliminated by using a dc blocker. Compared to the second term, the third term is much smaller and can be neglected. Then we can conclude that the output of the proposed PM-IM converter is proportional to the differential of the modulating signal $s(t)$, which implies that if the modulating signal is pre-processed to be the integral of $s(t)$ before driving the electrooptical phase modulator, the original information will be exactly recovered.

C. Unipolar-bipolar optical CDMA

A point-to-point link of the proposed unipolar-bipolar optical CDMA network is shown in Fig. 3. At the transmitter, an array of laser diodes (LDs) is employed as the light source. Through an optical star coupler, the combined light beams are fed to an electrooptical phase modulator which is driven by the pre-processed electrical signal that is expressed as

$$\upsilon(t) = \int_{-\infty}^{t} s(t)dt\,. \quad (5)$$

An array of N FBGs used as mirrors will perfectly reflect the N optical carriers at their reflection peaks to achieve code spreading. Either the input light wavelengths or the center

wavelengths of the FBGs are able to be shifted relative to each other; hence the individual chips of the coding sequence can be programmed to be either '1' (reflection) or '0' (no reflection), and can also be reconfigured. The encoded optical field is then written as

$$E_{encoded}(t) = \sum_{n=1}^{N} \cos[\omega_{c,n} t + \beta_{PM} \cdot \upsilon(t - nT_c)] \cdot a_n , \qquad (6)$$

where $\omega_{c,n}$ represents the angle frequency of the n-th carrier, a_n is the n-th chip that takes on 0 or 1, and T_c is the chip width, which is determined by the turn around optical path length between two adjacent FBGs. In a real system, the number of LDs can be less, which is determined by the weight of the coding sequence.

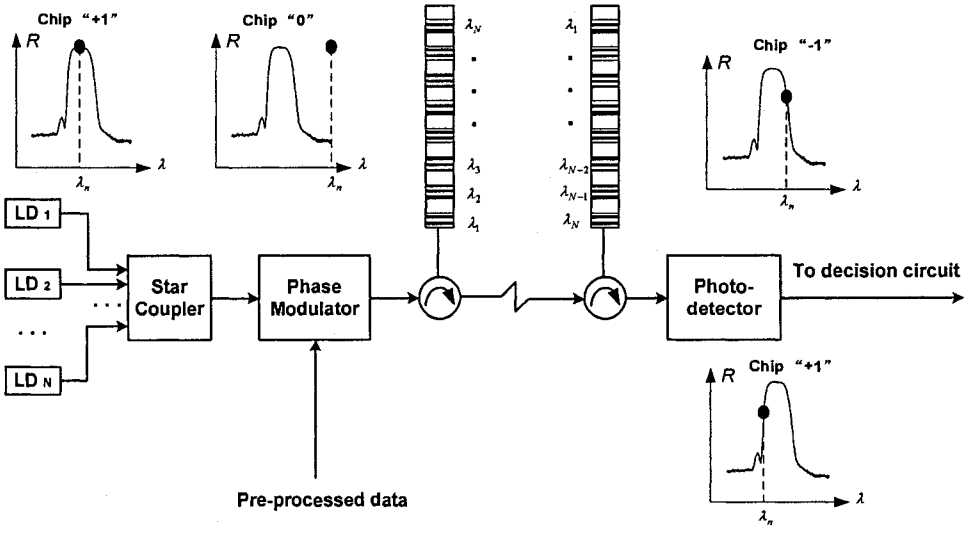

Fig. 3 Block diagram of a point-to-point link in the proposed unipolar-bipolar optical CDMA system.

At the receiver, an identical FBG array reversely placed is used as a matched filter. More importantly, as shown in Fig. 3, instead of reflecting the carriers at the reflection peaks in the encoder, the up or down slopes of the decoder FBGs are employed to reflect the corresponding carriers to achieve unipolar-bipolar correlation. The output of the photodetector can be written as

$$r_{decoder}(t) \propto \sum_{n=1}^{N} s(t - nT_c) \cdot a_n \cdot b_{N-n}, \quad (7)$$

where $a_n \in (0, 1)$, and $b_{N-n} = 2a_{N-n} - 1, \in (-1, +1)$. It has the same expression as the correlation output of an SIK CDMA system, which has been discussed in Sec. *A*. Compared to a unipolar-unipolar operation, the bipolar decoding presented in Eq. (7) has the same auto-correlation performance, but is able to significantly reduce cross-correlation peaks, and eventually suppresses the MAI induced by other user pairs.

3. Experiment

Based on the theoretical analysis in Sec. 2, we can see that the key element in the proposed unipolar-bipolar optical CDMA system is the FBG based PM-IM converter. Both the reflectivity and phase response at the slopes of the decoder FBGs should be linear and any nonlinearity will introduce distortion to the recovered electrical signal. However, this requirement may not be very critical since the electrical limiter and decision circuit after the photodetector can help the system tolerate signal distortion to some extend. The overall conversion efficiency and operational bit rate are determined by the steepness and bandwidth of the FBG slopes, which is an issue that needs to be addressed. In addition, at the transmitter, the encoder FBGs are desired to have flat top and broad bandwidth in reflection spectra to approach unaffected encoding. Therefore, both the encoder and decoder FBGs should be optimized. In [15], we have shown that by carefully choosing the FBG fabrication parameters, such as grating length, refractive index modulation depth and apodization profile, the system requirements can be met. In the following, a proof-of-principle experiment using a single FBG to achieve PM-IM conversion is presented.

The FBG fabricated in this experiment has a length of 10 mm, a peak power reflectivity of 90% and a Gaussian apodization profile. Additional inverse apodization is also applied during the FBG fabrication process to further suppress the sidelobes on short-wavelength side. Its reflectivity spectrum is shown in Fig. 4, which has a central wavelength at 1536.12 nm and a 3-dB bandwidth of 0.23 nm. A tunable laser with typical linewidth of 150 kHz is applied as a single wavelength light source. A 622 Mb/s electrical signal is generated using a bit-error-rate tester (BERT). Phase modulation is performed by using a $LiNbO_3$ straight-line phase

modulator. A digital communication analyzer is used to monitor the output of the photodetector. An erbium-doped fiber amplifier is incorporated in the system to compensate for the power loss in the system.

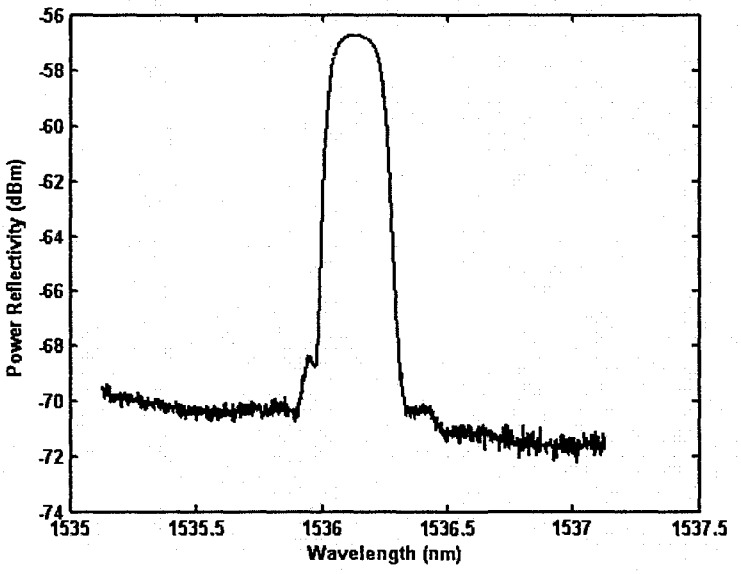

Fig. 4 Measured power reflection spectrum of the FBG used in the experiment.

To verify the theoretical analysis presented in Sec. *B*, we tune the carrier wavelength and make it be reflected at different locations of the grating reflection spectrum, i.e., the left slope, the middle, and the right slope. Fig. 5 shows the waveforms of the corresponding electrical outputs when the 622 MHz clock signal is applied to the phase modulator. Fig. 6 shows the eye diagram obtained when the carrier is tuned at the left slope of the FBG with a 622 Mb/s pseudo random bit sequence (PRBS) 2^7-1 signal is applied. The experimental results clearly show that 1) the output of the proposed FBG based PM-IM converter is the first derivative of the modulating signal, 2) the amplitude of the detected signals have different signs when the carrier wavelengths are located at the opposite slopes, 3) and no signal can be recovered if the carrier is located at the center of the reflection band. These features agree very well with the theoretical analysis and can be directly employed to achieving unipolar encoding and bipolar decoding in our proposed optical CDMA network.

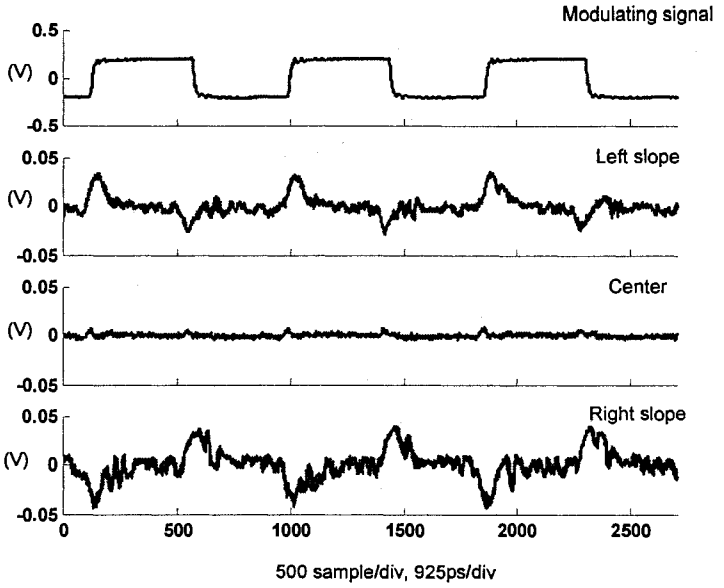

Fig. 5 Measured waveforms of the photodetector outputs when the wavelength of the optical carrier is tuned at different reflection points. The modulating signal is plotted as a reference (upper).

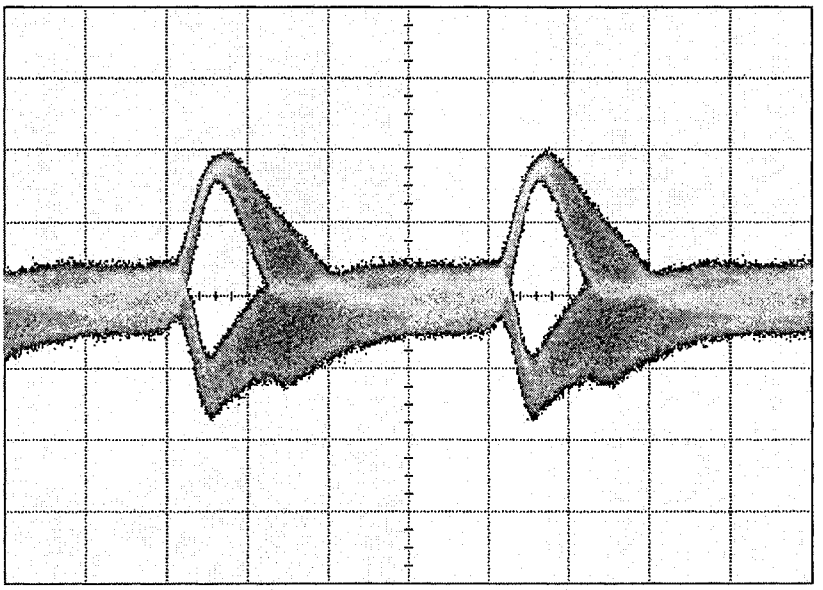

X axis: 200ps/div; Y axis: 20mV/div

Fig. 6 Measured eye diagram when 622 Mb/s PRBS 2^7-1 signal is applied.

4. Conclusions

A pair of all-optical encoder and decoder having equivalent performance as an SIK CDMA system was proposed in this paper. An electrooptical phase modulator and two fiber Bragg

grating (FBG) arrays are applied to manipulate the optical code signature. At the transmitter a low-bit-rate data sequence phase modulates the optical carriers and is then mapped to a high-rate optical sequence via the encoder FBG array in a unipolar way. At the receiver a similar FBG array functions as a matched filter and bipolar decoding is achieved by placing the optical carriers on either positive or negative slopes of the reflection responses of the decoder FBG array. The proposed encoding/decoding scheme can provide improved performance than the conventional incoherent scheme using optical orthogonal codes. In addition, compared with bipolar decoder applying balanced detection, this approach has a simpler and more compact architecture. Moreover, the proposed encoder/decoder can be quickly reconfigured by tuning either the wavelengths of the LDs or the FBGs. A proof-of-principle experiment using a single FBG to achieve PM-IM conversion was demonstrated. The experimental results showed excellent agreement with the theoretical analysis.

References

[1] M. B. Pursley, Spread-Spectrum Multiple-Access Communications in Multi-User Communication Systems, G. Longo, Ed. New York: Springer-Verlag, 1981.

[2] M. J. Parham, C. Smythe and B. L. Weiss, "Code division multiple-access techniques for use in optical-fiber local-area networks," J. Electron. Commun. Eng., pp. 203-212, Aug. 1992.

[3] P. R. Prucnal, M. A. Santoro, and T. R. Fan, "Spread spectrum fiber-optic local area network using optical processing," J. Lightw. Technol., vol. LT-4, pp. 547-554, May 1986.

[4] J. A. Salehi, "Code division multiple-access techniques in optical fiber networks-part I: fundamental principles," IEEE Trans. Commun., vol. 37, pp. 824-833, Aug. 1989.

[5] D. B. Hunter and R. A. Minasian, "Optical Programmable high-speed optical code recognition using fiber Bragg grating arrays," Electron. Lett., vol. 35, no. 5, pp. 412-414, Mar. 1999.

[6] G. J. Foschini and G. Vannucci, "Using spread-spectrum in a high-capacity fiber-optic local network," J. Lightw. Technol., vol. LT-6, pp. 370-379, Mar. 1988.

[7] D. D. Sampson and D. A. Jackson, "Spread-spectrum optical fiber network based on pulsed coherent correlation," Electron. Lett., vol. 26, pp. 1550-1552, 1990.

[8] N. Wada and K. I. Kitayama, "A 10Gb/s optical code division multiplexing using 8-chip optical bipolar code and coherent detection," J. Lightw. Technol., vol. 17, no. 10, pp. 1758-1765, Oct. 1999.

[9] C. M. Decusatis and P. K. Das, "Spread-spectrum techniques in optical communication using transform domain processing," IEEE J. Sel. Areas Commun., vol. 8, pp. 1608-1616, Aug. 1990.

[10] P. C. Teh, P. Petropoulos, M. Ibsen, and D. Richardson, "A comparative study of the performance of seven- and 63-chip optical code-division multiple-access encoders and decoders based on superstructured fiber Bragg gratings," J. Lightw. Technol., vol. 19, no. 9, pp. 1352-1365, Sept. 2001.

[11] T. O'Farrell and S. Lochmann, "Performance analysis of an optical correlator receiver for SIK DS-CDMA communication system," Electron. Lett., vol. 30, no. 1, pp. 63-65, Jan. 1994.

[12] I. Andonovic, L. Tancevski, M. Shabeer, and L. Bazgaloski, "Incoherent all-optical code recognition with balanced detection," J. Lightw. Technol., vol. 12, no. 6, pp. 1073-1080, Jun. 1994.

[13] C. F. Lam, D. T. K. Tong, M. C. Wu, and E. Yablonovitch, "Experimental demonstration of bipolar optical CDMA system using a balanced transmitter and complementary spectral encoding," IEEE Photon. Technol. Lett., vol. 10, no. 10, pp. 1504-1506, Oct. 1998.

[14] S. J. Kim, T. Y. Kim, Chul S. Park, and Chang S. Park, "10-Gb/s temporally coded optical CDMA system using bipolar modulation/balanced detection," IEEE Photon. Technol. Lett., vol. 17, no. 2, pp. 510-512, Feb. 2005.

[15] F. Zeng and J. P. Yao, "Frequency domain analysis of fiber Bragg grating based phase modulation to intensity modulation conversion," accepted for presentation at Photonics North 2005, 12-14 Sept., Toronto, Canada.

5.3 UWB pulse generation using an FBG-based frequency discriminator

UWB pulses are usually generated in the electrical domain for short-range high-data-rate wireless communications. To extend its coverage, UWB signal distributed over optical fiber is a topic of interest recently. Therefore, to fully exploit the advantages provided by optics, it is highly desirable that the distributed UWB pulse signals can be generated directly in the optical domain without the need of extra optical-electrical and electrical-optical conversions. In addition, with the current stage of technology, it is rather difficult to generate UWB pulses with a fractional bandwidth even greater than 100% at the central frequency of around 7 GHz. Hence, UWB pulse generation in the optical domain can also find application in instrumentations.

In this Section, two approaches using the FBG-based frequency discriminator for UWB pulse generation in the optical domain are presented. The use of the proposed all-optical signal processor to implement UWB pulse polarity and pulse shape modulation are also discussed which would provide the potential for fully exploiting the advantages provided by UWB-over-fiber networks.

5.3.1 UWB pulse signal generation based on EOPM

In this Section, we propose a hybrid system to generate UWB pulses. A Gaussian-shaped pulse train from an electrical pulse generator is applied to an EOPM to perform electrical to optical conversion. UWB monocycle or doublet pulses are generated at the output of a PD by performing PM-IM conversion using an FBG-based frequency discriminator, in which the optical carrier is located at the linear or the quadrature slopes of the FBG reflection spectrum.

Ultrawideband Signal Generation Using a High-Speed Electrooptic Phase Modulator and an FBG-Based Frequency Discriminator[8]

Fei Zeng, *Student Member, IEEE* and Jianping Yao, *Senior Member, IEEE*

Microwave Photonics Research Laboratory
School of Information Technology and Engineering
University of Ottawa, Ottawa, Ontario, Canada
Email: jpyao@site.uottawa.ca

Abstract

We propose a novel approach to generating UltraWideBand (UWB) pulse signals in the optical domain. The proposed system consists of a laser source, an electrooptic phase modulator (EOPM), a fiber Bragg grating (FBG), and a photodetector (PD). The light source is phase modulated by an electrical Gaussian pulse train via the EOPM. The optical phase modulation to intensity modulation conversion is achieved by reflecting the phase modulated light at the slopes of the FBG that serves as a frequency discriminator. Electrical monocycle or doublet pulses are obtained at the output of the PD by locating the optical carrier at the linear or the quadrature slopes of the FBG reflection spectrum. The use of the proposed configuration to implement pulse polarity and pulse shape modulation in the optical domain is discussed, which provide the potential for fully exploiting the advantages provided by UWB-over-fiber networks. Experimental measurements in both temporal and frequency domains are presented.

Index terms: microwave photonics, radio over fiber, UWB over fiber, all-optical signal processing, fiber Bragg grating, frequency discriminator

1. Introduction

UltraWideBand (UWB) impulse technology has been known for a few decades, but its applications for broadband wireless communications has been explored only recently. A lot of research efforts are being directed to the enhancement of the operational capabilities and the

[8] IEEE Photonics Technology Letters, vol. 18, no. 19, pp. 2062-2064, Oct.1, 2006.

cost-effectiveness of UWB systems for high-throughput wireless communications and sensor networks. Basically, the impulse signal in a UWB wireless system needs to achieve a fractional bandwidth larger than 20% or a 3-dB bandwidth of at least 500 MHz in the frequency range from 3.1 GHz to 10.6 GHz, as defined in part 15 of the Federal Communication Commission (FCC) regulations [1-3]. However, by wireless transmission, UWB signals are only limited in short distance of a few to tens of meters. To avoid such short-range networks operating only in a standalone mode, UWB-over-fiber technology can provide a very promising solution to integrate local UWB environment into the fixed wired networks or wireless wide-area infrastructures [4, 5].

Therefore, to fully exploit the advantages provided by optics, it is highly desirable that the distributed UWB pulse signals can be generated and modulated directly in the optical domain without the need of extra optical-electrical (O/E) and electrical-optical (E/O) conversions. In addition, using optical techniques to generate UWB pulses has many other advantages, such as light weight, small size, large tunability and the immunity to electromagnetic interference. Recently, we have proposed a method to generate and distribute UWB doublet pulses over a single-mode fiber (SMF) link. In the system, electrical Gaussian pulses were modulated on an optical carrier using an electrooptic phase modulator (EOPM). The optical phase modulation to intensity modulation (PM-IM) conversion was realized by changing the phase relationships among all the frequency components of the optical phase-modulated signal. The chromatic dispersion of the fiber link of a length of 25 km is used to achieving the desired phase changes. The PM-IM conversion has a transfer function equivalent to a microwave bandpass filter, by which the input Gaussian pulses were converted to UWB doublet pulses [6].

In this letter, we propose an approach to generating monocycle or doublet pulses in a structure without using a long optical fiber. In the proposed system, an optical carrier is phase modulated by a Gaussian pulse train via an EOPM. Instead of using a 25-km SMF to perform PM-IM conversion [6], the PM-IM conversion is achieved here by use of a fiber Bragg grating (FBG) that serves as a frequency discriminator [7]. By locating the optical carrier at the linear slope or the quadrature slope of the FBG reflection spectrum, monocycle or doublet pulses can be obtained at the output of a photodetector (PD). In addition, UWB pulses with opposite polarities can be generated by locating the optical carrier at the right (positive slope) or the left (negative

slope) side of the FBG reflection spectrum. This property is important, because the proposed system can be used to implement two different UWB pulse modulation schemes by shifting the optical carrier, the pulse shape modulation (PSM) (monocycle - doublet) and the pulse polarity modulation (PPM). Experiments are carried out to investigate the proposed UWB pulse generation system. Experimental measurements in both temporal and frequency domains are presented, which have good agreement with theoretical analysis.

2. Principle

The block diagram of the proposed UWB pulse generator is shown in Fig. 1. Light from a laser diode (LD) is fiber coupled to an EOPM which is driven by a sequence of Gaussian pulses. The phase-modulated optical signal is then applied to a uniform FBG via an optical circulator. The PM-IM conversion is achieved by using the FBG serving as a frequency discriminator. The PM-IM converted signal is then detected at a PD, which serves as an envelope detector.

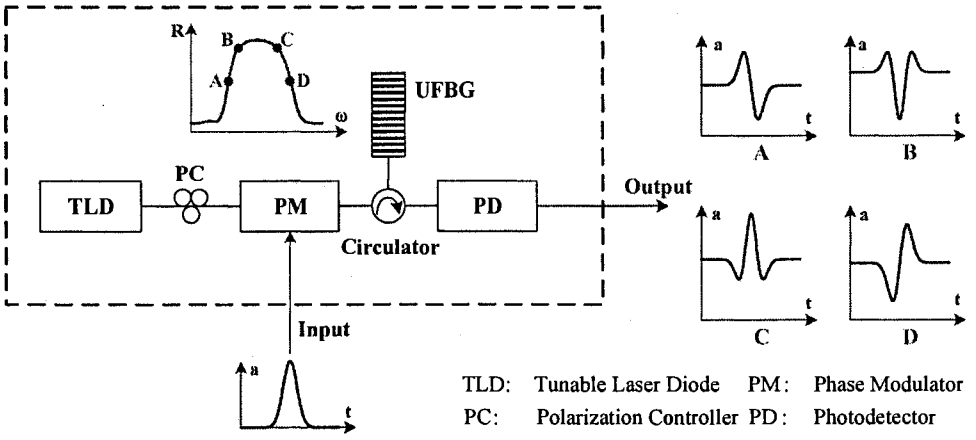

Fig. 1 Block diagram of the proposed UWB pulse generator.

The normalized optical field being phase-modulated by the Gaussian pulse train can be expressed in the form of

$$E_{PM}(t) = \exp[j\omega_c t + \beta_{PM} \cdot s(t)], \tag{1}$$

where ω_c is the angular frequency of the optical carrier, β_{PM} is the phase modulation index, and $s(t)$ is the pulse train represented by

$$s(t) = \sum_{n=-\infty}^{+\infty} \Omega(t - nT_r), \tag{2}$$

where T_r is the pulse repetition interval, and $\Omega(t)$ represents an ideal Gaussian pulse waveform. It is known that the energy spectral density of $\Omega(t)$ is large at dc and low-frequency region, which makes wireless transmission of such a signal impractical. Monocycle and doublet pulses that can be generated by performing the first-order and second-order derivatives of Gaussian pulses have a spectrum profile that can satisfy the FCC specified spectrum mask. Pulse waveforms for UWB applications can also be created by employing a high-pass filter to modify the spectrum of the Gaussian pulse, which is similar to the implementation of different orders of derivative of $\Omega(t)$ [1, 10]. For example, a Gaussian monocycle and a Gaussian doublet, that have very low spectral power at low-frequency region, can be respectively generated by performing the first-order and second-order derivatives of $\Omega(t)$. The approach proposed in this letter is to convert the Gaussian pulses into UWB pulses in the optical domain, which can be employed as UWB pulse source in a UWB-over-fiber network. In addition, in the proposed approach since the UWB signal is already modulated on optical carriers, optically controlled true time-delay beamforming structures [8] can be directly applied at the receiver front-end to improve the operational capabilities of the UWB impulse systems.

Based on the configuration shown in Fig. 1, when the phase modulated light is located at the linear region of the FBG reflection slopes, as shown in Fig. 1 at A, the ac part of the recovered signal at the output of the PD can be written as [7]

$$r(t) \sim \Re P \beta_{PM} K \cdot s'(t), \tag{3}$$

where $\Re$ is the responsivity of the PD, P is the optical power reflected from the FBG, K is the slope steepness factor of the FBG power spectrum, and $s'(t)$ is the first-order derivative of the modulating signal $s(t)$. Then the UWB monocycle pulses are obtained, which is denoted as $\Omega'(t)$.

Furthermore, when the optical carrier is located at the opposite slope of the FBG reflection spectrum, as shown in Fig. 1 at D, the output pulses will have a π phase difference. This

property is important, which has the potential to realize PPM when two optical carriers corresponding to these two out-of-phase pulses are employed and switched by the data sequence to be transmitted. More interestingly, if the optical carrier is located at the quadrature slopes of the FBG reflection response, as shown in Fig. 1 at B and C, doublet pulses will be generated. Therefore, by locating the optical carrier at different locations, UWB pulses with different shapes can be generated in the same configuration, and eventually the implementation of another pulse modulation scheme, i.e., PSM, is possible.

3. Experiment

The proposed UWB pulse generation system is experimentally implemented based on the configuration shown in Fig. 1. A tunable laser source with typical linewidth of 150 kHz is employed as the light source. The Gaussian-like pulse train is generated by a bit-error-rate tester (BERT). The temporal waveform representing a single input pulse can be found in Fig. 3(a) of [8], which has a full-width at half maximum amplitude of about 63 ps. Phase modulation is performed by using a $LiNbO_3$ straight-line phase modulator. An FBG with a length of 10 mm and a peak power reflectivity of 90% is fabricated and used as the frequency discriminator in the experiment. A proper Gaussian apodization is applied during the FBG fabrication process to suppress the reflection sidelobes. Its reflection spectrum is shown in Fig. 2, which has a central wavelength of 1536.12 nm and a 3-dB bandwidth of 0.23 nm.

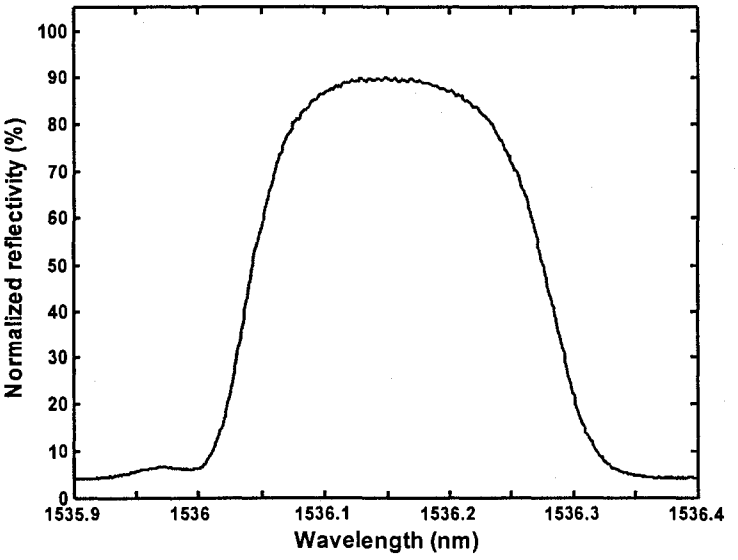

Fig. 2 Measured power reflection spectrum of the FBG used in the experiment.

First, the carrier wavelength λ_c is tuned at of 1536.032 nm, which is located at the left linear slope of the FBG. The signal at the output of the PD is then measured in both temporal and frequency domains by use of a high-speed sampling oscilloscope and an electrical spectrum analyzer, respectively. Fig. 3(a) shows the generated Gaussian monocycle pulse, which has an FWHM of about 52 ps. Fig. 3(b) shows the power spectrum of the Gaussian monocycle pulse signal, which has a central frequency of about 3.45 GHz, and a 10-dB bandwidth of about 7.94 GHz.

Then, the carrier wavelength is tuned at 1536.098 nm, which is located at the left turning corner (quadrature slope) of the FBG reflection spectrum, the output pulse turns to be a doublet with a negative mainlobe and two equal-time sidelobes having positive values, as shown in Fig. 4(a). Its FWHM is of about 42 ps. From its power spectrum shown in Fig. 4(b), we can see that the central frequency is increased to be about 7.14 GHz and the 10-dB bandwidth is about 8.8 GHz. These results are expected according to the mathematical definition of a Gaussian pulse with different orders of derivatives [9]. We then further tune the carrier wavelength and make it be reflected at the right turning corner and the right linear slope, respectively. As can be seen from Fig. 5, the generated pulses are actually the inverted versions of the ones shown in Fig. 4(a) and Fig. 3(a), respectively. These interesting results agree well with the theoretical analysis in Sec. 2.

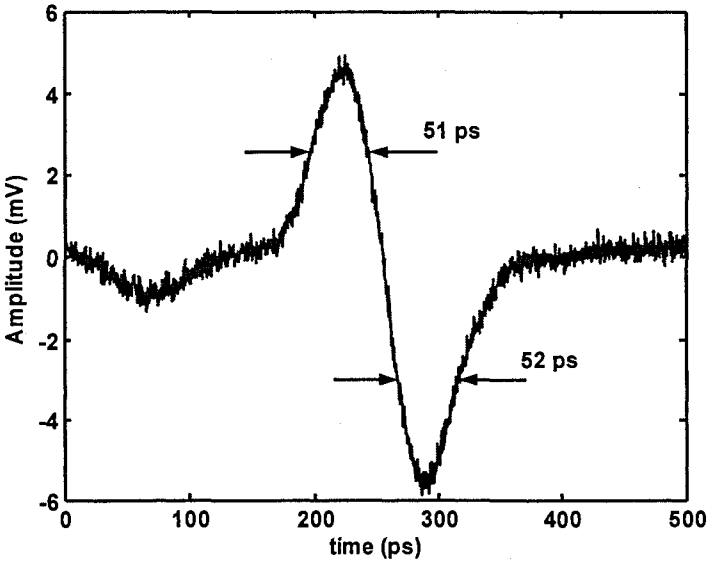

(a)

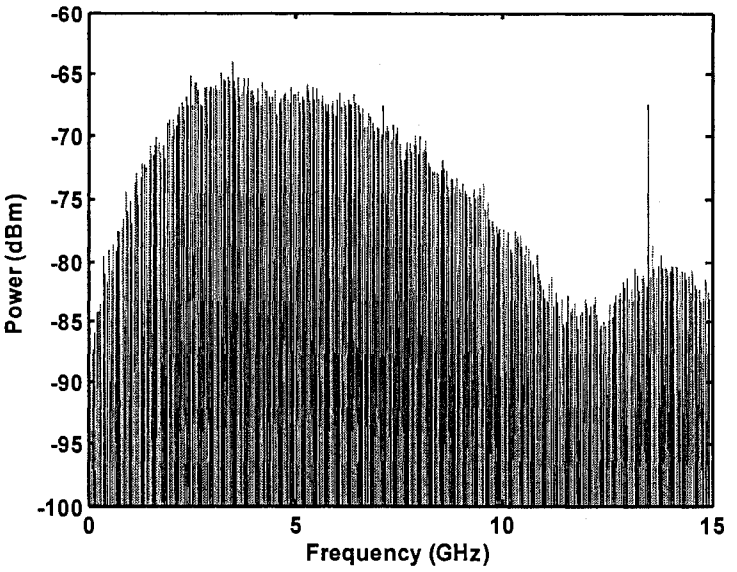

(b)

Fig. 3 When a 13.5 Gb/s PBRS 2^{10}-1 signal (generated by the BERT) is applied to the EOPM, the wavelength of the optical carrier λ_c =1536.032 nm, (a) the waveform showing a monocycle pulse, and (b) the power spectrum measured at the output of the PD.

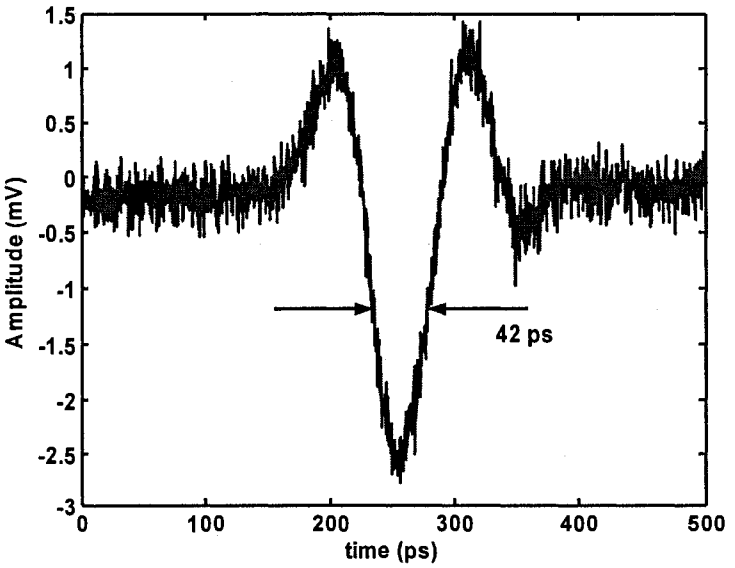

(a)

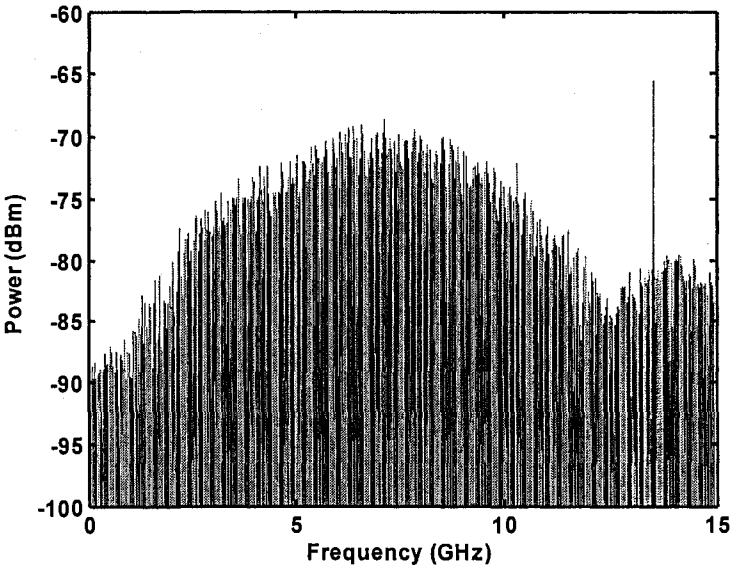

(b)

Fig. 4 (a) Waveform of the Gaussian doublet pulse, and (b) power spectrum of the shaped 13.5 Gb/s PBRS 2^{10}-1 signal obtained at the output of the PD. The wavelength of the optical carrier is λ_c =1536.098 nm.

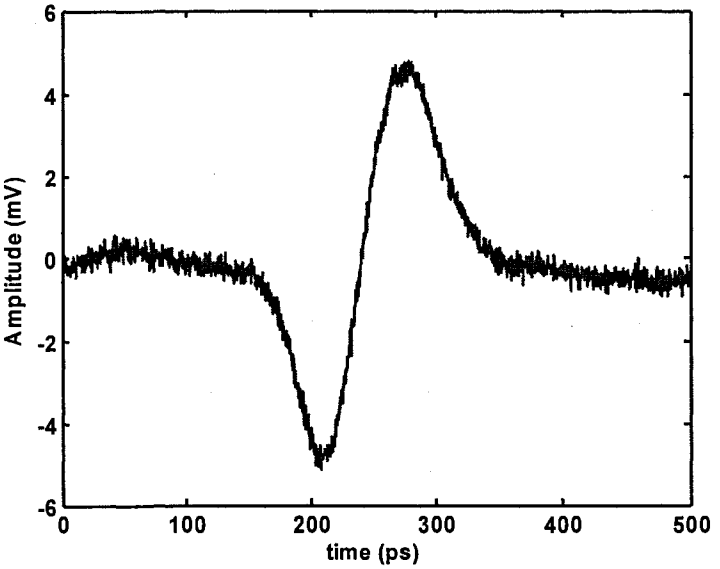

(a)

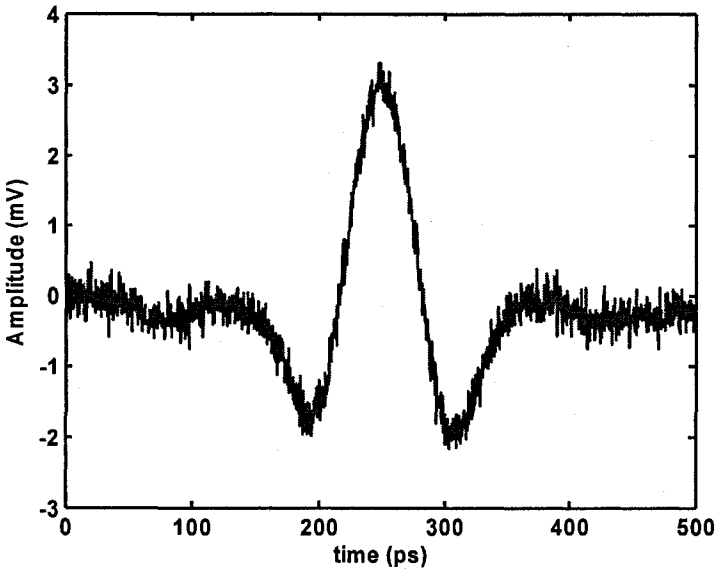

(b)

Fig. 5 Waveforms of the output pulses when the optical carrier is located at the opposite slope of the FBG: (a) λ_c =1536.272 nm, (b) λ_c =1536.210 nm.

4. Conclusion

An optical UWB pulse generator that can shape the input Gaussian pulses into monocycle or doublet pulses has been proposed and experimentally demonstrated. The proposed system was based on the optical PM-IM conversion that was realized by use of an EOPM and an FBG serving as an optical frequency discriminator. By locating the optical carrier at different locations of the FBG reflection spectrum, UWB pulses with inverted polarity or different shapes were obtained. This feature makes PPM and PSM schemes possible. In addition, since the UWB pulse signals were obtained directly in optical domain, the proposed approach can be well incorporated into UWB-over-fiber networks and eventually simplifies the entire networks by centralizing the operations at the central offices. In the proposed system, an electrical pulse source was needed. The system can be made all optical, if the electrical pulse source is replaced by an optical pulse source, such as a mode locked laser source.

References:

[1] M. Ghavami, L. B. Michael, and R. Kohno, Ultra Wideband Signals and Systems in Communication Engineering. West Sussex, England: Wiley, 2004.

[2] D. Porcine, P. Research, and W. Hirt, "Ultra-wideband radio technology: Potential and challenges ahead," IEEE Commun. Mag., vol. 41, no. 7, pp. 66-74, Jul. 2003.

[3] G. R. Aiello and G. D. Rogerson, "Ultra-wideband wireless systems," IEEE Microw. Mag., vol. 4, no. 2, pp. 36-47, Jun. 2003.

[4] T. Kawanishi, T. Sakamoto, and M. Izutsu, "Ultra-wide-band signal generation using high-speed optical frequency-shift-keying technique," in IEEE Int. Microwave Photonics, pp. 48-50, 2004.

[5] W. P. Lin and J. Y. Chen, "Implementation of a new ultrawide-band impulse system," IEEE. Photon. Technol. Lett., vol. 17, no. 11, pp. 2418-2420, Nov. 2005.

[6] F. Zeng and J. P. Yao, "An approach to Ultra-Wideband pulse generation and distribution over optical fiber," IEEE Photon. Technol. Lett., vol. 18, no. 7, pp. 823-825, Mar. 2006.

[7] F. Zeng and J. P. Yao, "Frequency domain analysis of fiber Bragg grating based phase modulation to intensity modulation conversion," in SPIE Proc., vol. 5971, Sept. 2005.

[8] H. Zmuda, R. A. Soref, P. Payson, S. Johns, and E. N. Toughlian, "Photonic beamformer for phased array antennas using a fiber grating prism," IEEE Photon. Technol. Lett., vol. 9, pp. 241-243, Feb. 1997.

[9] X. Chen and S. Kiaei, "Monocycle shapes for ultra wide-band system," in IEEE Int. Symp. Circuits and Systems, vol. 1, pp. 26-29, 2002.

5.3.2 All-optical UWB pulse signal generation based on XPM

In Sec. 5.3.1, a hybrid system to generate UWB pulses was presented, in which a sophisticated electrical pulse generator to generate the short Gaussian pulse train and a wideband EOPM to perform electrical to optical conversion are required. In this Section, we propose an all-optical system to generate UWB monocycle and doublet pulses in a structure without the need of either a high speed EOPM or an electrical short-pulse generator. In this approach, a CW optical probe is cross-phase modulated (XPM) in a nonlinear fiber by a pulsed light, which can be the output of a Q-switched or a mode-locked laser. UWB monocycles and doublets are generated by applying the XPM signal to an FBG-based frequency discriminator.

The investigation is performed by a two-step experiment. In the first step, we focus on the XPM effect in a nonlinear fiber. A CW light being intensity-modulated by an electrical pulse train is applied to a length of nonlinear fiber (25 km non-zero dispersion shifted fiber (NZ-DSF)) as a pulsed pump to perform XPM. UWB monocycles and doublets are then generated by applying the XPM signal to an FBG-based frequency discriminator. In the second step, we make the system all optical. An optical pulse train from a femtosecond pulse laser with proper spectrum slicing is used to generate the pulsed pump. The phase modulation is then realized in a length of nonlinear fiber (400 m dispersion shifted fiber (DSF)) to create XPM. Again, UWB monocycles and doublets are obtained by applying the XPM signal to the FBG-based frequency discriminator.

A. Operation principle

The block diagram of the proposed all-optical UWB pulse signal generator based on XPM is shown in Fig. 5.3.2.1. When a pulsed pump light is combined with a CW probe light and sent through a fiber, the optical pump pulses impose a phase modulation onto the CW light due to XPM. After the nonlinear fiber, an FBG combined with an optical circulator is used as an optical bandpass filter to eliminator the pump light. More importantly, its reflection slopes are used to perform frequency discrimination, to convert the cross-phase modulated probe light to intensity-modulated signals. When the optical carrier is located at the opposite slope of the FBG reflection spectrum, the output pulses will have a π phase difference, by which pulse polarity modulation can be realized. Furthermore, if the optical carrier is located at the

quadrature slopes of the FBG reflection response, as shown in Fig. 5.3.2.1 at B and C, doublet pulses will be also generated.

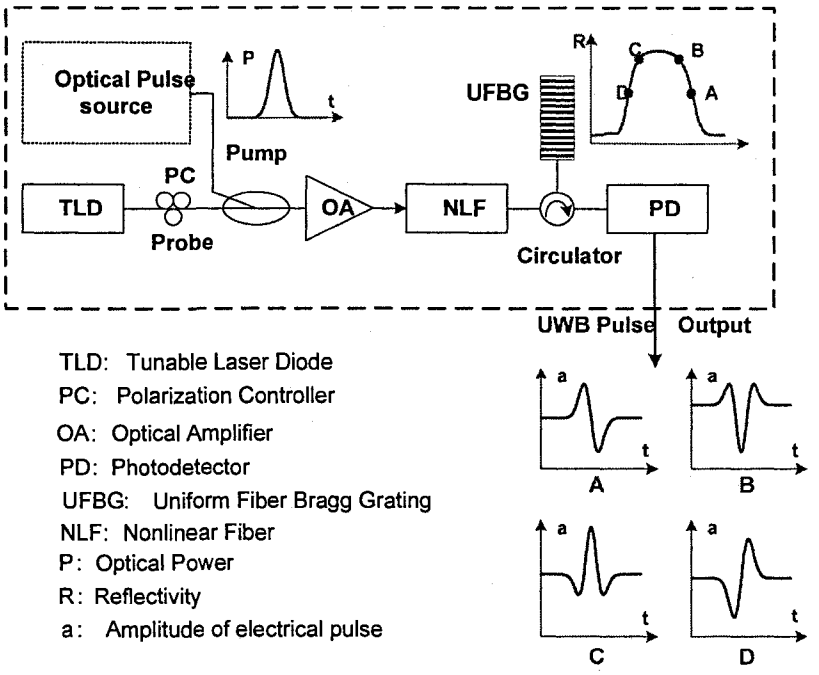

Fig. 5.3.2.1 Block diagram of the proposed UWB pulse generator.

B. An experiment using the intensity-modulated light as the pump- first step

In this step, we focus on the XPM effect in a nonlinear fiber. The optical pulses are generated by applying a 13.5 Gb/s bit sequence with a fixed pattern as 10000000000000001 (15 consecutive "0"s between two "1"s) to a CW LD at 1556.29 nm via an EOIM. The temporal waveform representing a single optical pulse can be found in Fig. 3(a) in Sec. 3.2, which has an FWHM pulse width of about 63 ps. The pump light is then combined with a CW light from a tunable laser source and amplified by an EDFA before being injected into 25 km NZ-DSF, which serves as the NLF shown in Fig. 5.3.2.1. The NZ-DSF has a chromatic dispersion of 5.6ps/nm/km at 1556 nm, a nonlinear refractive index n_2 of $2.3\times10^{-20}m^2$/km, and an effective mode-field area (MFA) of $72\mu m^2$. The optical spectra measured after the NZ-DSF with and without intensity modulation of the pump LD are shown in Fig. 5.3.2.2.

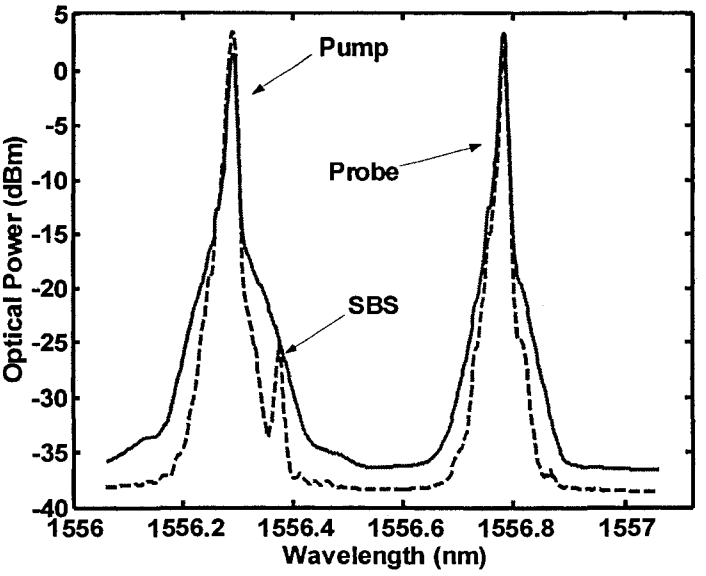

Fig. 5.3.2.2 Spectra measured at the output of the nonlinear fiber when the intensity modulation of the pump light is off (dashed line) and on (solid line). SBS: stimulated Brillouin scattering.

From Fig. 5.3.2.2, the spectrum of the probe light is broadened significantly when the pump light is being intensity modulated by the electrical pulses. This is due to the XPM, which makes the CW probe light be phase modulated, leading to an increased spectrum width. The stimulated Brillouin scattering (SBS) power level at the input side of the NZ-DSF is also monitored. A 20-dB SBS power reduction is observed when the electrical pulses are modulated on the pump light. It is known [1] that SBS could be suppressed if the spectrum of the light is broadened. In this system, the modulation of the pump light by the Gaussian pulses produces a broadened optical spectrum, which leads to a reduction in the stimulated Brillouin amplification. Thanks to the 20-dB SBS reduction, the SBS effect can be ignored in this system.

An FBG is applied as the frequency discriminator, which has a length of 10 mm and a peak amplitude reflectivity of 66%. A proper Gaussian apodization is applied during the FBG fabrication process to suppress the reflection sidelobes. Its reflection spectrum is shown in Fig. 5.3.2.3, which has a central wavelength of 1556.6 nm and a 3-dB bandwidth of 0.35 nm.

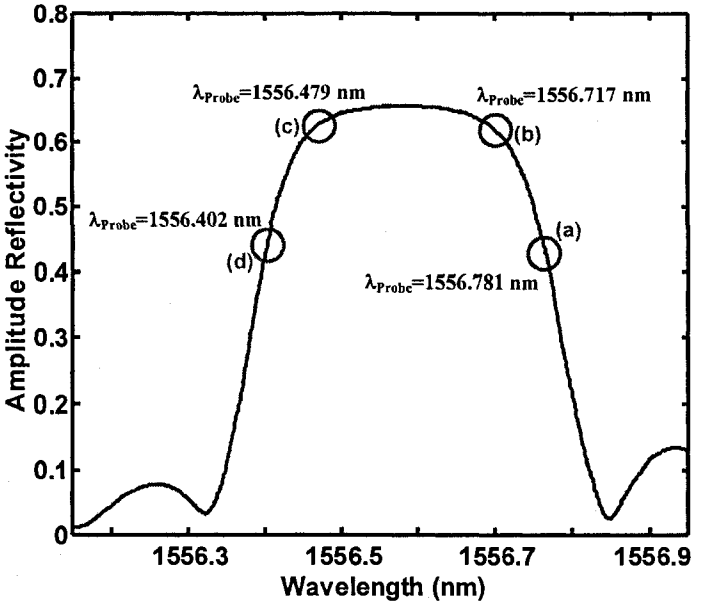

Fig. 5.3.2.3 Measured amplitude reflection spectrum of the FBG used in the experiment.

First, the wavelength of the probe light, λ_{probe}, is tuned at 1556.781 nm, which is located at the right linear slope of the FBG. The signal at the output of the PD is then measured by use of a high-speed sampling oscilloscope. Fig. 5.3.2.4(a) shows the generated Gaussian monocycle pulse, which has a null-to-null of about 110 ps. A small asymmetry between the positive and the negative part of the pulse is observed, which is due to the dispersion walkoff between the pump light and the probe light. By using a highly nonlinear fiber [2], it is possible to decrease the required optical pulse power, or use a shorter fiber, where the dispersive walkoff would be much less significant.

Then, the carrier wavelength is tuned at 1556.717 nm, which is located at the right turning corner of the FBG reflection spectrum, the output pulse turns to be a doublet with a negative mainlobe and two equal time sidelobes having positive values, as shown in Fig. 5.3.2.4(b). We further tune the carrier wavelength and make it be reflected at the left turning corner and the left linear slope, respectively. As can be seen from Figs. 5.3.2.4(c) and (d), the generated pulses are actually the inverted versions of those shown in Figs. 5.3.2.4(b) and (a), respectively. These interesting results agree well with the theoretical analysis in Sec. 5.3.1, and can be directly applied to implement different pulse modulation schemes.

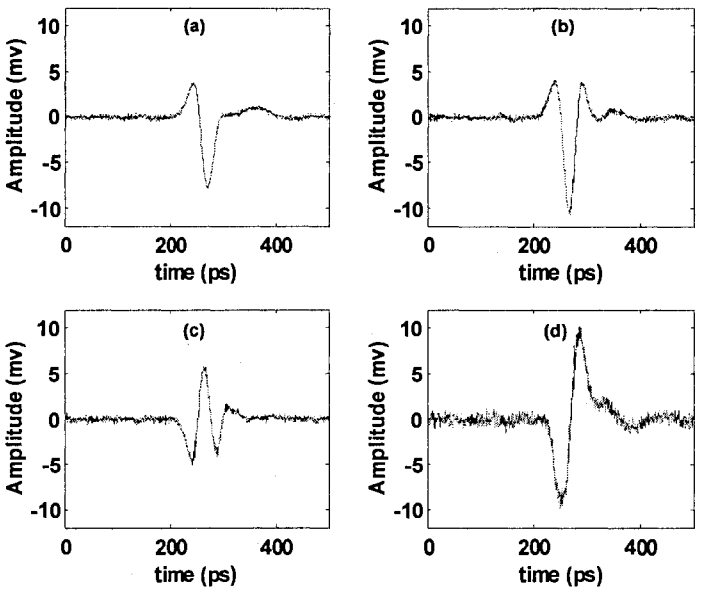

Fig. 5.3.2.4 Waveforms of the output pulses, when the wavelengths of the probe light are (a) 1556.781nm, (b) 1556.717nm, (c) 1556.479nm (d) 1556.402nm.

C. An experiment using a femtosecond pulse laser as the pump- second step

In the previous experiment, a CW light was intensity-modulated by an electrical pulse train to serve as the pump light; therefore an electrical short pulse generator was still required. In addition, the use of a long NZ-DSF fiber (25 km) led to a significant walk off between the pump and the probe. Since in a dispersive fiber, the frequency response of XPM index is approximately inversely proportional to the product of frequency, fiber dispersion, and wavelength separation between the pump and the probe [3]. So when the wavelength separation ($\Delta\lambda$) between the pump and the probe is large (that is the case always required for suppressing the pump in the processing of the probe signal), only a smaller fraction of the frequency components of the pump pulse will generate XPM efficiently, i.e., the low frequency components induce stronger XPM than that from the high frequencies. Consequently the shape of the pump pulse cannot be preserved in the phase change of the probe light, which eventually reflects as distortion of the generated UWB pulses.

In this step, a fully all-optical UWB pulse generator is experimentally implemented to solve these problems. Instead of using an electrical short pulse generator and a high-speed optical

intensity modulator to create the optical pulse train, a femtosecond pulse laser (FSPL) is applied. The output of the FSPL has a pulse width of 475 fs with a repetition rate of 48.6 MHz, which has a 3dB spectral bandwidth of 7.9 nm. However, such pulses are too short for UWB wireless applications. To obtain a proper pulse width, a tunable grating filter (TGF), which has a 3dB bandwidth of 0.23 nm and a tunable range covered the entire C band, is used to slice the spectrum of the FSPL and broaden the pulse width. The comparison of the spectra and temporal waveforms representing a single optical pulse measured before and after the TGF can be found in Fig. 5.3.2.5. We can see that after the spectrum slicing, the pulse width extends to 20 ps.

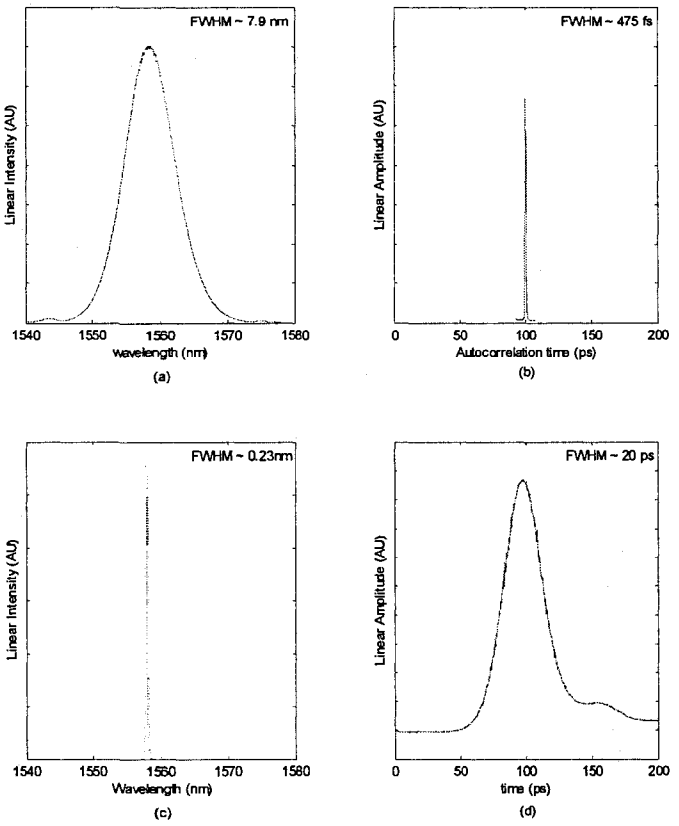

Fig. 5.3.2.5 (a) spectrum and (b) autocorrelation trace measured at the output of the FSPL, (c) spectrum and (d) temporal waveform measured at the output of the TGF.

The pump light is then combined with a CW light from a tunable LD and amplified by an EDFA before being injected into a length of 400m DSF, which has a chromatic dispersion of -3.4ps/nm/km at 1558nm, a nonlinear coefficient γ of $2.7W^{-1}km^{-1}$, and an effective MFA of

51.5μm^2. Compared to the 25km NZ-DSF used in the previous experiment, the length of the fiber to achieve sufficient XPM depth is significantly reduced, mainly due to two reasons: 1) the pump pulse obtained from the FSPL has short duration, very small duty cycle, and higher extinction ratio; and 2) the deployed DSF has a smaller effective MFA which leads to a larger nonlinear coefficient.

The central wavelength of the TGF is tuned at 1561.5 nm, which is about 5 nm away from the peak of the FBG reflection spectrum. The average optical power of the pump light measured before being injected into the DSF is 8 dBm, and that of the probe light is about 4 dBm. For the wavelength separation $\Delta\lambda$ of 5 nm, the DSF gives a walk-off of 6.8 ps, while this value will be around 620 ps if the 25 km NZ-DSF is used. Thanks to the large $\Delta\lambda$ applied in this experiment, after the DSF, the pump can be easily filtered out with high suppression ratio by the FBG. Again, by tuning the wavelength of the probe, λ_{probe}, at four different locations of the FBG reflection spectrum, we obtain four different UWB pulses, as shown in Fig. 5.3.2.6. UWB monocycles are generated by locating the probe at the linear slopes of the FBG reflection spectrum and UWB doublets are generated by locating the probe at the quadrature slopes of the FBG reflection spectrum. In addition, the two monocycles or the two doublets are out of phase. For the four pulses, a slight asymmetry is observed, which is mainly due to the self phase modulation (SPM) of the pump pulse in the DSF, which leads to the pulse broadening and distortion.

In this experiment, since the optical pulse is generated using an FSPL, no sophisticate electrical pulse generator is required. In addition, thanks to the use of the ultrafast optical pulse source and the DSF with a larger nonlinear coefficient, a much shorter fiber length (~ 400m) is required which reduces significantly the wavelength walk off effect during the XPM and the system stability is improved as well.

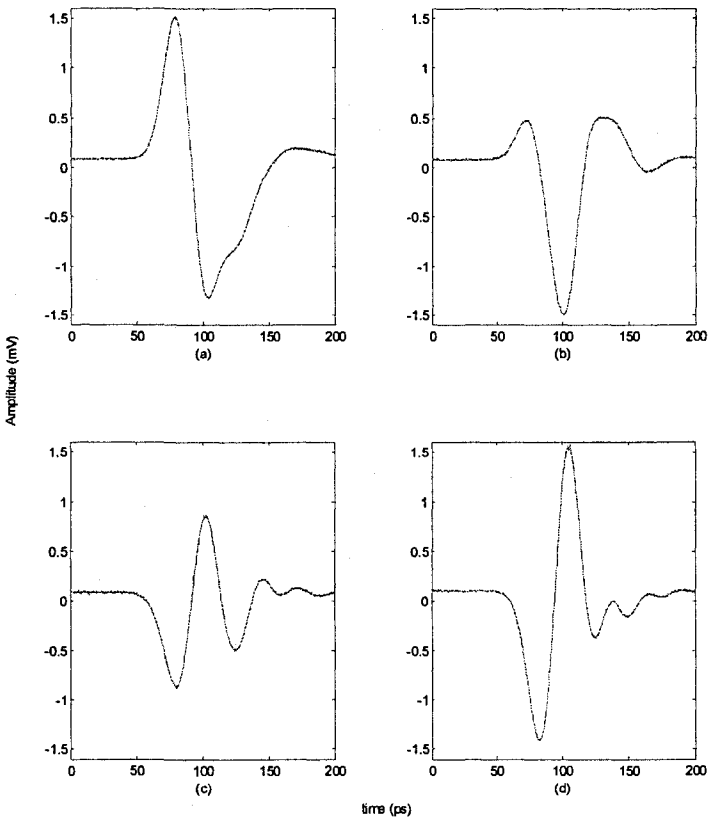

Fig. 5.3.2.6 Temporal waveforms of the output pulses, when the probe wavelength is located at different locations of the FBG reflection spectrum (A, B, C and D shown in Fig. 1)

References

[1] A. R. Chraplyvy, "Limitations on lightwave communications imposed by optical-fiber nonlinearities," J. Lightwave Technol., vol. 8, no. 10, pp. 1548-1557, Oct. 1990.

[2] M. Onishi, T. Okuno, T. Kashiwada, S. Ishikawa, N. Akasaka, and M. Nishimura, "Highly nonlinear dispersion-shifted fibers and their application to broadband wavelength converter," Opt. Fiber Technol., vol. 4, no. 2, pp. 204-214, 1998.

[3] T.-K. Chiang, N. Kagi, M. E. Marhic, and L. G. Kazovsky, "Cross-phase modulation in fiber links with multiple optical amplifiers and dispersion compensators," J. Lightw. Technol., Vol. 14, pp. 249-260, March 1996.

CHAPTER 6

CONCLUSIONS AND FUTURE WORK

6.1 Conclusions

In this thesis, a theoretical and experimental study of optical phase modulation and its applications in all-optical microwave signal processing were presented, which include all-optical microwave filtering, all-optical microwave mixing, optical CDMA coding, and UWB pulse signal generation.

In Chapter 2, a comprehensive study on optical phase modulation and its comparison with intensity modulation were made. Then, two different methods to realize PM-IM conversions were proposed. In the first approach, a dispersive device, such as a length of dispersive fiber or a LCFBG was used to alter the phase relationships among the sidebands and the optical carrier of a phase-modulated optical signal, leading to the PM-IM conversion. In the second approach, an optical filter, such as a fiber-based Sagnac-loop filter or an FBG, served as an optical frequency discriminator to achieve the PM-IM conversion. We showed that the PM-IM conversions would present some interesting features which are useful for all-optical signal processing: 1) the frequency response of a PM-IM conversion has a notch at dc, which would eliminate the baseband resonance and can be directly used to achieve microwave bandpass filtering; 2) a PM-IM conversion can generate two microwave signals that are out of phase by using two dispersive devices with opposite dispersions or an optical bandpass filters with opposite frequency response slopes. This feature was proved to be very useful that it would provide the possibility to implement bipolar operations, to achieve more complex signal processing functionalities with flexible structures.

In Chapter 3, three different approaches based on the proposed PM-IM conversions to achieving all-optical microwave bandpass filtering were presented. In the first approach, an equivalent

bandpass filter with only a single tap was experimentally implemented. The filter was used to shape the spectrum of a Gaussian pulse train to generate UWB doublet for UWB radio over fiber applications. In the second approach, all-optical microwave bandpass filter with multiple taps was experimentally implemented. It was different from the single-tap microwave bandpass filter where a single wavelength laser source was employed. In the second approach, a laser-array was used to generate multiple taps. The filter performances, including the mainlobe to sidelobe suppression ratio, the reconfigurability, tunability, and the dynamic range, were also investigated. In the first two approaches, the bandpass operation was realized by eliminating the baseband resonance with a dc notch of the PM-IM conversion. No negative coefficients were actually generated. In the third approach, a microwave bandpass filter with negative coefficients was proposed and experimentally demonstrated.

In Chapter 4, an electrooptic phase modulation based all-optical signal processor that could perform both microwave mixing and bandpass filtering simultaneously in a radio-over-fiber link was presented. First, a prove-of-concept experiment to up convert a subcarrier frequency from 3 GHz to 11.8 GHz using an EOPM-based signal processor with a local oscillator frequency of 8.8 GHz was implemented. Then, a further investigation of subcarrier frequency up conversion with data modulation was performed. The system performance was also studied.

In Chapter 5, an extensive investigation of an FBG-based frequency discriminator and its applications for all-optical microwave signal processing were performed. First, PM-IM conversion by use of an FBG-based frequency discriminator was presented. Both the magnitude and phase responses of the FBG are taken into account to build a numerical model in the frequency domain. A Gaussian-apodized FBG was fabricated to carry out the experiments. By using the FBG-based frequency discriminator, an approach to implementing unipolar-bipolar phase-time encoding/decoding in an optical CDMA system was presented. Two FBG arrays would be employed to perform the en/de coding and the proposed scheme was equivalent to a sequence inversion keyed (SIK) direct-sequence CDMA, which would provide an improved performance compared to the conventional incoherent scheme using optical orthogonal codes. The use of the FBG-based frequency discriminator to generate UWB pulses was also investigated. Two UWB pulse generation systems were proposed and experimentally

demonstrated. The first system was a hybrid system which required using an electrical pulse generator to generate the Gaussian pulse train. The optical phase modulation was realized using an EOPM. The second system was all optical, no electrical pulse generator and EOPM were used. In the second system, the optical pulse train was generated by a femtosecond laser source and the phase modulation was implemented in the optical domain based on XPM in a nonlinear fiber. The use of the proposed all-optical signal processor to implement UWB pulse polarity and pulse shape modulation was also discussed.

We should note that the proposed optical phase modulation based approaches present a general form of all-optical microwave signal processing using external electrooptic modulation. The approaches based on an MZI intensity modulator can be considered as a special case, because an EOPM is located at one of the two branches of the MZI and PM-IM conversion is achieved by using the MZI itself as an optical filter. However, in the approaches presented in this thesis, the PM-IM conversions are achieved by using two different methods (chromatic dispersion based and frequency discriminator based) with different architectures, which provide much more flexibility in implementing all-optical signal processing systems with various functionalities.

6.2 Future work

First, the impact of phase noise of the light source on the performance of the proposed systems needs to be studied. Since the phase of the laser source itself varies randomly with time and the photonic circuits also introduce additional random phase fluctuations due to the temperature and mechanical vibrations, the proposed PM-IM conversions will convert the phase noise to intensity noise, which would introduce additional noise to the system output. A theoretical and experimental study on the noise generated by PM-IM conversion and its impact on the system performance would be investigated.

Optical phase modulation based on XPM and SPM for all-optical signal processing needs to be further investigated. By using optical XPM and SPM techniques, no broadband EOPM is required, which is highly desirable for all-optical applications. For instance, in the UWB signal

generator presented in Sec. 5.3.2, neither an electrical pulse generator nor a high-speed EOPM was required, which made the system all optical. An all-optical system has the potential for integration using photonic integrated circuit technology. However, to fully exploit the advantages brought by XPM and SPM, more research work needs to be carried out.

Another important issue that should be tackled in the future is to reduce the overall system loss. Although the state-of-the-art optical fibers have extremely low loss, the overall system loss is still very high because of the poor efficiency of the E/O (using an electro-optic modulator) and the O/E (using a PD) conversions. A solution to this problem is to use optical amplifiers to compensate for the loss. An ultimate solution is to develop opto-electronic devices with higher conversion efficiency.

Finally, for practical applications, extensive research efforts need to be invested to improve the system performance and to reduce the cost. A promising solution is to use integrated photonic circuits to realize the functionality of the systems. The ultimate goal is to design a complete system on the same substrate thus realizing the system-on-substrate or system-on-chip for microwave photonic applications.

Publications

Refereed journal papers:

1 C. Wang, F. Zeng, and J. P. Yao "All-fiber Ultra Wideband pulse generation based on spectral shaping and dispersion-induced frequency-to-time conversion," IEEE Photonics Technology Letters, in press.

2 Q. Wang, H. Rideout, F. Zeng, and J. P. Yao, "Millimeter-wave frequency tripling based on four-wave mixing in a semiconductor optical amplifier," IEEE Photonics Technology Letters, vol. 18, no. 23, pp. 2460-2462, December 2006

3 F. Zeng and J. P. Yao, "Ultrawideband signal generation using a high-speed electrooptic phase modulator and an FBG-based frequency discriminator," IEEE Photonics Technology Letters, vol. 18, no. 19, pp. 2062-2064, October 1, 2006.

4 Q. Wang, F. Zeng, S. Blais, and J. P. Yao, "Optical UWB monocycle pulse generation based on cross-gain modulation in a semiconductor optical amplifier," Optics Letters, vol. 31, no. 21, pp. 3083-3085, November 2006.

5 F. Zeng and J. P. Yao, "An approach to Ultra-Wideband pulse generation and distribution over optical fiber," IEEE Photonics Technology Letters, vol. 18, no. 7, pp. 823-825, March 2006.

6 J. Wang, F. Zeng, and J. P. Yao, "All-optical microwave bandpass filters with negative coefficients based on PM-IM conversion," IEEE Photonics Technology Letters, vol. 17, no.10, pp. 2176-2178, October 2005.

7 F. Zeng, J. Wang, and J. P. Yao, "All-optical microwave bandpass filter with negative coefficients based on an electro-optic phase modulator and linearly chirped fiber Bragg gratings," Optics Letters, vol. 30, no. 17, pp. 2203-2205, September 2005.

8 J. Wang, F. Zeng, and J. P. Yao, "All-optical microwave bandpass filters implemented in a radio-over-fiber link," IEEE Photonics Technology Letters, vol. 17, no. 8, pp. 1737-1739, August 2005.

9 X. F. Chen, J. P. Yao, F. Zeng and Z. Deng, "Single-longitudinal-mode fiber ring laser employing an equivalent-phase-shift fiber Bragg grating," IEEE Photonics Technology Letters, vol. 17, no. 7, pp. 1390-1392, July 2005.

10 F. Zeng and J. P. Yao, "Investigation of phase modulator based all-optical bandpass filter," IEEE Journal of Lightwave Technology, vol. 23, no. 4, pp.1721-1728, April 2005.

11 F. Zeng and J. P. Yao, "All-optical microwave mixing and bandpass filtering in a radio-over-fiber link," IEEE Photonics Technology Letters, vol. 17, no. 4, pp. 899-901, April 2005.

12 F. Zeng and J. P. Yao, "All-optical microwave filters using uniform fiber Bragg gratings with identical reflectivities," IEEE Journal of Lightwave Technology, vol. 23, no. 3, pp. 1410-1418, March 2005.

13 F. Zeng and J. P. Yao, "All-optical bandpass microwave filter based on an electro-optic phase modulator," Optics Express, vol. 12, no. 16, pp. 3814-3819, August 2004.

14 F. Zeng, J. P. Yao, and S. Mihailov, "Genetic algorithm for fiber Bragg grating based all-optical microwave filter synthesis," Optical Engineering, vol. 42, no. 8, pp. 2250-2256, August 2003.

Refereed conference papers:

1 Y. Yan, F. Zeng, Q. Wang, and J. P. Yao, "Photonic microwave filter with negative coefficients based on cross polarization modulation in a semiconductor optical amplifier," accepted for oral presentation in OFC 2007.

2 F. Zeng and J. P. Yao, "Optical generation and distribution of UWB signals," presented at the 19th Annual Lasers and Electro Optics Society (LEOS) meeting, Montreal, Canada, November 2006. (Invited paper)

3 F. Zeng, Q. Wang, and J. P. Yao, "An approach to all-optical UWB pulse generation," presented at Microwave Photonics, Grenoble, France, October 2006.

4 Q. Wang, F. Zeng, and J. P. Yao, "Millimeter-wave generation based four-wave mixing in an SOA," presented at Microwave Photonics, Grenoble, France, October 2006.

5 F. Zeng and J. P. Yao, "Optical generation and distribution of UWB signals," presented at ICCCAS, Guilin, China, June 2006. (Invited paper)

6 F. Zeng and J. P. Yao, "Generation and distribution of UWB pulse signals by use of optical phase modulation and PM-IM conversions," presented at Photonics North, Quebec City, Canada, June 2006.

7 F. Zeng, Qing Wang, and J. P. Yao, "All-optical UWB pulse generation based on XPM and FBG-based frequency discriminator," presented at Asia-Pacific Microwave Photonics Conference, Kobe, Japan, April 2006. (Post-deadline paper)

8 C. Bélisle, S. Paquet, J. Seregelyi, G. Qi, F. Zeng, J. P. Yao, V. Aimez, J. Beauvais, W. Wang, and M. Cada, "All-optical microwave front end SDR," presented at 2005 Software Defined Radio Technical Conference and Product Exposition, Hyatt Regency - Orange County, California, United States, November 2005.

9 F. Zeng and J. P. Yao, "Performance evaluation of a novel all-optical microwave mixing and filtering system for radio-over-fiber applications," Proceedings of SPIE, vol. 5971, September 2005.

10 F. Zeng and J. P. Yao, "Experimental demonstration of bipolar optical CDMA encoder/decoder using electro-optic phase modulator and fiber Bragg grating arrays," presented at Photonics North, Toronto, Canada, September 2005.

11 F. Zeng and J. P. Yao, "Frequency domain analysis of fiber Bragg grating based phase modulation to intensity modulation conversion," Proceedings of SPIE, vol. 5971, September 2005.

12 F. Zeng and J. P. Yao, "Dispersion effects on fiber Bragg gratings-based all-optical microwave filters," Proceedings of SPIE, vol. 5466, pp. 61-71, April 2004.

13 F. Zeng and J. P. Yao, "Tunable all-optical microwave filter using uniform fiber Bragg gratings with identical reflectivities," Proceedings of SPIE, vol. 5466, pp. 44-53, April 2004.

14 F. Zeng and J. P. Yao and Tet Yeap, "Dispersion effects and implementation errors on uniform fiber Bragg grating based true-time-delay beamforming networks," Proceedings of 2003 IEEE International Topical Meeting on Microwave Photonics, pp. 337-340, 10-12 September 2003.

15 F. Zeng and J. P. Yao, "Dispersion effects of fiber Bragg gratings on true-time-delay beamforming networks," 2003 IEEE Canadian Conference on Electrical and Computer Engineering, vol. 1, pp. 299 - 302, 4-7 May 2003.

LIST OF ACRONYMS

A

AP	Access Point
ASE	Amplified Spontaneous Emission
AWG	Arrayed Wave Guide

B

BERT	Bit-Error-Rate Tester
BPSK	Binary Phase Shift Keying

C

CDMA	Code Division Multiple Access
CS	Central Office
CW	Continuous Wave

D

DD	Direct Detection
DFB	Distributed-Feedback
DPSK	Differential Phase Shift Keying
DSF	Dispersion Shifted Fiber

E

EDFA	Erbium Doped Fiber Amplifier
EMI	Electromagnetic Interference
E/O	Electrical to Optical
EOM	Electro-Optic Modulator
EOIM	Electro-Optic Intensity Modulator
EOPM	Electro-Optic Phase Modulator
ESA	Electrical Spectrum Analyzer

F

FBG	Fiber Bragg Grating
FIR	Finite Impulse Response
FM	Frequency Modulation
FP	Fabry-Perot
FSK	Frequency Shift Keying
FSPL	Femtosecond Pulsed Laser
FSR	Free Spectral Range
FTTH	Fiber-to-the-Home
FWHM	Full Width at Half Maximum

G

GD	Group Delay

I

IM	Intensity Modulation

L

LAN	Local Area Network
LCFBG	Linearly Chirped FBG
LD	Laser Diode
LED	Light Emission Diode
$LiNbO_3$	Lithium Niobate

M

MAI	Multiple Access Interference
MFA	Mode Field Area
MSR	Mainlobe-to-Sidelobe Ratio
MZI	Mach-Zehnder Interferometer

N

NZ-DSF	Non-Zero Dispersion Shifted Fiber

O

O/E	Optical to Electrical
OOC	Optical Orthogonal Code
OOK	On-Off-Keying
OSA	Optical Spectrum Analyzer

P

PC	Polarization Controller
PD	Photodetector
PM	Phase Modulation
PPM	Pulse Polarity Modulation
PRBS	Pseudo-Random Bit Sequence
PSK	Phase Shift Keying
PSM	Pulse Shape Modulation

R

RF	Radio Frequency
RoF	Radio over Fiber

S

SBS	Stimulated Brillouin Scattering
SIK	Sequence Inversion Keying
SMF	Single Mode Fiber
SNR	Signal-to-Noise Ratio
SOA	Semiconductor Optical Amplifier
SPM	Self-Phase Modulation

U

UFBG	Uniform Fiber Bragg Grating
UV	Ultraviolet
UWB	Ultra-Wideband

X

XGM	Cross-Gain Modulation
XPM	Cross-Phase Modulation